Stratigraphic Studies of a Late Quaternary Barrier-Type Coastal Complex, Mustang Island–Corpus Christi Bay Area, South Texas Gulf Coast

U.S. GEOLOGICAL SURVEY PROFESSIONAL PAPER 1328

COVER: Landsat image showing a regional view of the South Texas coastal zone.

LIBRARY
U. S. BUREAU OF MINES
Western Field Operation Center
East 360 3rd Ave.
Spokane, Washington 99202

BUREAU OF MINES
LIBRARY
SPOKANE WASH.
FEB 19 1987
PLEASE RETURN
TO LIBRARY

Stratigraphic Studies of a Late Quaternary Barrier-Type Coastal Complex, Mustang Island–Corpus Christi Bay Area, South Texas Gulf Coast

Edited by GERALD L. SHIDELER

U.S. GEOLOGICAL SURVEY PROFESSIONAL PAPER 1328

UNITED STATES GOVERNMENT PRINTING OFFICE, WASHINGTON : 1986

DEPARTMENT OF THE INTERIOR

DONALD PAUL HODEL, *Secretary*

U.S. GEOLOGICAL SURVEY

Dallas L. Peck, *Director*

Library of Congress Cataloging-in-Publication Data
Main entry under title:

Stratigraphic studies of a late Quaternary barrier-type coastal complex, Mustang Island-Corpus Christi Bay area, South Texas Gulf Coast.

(U.S. Geological Survey professional paper ; 1328)

Supt. of Docs. no.: I 19.16:1328
Contents: Stratigraphic studies of a late Quaternary coastal complex, South Texas / by Gerald L. Shideler—Seismic and physical stratigraphy of late Quaternary deposits, South Texas coastal complex / by Gerald L. Shideler—Ostracodes from late Quaternary deposits, South Texas coastal complex / by Thomas M. Cronin—[etc.]

1. Barrier islands—Texas—Gulf Region—Addresses, essays, lectures. 2. Geology, Stratigraphic—Quaternary—Addresses, essays, lectures. I. Shideler, Gerald L. II. Series: U.S. Geological Survey professional paper ; 1328.
GB465.T4S87 1986 551.4'23'09764 84-600246

For sale by the Books and Open-File Reports Section, U.S. Geological Survey,
Federal Center, Box 25425, Denver, CO 80225

CONTENTS

[Letters designate the chapters]

Stratigraphic Studies of a Late Quaternary Coastal Complex, South Texas— Introduction and Geologic Framework

By GERALD L. SHIDELER

STRATIGRAPHIC STUDIES OF A
LATE QUATERNARY BARRIER-TYPE COASTAL COMPLEX,
MUSTANG ISLAND–CORPUS CHRISTI BAY AREA,
SOUTH TEXAS GULF COAST

U.S. GEOLOGICAL SURVEY PROFESSIONAL PAPER 1328–A

CONTENTS

ILLUSTRATIONS

STRATIGRAPHIC STUDIES OF A LATE QUATERNARY COASTAL COMPLEX, SOUTH TEXAS— INTRODUCTION AND GEOLOGIC FRAMEWORK

By GERALD L. SHIDELER

ABSTRACT

An understanding of the origin and behavior of modern barrier-island systems is an important factor in the implementation of effective coastal-zone-management programs. Similarly, an understanding of the ancient barrier-lagoonal analogues within the stratigraphic record is important in designing effective sedimentary-facies models used in the exploration for mineral resources. These factors prompted the initiation in 1979 of the study described in this volume. The purpose of this study was to investigate the stratigraphic history of a late Quaternary coastal complex of the South Texas Coastal Plain province, a complex that includes both Pleistocene and Holocene barrier systems. The study is based on 247 m of continuous cores obtained at seven sites and 70 km of high-resolution seismic-reflection profiles, which were used to analyze the uppermost 60 m of Quaternary coastal-plain deposits. The age of the studied stratigraphic section ranges from Pleistocene (post-Aftonian) to Holocene.

Quaternary sedimentation was controlled largely by glacioeustatic movements. During interglacial high stands of sea level, coastal-plain depositional sequences were formed of alluvial, deltaic, coastal-interdeltaic, and marine deposits. The coastal-plain sequences are separated by unconformities formed during erosional intervals associated with glacial low stands of sea level.

The immediate study area encompasses southern Mustang Island, northern Laguna Madre, southern Corpus Christi Bay, and the adjacent mainland. This part of the Texas Coastal Plain province consists of a modern barrier-island chain and an extensive lagoonal-estuarine system. Corpus Christi Bay is separated from the Gulf of Mexico by Mustang Island and represents a bar-built variety of estuary that is typical of the Texas Gulf Coast. The mainland is underlain by the upper Pleistocene Beaumont Formation, which consists mainly of fluvial-deltaic deposits but which also includes the Ingleside barrier-beach facies.

The chapters in this volume present the results of different facets of the study. Subsequent chapters present the following topics: the seismic and physical stratigraphy of the study area, ostracode assemblages and their paleoenvironmental significance, the petrology and diagenetic features of sand units, and the geochemistry and mineralogy of fine-grained sediments.

INTRODUCTION

During the past decade, the number of geologic studies related to the origin and behavior of Quaternary barrier-island systems has increased greatly. This increased research effort has been prompted by the increasing intensity of national environmental problems associated with coastal-zone development, the implementation of the national Coastal Zone Management Act, and the need for a solid scientific understanding of highly dynamic barrier environments in formulating coastal-management decisions. Additional impetus also has been provided by the importance of coastal barriers and associated backbarrier facies within the stratigraphic record and their relevance to the design of exploration models for hydrocarbons, coal deposits, and mineral resources.

In response to the widespread interest in barrier systems, the present study was initiated in 1979 to investigate the local stratigraphic history of a Quaternary coastal complex containing barrier systems on the South Texas Gulf Coast (fig. 1). The coastal complex is near the City of Corpus Christi; it includes the modern southern Mustang Island barrier and the backbarrier environments of southern Corpus Christi Bay and northern Laguna Madre. The complex also includes the adjacent mainland, which consists of a Pleistocene barrier system. Thus, the local study site was selected because it is a small and compact area that contains two Quaternary barrier systems, resulting in a maximum amount of stratigraphic information. Specific objectives of the present study were to investigate the general stratigraphic evolution of this Pleistocene-

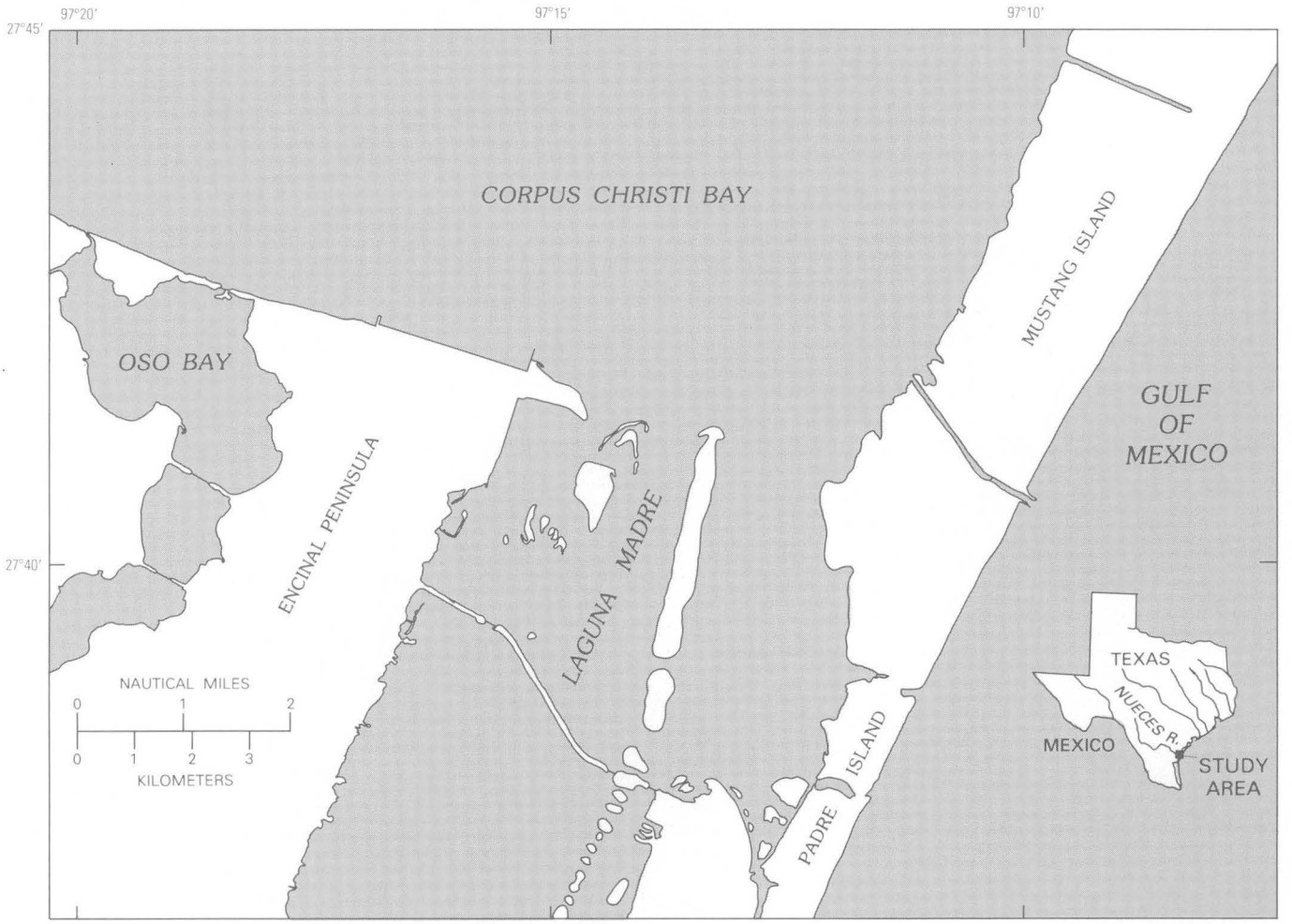

FIGURE 1.—Map showing locations of features within the southern Mustang Island–Corpus Christi Bay study area on the South Texas Gulf Coast. The modern Mustang Island–Padre Island barrier chain separates Corpus Christi Bay and northern Laguna Madre from the Gulf of Mexico. The mainland consists of the Encinal Peninsula–Oso Bay area, which is within the City of Corpus Christi.

Holocene coastal complex and to gain insight regarding the origin and stability of the associated barrier systems.

The subsurface information that formed the basis for this stratigraphic analysis consists of continuous cores from seven bored holes, most of which penetrated to depths of about 60 m. The continuous cores provided stratigraphic data that are much more reliable than data from well cuttings obtained from rotary, auger, or jet-down holes. Additional subsurface data consist of about 70 km of high-resolution seismic-reflection records obtained throughout the study area. The seismic records, in conjunction with the cores, were utilized to establish the seismic and physical stratigraphy of the area (Shideler, Chap. B, this volume). Samples from the cores were analyzed by Cronin (Chap. C, this volume) for microfossils, especially ostracode assemblages, which were used for paleoenvironmental inferences. Flores and Keighin (Chap. D, this volume) studied the petrology and diagenetic features of the sand units sampled by the cores. The bulk geochemistry and mineralogy of fine-grained sediments within the cored stratigraphic section also were studied (Flores and Shideler, Chap. E, this volume). These individual studies have collectively contributed to an overall understanding of the geologic history of the study area.

GEOLOGIC FRAMEWORK

PHYSIOGRAPHIC SETTING

The study area is a part of the South Texas coastal zone, which is characterized by an essentially continuous, modern barrier-island chain (Mustang Island and Padre Island) that extends from the Aransas Pass tidal inlet southward to the United States–Mexico border (fig. 2). This barrier chain is approximately 225 km long; about one-half of it is within the Padre Island

FIGURE 2.—Landsat image showing a regional view of the South Texas coastal zone. The image shows the modern Mustang Island–Padre Island barrier chain extending southward from the Aransas Pass tidal inlet of Corpus Christi Bay to the dredged Port Mansfield Channel. The backbarrier lagoonal-estuarine system consists of Corpus Christi Bay, Baffin Bay, and Laguna Madre. Note southward reduction in coastal vegetation and corresponding increase in active sand migration.

National Seashore. The barrier chain is separated from the mainland by a lagoonal-estuarine system consisting of Corpus Christi Bay, Baffin Bay, and Laguna Madre. The tidal range during fair weather is generally less than 0.3 m in the open Gulf of Mexico (Marmer, 1954), and it is even lower in the backbarrier lagoonal-estuarine system. Consequently, the South Texas barriers are of the microtidal variety (tidal range <2 m); waves and wind are the dominant formative agents, and tidal effects are minimal.

The climate of the South Texas coastal zone is subtropical and semiarid. Average annual rainfall ranges from about 29 in. (74 cm) near Corpus Christi Bay to 26 in. (66 cm) at the United States–Mexico border, and average annual temperatures range from about 72°F (22°C) near the bay to 74°F (23°C) at the border (Carr, 1967). The southward reduction in annual rainfall, in conjunction with a southward increase in temperature and evaporation rates, results in a progressive southward increase in aridity and a reduction in coastal vegetation. Consequently, the effects of wind in controlling coastal processes increase southward. For South Texas, the prevailing winds are southeasterly onshore winds and are most consistent during the summer. During the winter, the winds are more variable; the southeasterly winds are interrupted by frequent higher velocity northerly winds that are associated with southward-moving cold fronts.

The Texas barrier islands are highly susceptible to modifying effects from tropical storms and hurricanes. The past effects of hurricanes on Texas barriers have been discussed by Hayes (1967). More recent effects of Hurricane Allen (August 1980) on the South Texas barriers were described by Miller and others (1981), who noted extensive breaching of the barrier by storm channels and the large-scale transport of barrier-beach sand into adjacent Laguna Madre as washover fans. These effects were most pronounced on southern Padre Island where the hurricane eye made landfall.

Within the immediate study area (fig. 3), Corpus Christi Bay is the dominant physiographic feature. It is a highly restricted bar-built variety of estuary (Pritchard, 1967), which is typical of the Texas Coastal Plain. It is relatively shallow (<5 m deep) and is separated from the Gulf of Mexico by the Mustang Island barrier. Corpus Christi Bay's main tidal inlet is Aransas Pass at the northern terminus of Mustang Island. The main fluvial input into the estuarine system is from the Nueces River, which discharges directly into satellite Nueces Bay. This shallow bay (<2 m deep) is connected by an inlet to Corpus Christi Bay, which has water exchange with shallow (<2 m) Laguna Madre to the south and Redfish Bay to the north. Minor stream discharge also enters Corpus Christi Bay along its southern shore from the shallow (<1 m) Oso Bay–Oso Creek tributary.

REGIONAL GEOLOGY

The study area is a part of the Gulf Coastal Plain province and is underlain by a thick gulfward-dipping sequence of clastic deposits of Quaternary age. Some early discussions of Quaternary deposits of the Texas Coastal Plain are presented in the works of Deussen (1914, 1924), Barton (1930a, b), Price (1933, 1958), and Doering (1935, 1956, 1958). Previous studies of the Quaternary geology of the Gulf Coastal Plain have been well summarized by Murray (1961) and by Bernard and LeBlanc (1965).

In general, the geologic evolution of the Quaternary Coastal Plain of Texas was controlled mainly by glacioeustatic fluctuations. During high stands of sea level associated with the Pleistocene interglacial stages, four distinct coastal-plain depositional sequences were formed. Each coast-parallel sequence consists of alluvial, deltaic, coastal-interdeltaic, and marine deposits having facies relationships similar to those of modern coastal-plain deposits. A general downdip gradation exists from continental to marine deposits in a gulfward direction. The four Pleistocene coastal-plain sequences are separated from each other by unconformities that reflect weathering and erosion that took place during low stands of sea level associated with glacial stages. During the Holocene transgression, the modern coastal-plain sequence formed, reflecting the present high stand of sea level.

The five Quaternary coastal-plain sequences dip gulfward and are progressively younger from inland areas toward the coast; each coastal-plain sequence overlies and offlaps the next older sequence in a gulfward direction. The surface of each progressively younger coastal-plain sequence decreases in both elevation and seaward slope toward the coast. The progressive increase in surface gradients of the coastal plains with age reflects the continued regional subsidence of the Gulf Coast during Quaternary sedimentation. Some of the Quaternary coastal-plain sequences of the Gulf Coast have formation status, and their nomenclature and correlation have been the subjects of numerous studies. In the present study, the nomenclature presented by Bernard and LeBlanc (1965) is used (fig. 4).

The five Quaternary coastal-plain sequences in Texas are, from oldest to youngest, the Willis Formation, Lissie Formation (lower and upper parts), Beaumont Formation, and unnamed Holocene deposits. This Quaternary section of coastal-plain deposits shows substantial variations in thickness. Bernard and LeBlanc (1965) noted that in the Texas Coastal Plain, each Pleistocene sequence can range in thickness from a few feet to 50 ft (15 m) in interdeltaic or interfluve areas and from less than 10 ft (3 m) to about 150–200 ft (45–60 m) within entrenched alluvial valleys. The Quaternary section is underlain by the Goliad Formation of Pliocene age. For further details regarding the regional Quaternary geology of the Texas Gulf Coast, the reader is referred to review papers by Doering (1956), Price (1958), Murray (1961), and Bernard and LeBlanc (1965).

FIGURE 3.—Aerial photograph showing a local view of the southern Mustang Island–Corpus Christi Bay study area. The photograph was taken from an altitude of about 18,300 m during a NASA (U.S. National Aeronautics and Space Administration) overflight on August 20, 1980.

Series	Glaciation and interglaciation	Texas	Louisiana
Holocene		Unnamed deposits	Unnamed deposits
Pleistocene	Wisconsin	Beaumont Formation	Prairie Formation
	Sangamon-late Illinoian	Lissie Formation (upper part)	Montgomery Formation
	Yarmouth-late Kansan	Lissie Formation (lower part)	Bentley Formation
	Aftonian-late Nebraskan	Willis Formation	Williana Formation
Pliocene		Goliad Formation	Goliad Formation

FIGURE 4.—Quaternary and Pliocene stratigraphic nomenclature for Texas and Louisiana modified from Bernard and LeBlanc (1965).

LOCAL GEOLOGY

The geology of the region including the southern Mustang Island–Corpus Christi Bay study area has been mapped by the University of Texas Bureau of Economic Geology (Texas University Bureau of Economic Geology, 1975). The entire mainland area surrounding the Corpus Christi Bay estuarine system is underlain by the Pleistocene Beaumont Formation (fig. 5). The Beaumont is a highly heterogeneous clastic unit composed of fluvial, deltaic, coastal, and shallow-marine deposits. A separate barrier-island and beach sand facies of the Beaumont Formation has been mapped both south (Encinal Peninsula) and north (Live Oak Ridge) of Corpus Christi Bay. This facies represents the Ingleside sand body, which forms a low (3–9 m), segmented, coast-parallel ridge system along the Texas mainland from Matagorda Bay southward to Baffin Bay, a distance of about 145 km. The exact age and origin of the Ingleside sand body are controversial. It has been interpreted as a transgressive offshore bar or barrier-island chain analogous to the modern Texas barrier system (Price, 1933). An alternate interpretation was proposed by Wilkinson and others (1975); they considered the Ingleside to be a regressive strandplain sheet sand similar to that on the west coast of Mexico described by Curray and others (1969) or similar to the Chenier plain of southwestern Louisiana described by Gould and McFarlan (1959).

Further gulfward are Holocene deposits composing the modern barrier-island chain and the backbarrier lagoons, marshes, and tidal flats. Holocene alluvial deposits of the Nueces River are present at the head of Nueces Bay; alluvium is also present along Oso Creek. Both fill and dredged spoil materials are locally distributed throughout the area. The mapping of Holocene bay-floor sediments within the Corpus Christi Bay estuarine system illustrates that the interior areas of Corpus Christi Bay, Nueces Bay, and Oso Bay are depocenters for terrigenous silt and clay (Shideler and others, 1981); the main sources of mud influx into the estuarine system are the Nueces River, Oso Creek, and shoreline erosion of the mud-rich Beaumont Formation substrate. Most of the peripheral areas of the bays are composed of sandy sediments that appear to be mainly lag deposits from shoreline erosion.

In the Gulf of Mexico, Holocene sea-floor sediments have been mapped on the Inner Continental Shelf adjacent to Mustang Island and northern Padre Island (Shideler and Berryhill, 1977). With the exception of a hydraulically complex sector near the Aransas Pass tidal inlet, the sea-floor sediments illustrate a size-graded shoreface and inner shelf zone characterized by a well-defined gradient of decreasing sand content seaward. In water depths shallower than about 15 m, sand constitutes more than 90 percent of the sea-floor sediment; mud is the dominant sea-floor sediment component (more than 50 percent) in water depths greater than 20 m. The shallow sandy shoreface and inner shelf sector exerts an important influence on the Mustang Island–Padre Island barrier system. The upper shoreface is characterized by a migrating bar-and-

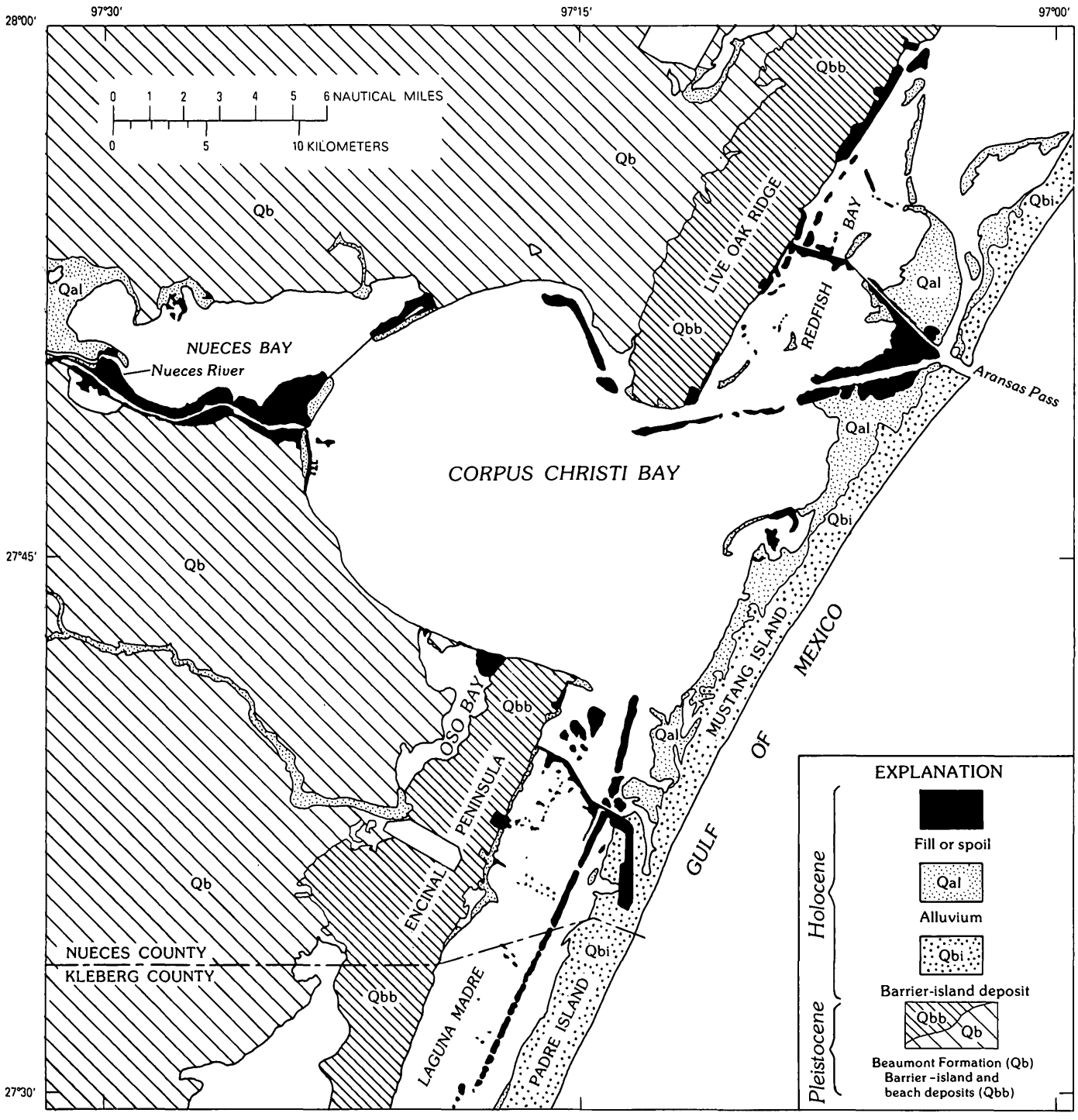

FIGURE 5.—Geologic map of the southern Mustang Island–Corpus Christi Bay study area and surrounding region (modified from Texas University Bureau of Economic Geology, 1975).

trough system that is in dynamic equilibrium with the barrier beach. The offshore bars are sand reservoirs for the natural replenishment of barrier beaches during seasonal beach cycles and, thus, are an influential factor in the sediment budget and response characteristics of the adjacent barrier system.

REFERENCES CITED

Barton, D. C., 1930a, Surface geology of coastal southeast Texas: American Association of Petroleum Geologists Bulletin, v. 14, no. 10, p. 1301–1320.

———1930b, Deltaic coastal plain of southeastern Texas: Geological Society of America Bulletin, v. 41, no. 3, p. 359–382.

Bernard, H. A., and LeBlanc, R. J., 1965, Résumé of the Quaternary geology of the northwestern Gulf of Mexico province, *in* Wright, H. E., Jr., and Frey, D. G., eds., The Quaternary of the United States: Princeton, N.J., Princeton University Press, p. 137–185.

Carr, J. T., Jr., 1967, The climate and physiography of Texas: Texas Water Development Board Report 53, 27 p.

Curray, J. R., Emmel, F. J., and Crampton, P. J. S., 1969, Holocene history of a strand plain, lagoonal coast, Nayarit, Mexico, *in* Ayala Castañares, Agustín, and Phleger, F. B., eds., Coastal lagoons, a symposium—UNAM–UNESCO, México, D.F., 1967: México, D.F., Universidad Nacional Autónoma de México, p. 63–100.

Deussen, Alexander, 1914, Geology and underground waters of the southeastern part of the Texas Coastal Plain: U.S. Geological Survey Water-Supply Paper 335, 365 p.

———1924, Geology of the Coastal Plain of Texas west of Brazos River: U.S. Geological Survey Professional Paper 126, 139 p.

Doering, John, 1935, Post-Fleming surface formations of coastal southeast Texas and south Louisiana: American Asssociation of Petroleum Geologists Bulletin, v. 19, no. 5, p. 651-688.

———1956, Review of Quaternary surface formations of Gulf Coast region: American Association of Petroleum Geologists Bulletin, v. 40, no. 8, p. 1816–1862.

———1958, Citronelle age problem: American Association of Petroleum Geologists Bulletin, v. 42, no. 4, p. 764–786.

Gould, H. R., and McFarlan, Edward, Jr., 1959, Geologic history of the chenier plain, southwestern Louisiana: Gulf Coast Association of Geological Societies Transactions, v. 9, p. 261–270.

Hayes, M. O., 1967, Hurricanes as geological agents—Case studies of hurricanes Carla, 1961, and Cindy, 1963: Texas University Bureau of Economic Geology Report of Investigations 61, 56 p.

Marmer, H. A., 1954, Tides and sea level in the Gulf of Mexico, *in* Galtsoff, P. S., coordinator, Gulf of Mexico, its origin, waters, and marine life: U.S. Fish and Wildlife Service Fishery Bulletin, v. 55 (Fishery Bulletin 89), p. 101–118.

Miller, R. J., Kindinger, J. L., Berryhill, H. L., Jr., and Bouma, A. H., 1981, Sedimentological effects of Hurricane Allen on South Texas coast; model of storm influence on barrier-island coast evolution [abs.]: Gulf Coast Association of Geological Societies Transactions, v. 31, p. 433.

Murray, G. E., 1961, Geology of the Atlantic and Gulf Coastal Province of North America: New York, Harper and Brothers, 692 p.

Price, W. A., 1933, Role of diastrophism in topography of Corpus Christi area, south Texas: American Association of Petroleum Geologists Bulletin, v. 17, no. 8, p. 907–962.

———1958, Sedimentology and Quaternary geomorphology of south Texas: Gulf Coast Association of Geological Societies Transactions, v. 8, p. 41–75.

Pritchard, D. W., 1967, What is an estuary—Physical viewpoint, *in* Lauff, G. H., ed., Estuaries: American Association for the Advancement of Science Publication 83, p. 3–5.

Shideler, G. L., and Berryhill, H. L., Jr., 1977, Map showing sea-floor sediment texture on the South Texas Inner Continental Shelf, Corpus Christi Bay to Baffin Bay: U.S. Geological Survey Miscellaneous Field Studies Map MF–901.

Shideler, G. L., Stelting, C. E., and McGowen, J. H., 1981, Maps showing textural characteristics of benthic sediments in the Corpus Christi Bay estuarine system, south Texas: U.S. Geological Survey Miscellaneous Field Studies Map MF–1275.

Texas University Bureau of Economic Geology, 1975, Geologic atlas of Texas, Corpus Christi sheet: Austin, scale 1:250,000.

Wilkinson, B. H., McGowen, J. H., and Lewis, C. R., 1975, Ingleside strandplain sand of central Texas coast: American Association of Petroleum Geologists Bulletin, v. 59, no. 2, p. 347–352.

Seismic and Physical Stratigraphy of Late Quaternary Deposits, South Texas Coastal Complex

By GERALD L. SHIDELER

STRATIGRAPHIC STUDIES OF A
LATE QUATERNARY BARRIER-TYPE COASTAL COMPLEX,
MUSTANG ISLAND–CORPUS CHRISTI BAY AREA,
SOUTH TEXAS GULF COAST

U.S. GEOLOGICAL SURVEY PROFESSIONAL PAPER 1328–B

CONTENTS

ILLUSTRATIONS

[Plates are in pocket]

TABLES

STRATIGRAPHIC STUDIES OF A LATE QUATERNARY BARRIER-TYPE COASTAL COMPLEX, MUSTANG ISLAND–CORPUS CHRISTI BAY AREA, SOUTH TEXAS GULF COAST

SEISMIC AND PHYSICAL STRATIGRAPHY OF LATE QUATERNARY DEPOSITS, SOUTH TEXAS COASTAL COMPLEX

By GERALD L. SHIDELER

ABSTRACT

A high-resolution seismic-reflection survey and continuous cores from seven localities were used to study the late Quaternary stratigraphy of the southern Mustang Island–Corpus Christi Bay area, South Texas Gulf Coast, to a depth of 60 m. The stratigraphic section ranges in age from Pleistocene (post-Aftonian) to Holocene and is a lithologically heterogeneous assemblage of unconsolidated to poorly consolidated clastic deposits that consist mainly of alternating sand and mud lithosomes. The section shows a high degree of vertical and lateral facies variability, extensive internal channeling and truncation, and a general absence of persistent horizons for correlation. The stratigraphic characteristics indicate multiple transgressive-regressive sequences resulting mainly from glacioeustatic movements.

The Pleistocene section shows facies relationships that indicate transitions among the following paleoenvironments: alluvial plain, upper and lower deltaic plains, subaqueous deltaic plain, and barrier-strandplain. The deposits record at least two major transgressions probably associated with the Sangamon interglacial stage and a mid-Wisconsin interstade. The Ingleside barrier-strandplain sand body of the mainland appears to be a composite transgressive-regressive structure that formed at the high stand of sea level near the end of the mid-Wisconsin interstade (about 25,000 years ago) and during the early phases of the subsequent late Wisconsinan regression. During the latter regression, the Ingleside sand body and subjacent fluvial-deltaic plain of the Beaumont Formation were dissected by the ancestral Nueces River system, which drained to the southeast; the result was the development of a prominent unconformity having more than 35 m of local relief.

The Holocene section attains a maximum local thickness of 36 m and is composed of a transgressive sequence of fluvial-estuarine, lagoonal, and barrier-island deposits formed during the past 10,000 years. The section shows multiple episodes of channel dissection and infilling by the ancestral Nueces River system, indicating that the Holocene transgression was interrupted by one or more sea-level stillstands or minor regressive phases. During that transgression, Holocene sedimentation was controlled largely by late Pleistocene paleotopography. The thickest and most complete Holocene sections accumulated within the incised ancestral valleys of the Nueces River system; the topographically higher ancestral interfluve areas accumulated thinner deposits.

The modern Mustang Island barrier probably began to form locally approximately 8,500 years ago. Facies relationships indicate that the primordial barrier originated somewhat seaward of the present barrier position and that, as transgression continued, vertical sand accretion and landward migration resulted in the evolution of the modern Mustang Island barrier. In turn, barrier development caused the progressive restriction of Corpus Christi Bay and Laguna Madre, which resulted in the accumulation of backbarrier estuarine-lagoonal deposits. Average barrier sedimentation rates during the last 5,000 years indicate that the landward migration of Mustang Island has continued into modern time.

INTRODUCTION

The purpose of this study was to investigate the stratigraphic evolution of a late Quaternary barrier-type coastal complex within the Coastal Plain province of South Texas. The study area encompasses southern Mustang Island, northern Laguna Madre, southern Corpus Christi Bay, and the adjacent mainland (fig. 1). This stratigraphic study is based on both a high-resolution seismic survey of the area and complementary continuous cores from seven selected localities. These data permitted an investigation of the Pleistocene-Holocene section to a depth of approximately 60 m.

The South Texas Coastal Plain province in the study area is composed of a thick sequence of gulfward-dipping clastic deposits of Quaternary age. The general geology of the Coastal Plain in the immediate Mustang

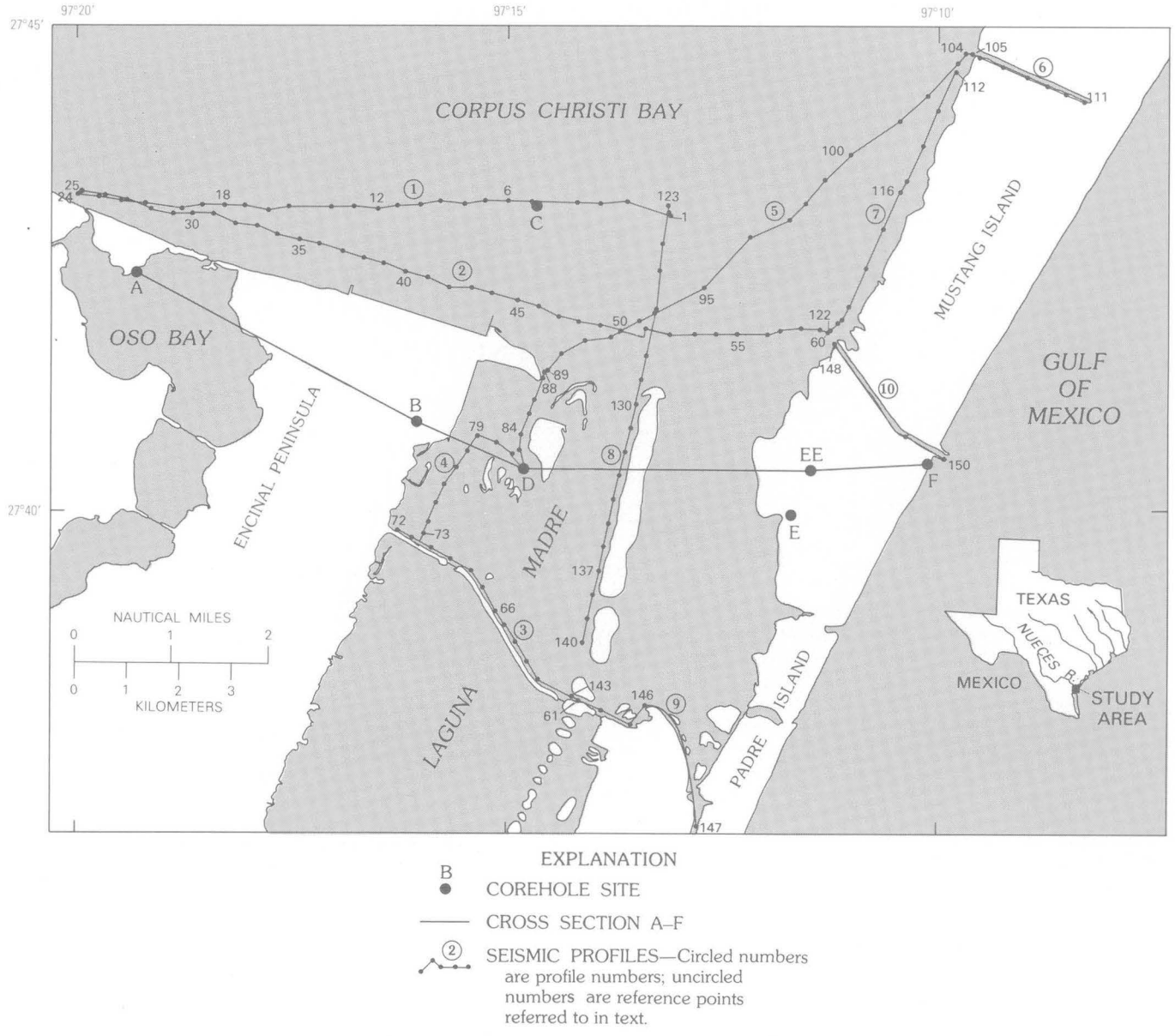

FIGURE 1.—Map of the southern Mustang Island-Corpus Christi Bay study area on the South Texas Gulf Coast showing the locations of the seismic-profile network, the coreholes, and the line along which the generalized stratigraphic cross section A–F was constructed.

Island–Corpus Christi Bay area has been mapped by the University of Texas Bureau of Economic Geology (Texas University Bureau of Economic Geology, 1975). The substrate of the bay and adjacent mainland consists of Pleistocene fluvial-deltaic deposits of the Beaumont Formation and underlying Lissie Formation. A separate barrier-island and beach facies of the Beaumont Formation has been mapped both north and south of the bay and is locally referred to as the Ingleside sand body. The Ingleside, which composes the Encinal Peninsula on the mainland, is a controversial facies in terms of age and origin (Price, 1933, 1958; Wilkinson and others, 1975a,b; Otvos, 1975). One objective of the present study was to further investigate the nature of the Pleistocene Ingleside facies and associated fluvial-deltaic deposits of the Beaumont Formation. Overlying the Pleistocene Beaumont Formation are Holocene deposits of modern Corpus Christi Bay, Oso Bay, Laguna Madre, and the Mustang Island–Padre Island barrier chain. Investigating the stratigraphic evolution of these Holocene coastal-zone features was another major objective of this study.

METHODS

SEISMIC TECHNIQUES

A high-resolution seismic-reflection survey was conducted of subaqueous parts of the study area; a Del Norte[1] minisparker system operating at a 175-joule power output was used. The seismic signals were broad-band filtered and recorded on magnetic tape. The seismic survey was conducted aboard small coastal vessels, and navigation was provided by a Motorola Mini-Ranger System III, resulting in a plotting accuracy of ±30 m. The survey resulted in the acquisition of about 70 km of seismic profiles (numbered 1–10) throughout southern Corpus Christi Bay and northern Laguna Madre and across Mustang Island (fig. 1). In the laboratory, the final seismic records were produced from magnetic-tape playback and were recorded at a 1/8-s sweep speed. In interpretations of the seismic profiles, depth relationships were based on an assumed average velocity of 1,700 m/s for both the sediments and overlying water column. Major reflector trends were delineated on the individual profiles (pls. 1, 2).

CORE ACQUISITION AND ANALYSIS

The seven cores (designated A, B, C, D, E, EE, and F) were taken from five subaerial and two subaqueous sites (fig. 1, table 1). Penetrated depths of individual coreholes range from a minimum of 10.75 m (corehole C) to a maximum of 62.0 m (corehole D); five of the coreholes exceed 60.0 m in depth. The drilling was done by a truck-mounted Failing 1500 drilling rig; at the subaqueous sites C and D, a spud barge was used as an operational platform for the drilling-rig truck and support vehicles. Continuous cores were obtained by use of a rotary-type modified Denison core barrel fitted with an acrylic core liner; the core barrel produced core segments having a diameter of 9.5 cm and a maximum length of 1.5 m. Average core recovery for the seven coreholes was 74 percent, resulting in a total acquisition of 247 m of core. After the completion of coring operations at each site, the corehole was conditioned and the following corehole logs were obtained: caliper, resistivity, gamma ray, and density logs. Field locations of all coreholes were determined by standard surveying techniques.

In the laboratory, the cores were longitudinally split in half and stored in capped water-tight D-tubing to retain their moisture content. One split of the cores was used for petrological, geochemical, and mineralogical analyses (Chaps. D and E, this volume). The other split of the cores was processed in the following manner.

TABLE 1.—*Locations and elevations of coreholes A–E, EE, and F*
[All coreholes are in Nueces County, Tex. MLW, mean low water]

Corehole	Location and elevation
A	At MLW on the Ward Island wind-tidal flat, lat 27°42′29″N., long 97°19′18″W., in Oso Creek NW Quadrangle.
B	3 m above MLW on the Corpus Christi Naval Air Station, lat 27°40′56″N., long 97°16′04″W., in Oso Creek NE Quadrangle.
C	In southeastern Corpus Christi Bay in a water depth of 4 m, lat 27°43′09″N., long 97°14′40″W., in Crane Islands NW Quadrangle.
D	In northern Laguna Madre in a water depth of 1 m, lat 27°40′27″N., long 97°14′49″W., in Crane Islands NW Quadrangle.
E	0.6 m above MLW on the wind-tidal flat of southern Mustang Island, lat 27°39′58″N., long 97°11′42″W., in Crane Islands NW Quadrangle.
EE	0.6 m above MLW on the wind-tidal flat of southern Mustang Island, lat 27°40′26″N., long 97°11′28″W., in Crane Islands NW Quadrangle.
F	1 m above MLW on the beach berm of southern Mustang Island, lat 27°40′30″N., long 97°10′05″W., in Crane Islands NW Quadrangle.

An X-radiograph (1:1) was made of each core to determine sedimentary structures and to estimate the amount of bioturbation. The cores and X-radiographs were then described megascopically. The color of wet sediment was compared to the standard Geological Society of America rock-color chart based on the Munsell system (Goddard and others, 1948).

After the cores were described, they were sampled for textural analyses; textural samples were obtained from each core segment and at each observable change in lithology. The textural samples were oxidized with hydrogen peroxide to remove organic matter, desalinized, and dispersed in a standard sodium hexametaphosphate solution (5 g/L). After dispersion, the samples were fractionated by wet sieving into gravel (>2 mm), sand (2 mm–63 μm), and mud (<63 μm) fractions. The gravel was mainly bioclastic material, primarily molluscan shell fragments; however, terrigenous quartz granules and pebbles also were present in a few of the samples. Because the gravel fraction was a very minor component, only its total weight percentage was determined; the gravel fraction was then excluded from further size analysis.

Grain-size distributions of the sand fractions were determined by means of a Rapid Sediment Analyzer settling tube (1 m long) and techniques described by Schlee (1966). Grain-size distributions of the mud fractions were determined electronically by a Coulter Counter (Model TA) and techniques described by

[1]Any use of trade names in this report is for descriptive purposes only and does not constitute endorsement by the U.S. Geological Survey.

Shideler (1976). Composite size-frequency distributions of the total nongravel fractions of the sediment were determined at a 0.5-ϕ interval ($\phi = -\log_2 D$, where D = diameter in millimeters), which provided the basis for the computer derivation of statistical grain-size parameters that include mean diameter and standard deviation (first and second moments) and modal diameter.

In addition to samples used for textural analyses, separate 10-g samples were analyzed to determine total carbonate content. The weighed samples were digested in 6*N* HCl, the insoluble residues were weighed, and the percentages of soluble carbonates were determined. Separate samples also were obtained for microfaunal analysis (Chap. C, this volume).

A total of 18 selected samples of wood and shell materials were analyzed by Beta Analytical, Inc., for radiocarbon dates and stable-isotope ratios ($^{13}C/^{12}C$, $^{18}O/^{16}O$). The stable-isotope ratios were used to correct the carbon-14 dates (table 2). Radiocarbon dates were calculated by using the Libby half-life of 5,568 years and 95 percent of the NBS (U.S. National Bureau of Standards) oxalic-acid activity as the modern standard; the errors are within one standard deviation. All B.P. (before present) dates are referenced to A.D. 1950. Stable carbon and oxygen were measured relative to the PDB–1 international standard, and the corrected ages were normalized to −25 ppt (parts per thousand). No corrections were made for reservoir effect.

In describing the sections penetrated by the seven coreholes (pls. 3–9), I used the relative proportions of sand, silt, and clay components and Shepard's (1954) sediment-classification system to differentiate discrete lithologic units; further differentiation of the sand units was based on their modal diameters. All size terminology is in accordance with the Udden-Wentworth grade scale (Wentworth, 1922). The lithology of nonrecovery zones was inferred from adjacent core segments

TABLE 2.—*Radiocarbon dates and stable-isotope ratios from core samples*
[All analyses by Beta Analytical, Inc. USGS, U.S. Geological Survey; B.P., before A.D. 1950; σ, standard deviation]

Core	Sample depth (meters)	Sample material	USGS sample number	Lab. number	^{14}C age (years B.P. ± 1σ)	$^{13}C/^{12}C$	$^{18}O/^{16}O$	Corrected ^{14}C age (years B.P. ± 1σ)
A	20.7	*Argopectin* shells	A–17–1A	Beta-2218	25,090 ± 670	− 5.18	− 2.23	25,410 ± 700
B	14.0	Indurated molluscan coquina bed.	B–10–1A	Beta-2219	28,930 ± 600	− 5.15	− 3.31	29,260 ± 630
B	29.8	*Crassostrea virginica* shell.	B–23–1A	Beta-2220	> 37,030	− 2.39	− 1.08	> 37,030
C	3.3	*Mercenaria* shell	C–4–1A	Beta-2222	4,055 ± 80	− 1.38	− 0.59	4,440 ± 90
D	29.2	*Crassostrea virginica* shell.	D–24–1A	Beta-2223	33,210 ± 850	− 2.55	− 2.59	33,580 ± 890
D	42.6	*Rangia cuneata* shells	D–37–1A	Beta-2224	32,330 ± 670	− 6.05	− 8.30	32,640 ± 700
D	44.2	Wood fragments	D–38–1A	Beta-2225	32,130 ± 880	− 27.50	--	32,090 ± 880
EE	4.0	*Chione cancellata* shells.	EE–4–1A	Beta-2187	1,110 ± 70	+ 0.36	− 0.30	1,520 ± 80
EE	12.3	*Chione cancellata* shells.	EE–10–1A	Beta-2188	910 ± 70	− 0.17	− 0.76	1,320 ± 80
EE	15.0	*Chione* and *Anadara* shells.	EE–13–1A	Beta-2189	1,130 ± 60	+ 0.21	− 0.84	1,580 ± 70
EE	18.8	*Macrocallista nimbosa* shells.	EE–16–1A	Beta-2190	8,080 ± 100	− 1.92	− 0.84	8,460 ± 110
EE	44.8	*Corbula* and *Rangia* shells.	EE–35–1A	Beta-2191	24,940 ± 650	− 1.37	− 1.46	25,330 ± 680
EE	60.5	*Crassostrea virginica* shell.	EE–49–1A	Beta-2192	34,520 ± 810	− 2.21	− 1.83	34,900 ± 850
F	8.5	*Argopectin, Donax,* and *Mulinia* shells.	F–6–1A	Beta-2193	4,200 ± 130	− 0.19	− 0.12	4,620 ± 130
F	14.5	*Anadara, Argopectin, Cardita, Donax, Mulinia,* and *Tellidora* shells.	F–11–1A	Beta-2194	6,050 ± 100	+ 0.15	− 0.02	6,460 ± 100
F	22.3	*Argopectin, Chione,* and *Mercenaria* shells.	F–17–1A	Beta-2195	6,240 ± 110	− 0.64	− 0.73	6,640 ± 120
F	34.0	*Crassostrea virginica* shell.	F–25–1A	Beta-2196	9,480 ± 100	− 3.26	+ 0.35	9,840 ± 110
F	51.8	Wood fragments	F–44–1A	Beta-2197	24,720 ± 1600	− 29.72	--	24,640 ± 1,580

and the corehole logs. Lithologic logs were prepared for each corehole, and individual lithologic units were numbered sequentially from oldest to youngest (pls. 3–9). Also included on the lithologic logs are observed sedimentary structures, estimates of the percentage of bioturbation, and the radiocarbon dates. Additional lithologic details, including sediment color, are described elsewhere (Shideler, 1982). In addition to lithologic logs, plates 3–9 show supplemental logs of the coreholes to illustrate variations with depth of the following parameters: central tendency measures (mean and modal diameters) of the nongravel fraction, sorting (standard deviation) of the nongravel fraction, and weight percentages of both carbonate material and gravel, which are relatively minor components.

SEISMIC STRATIGRAPHY

BASIC SEISMIC STRATIGRAPHY OF THE STUDY AREA

The seismic stratigraphy of the study area was investigated by using the approaches outlined by Mitchum and others (1977). In general, the late Quaternary stratigraphic section of the area can be characterized as a heterogeneous sequence of unconsolidated to poorly consolidated paralic deposits that have complex facies relationships. The section shows a great amount of fluvial channeling and truncation and a general absence of persistent reflectors throughout the area. The only correlatable reflector is a distinctive surface of seismic discontinuity, which is interpreted as the Pleistocene-Holocene unconformity formed during the late Wisconsinan lowering of sea level. This unconformity was delineated on the basis of its strong reflectivity, the termination of subjacent reflections attributed to the erosional truncation of underlying strata, and supplemental age and lithologic data from cores. The unconformity was used to separate the stratigraphic section into Pleistocene and Holocene seismic sequences; these two sequences and the intervening unconformity formed the basic stratigraphic framework of the area.

Within both the Pleistocene and Holocene seismic sequences, strong reflector trends were delineated to outline major structural features. In addition, a qualitative lithologic appraisal of seismic facies was made on the basis of reflector characteristics and local lithologic data from cores. Two distinct seismic facies were distinguishable within the study area: (1) a parallel- and subparallel-reflector facies characterized by strata that produce relatively strong parallel to subparallel reflections that have a high degree of continuity; and (2) a chaotic-reflector facies characterized by strata that produce relatively weak and incoherent discontinuous reflections. Lithologic data from core F indicate that the parallel- and subparallel-reflector facies represents a predominantly muddy lithosome, whereas the chaotic-reflector facies represents a predominantly sandy lithosome. Because the proportions of sand and mud are highly variable within the stratigraphic section, the distinctness of these two basic seismic facies varies throughout the area.

DISCUSSION OF SEISMIC PROFILES

In all, 10 high-resolution seismic profiles were obtained from the study area (fig. 1). These profiles are discussed individually and are shown in plate 1 (profiles 1–5) and plate 2 (profiles 6–10).

Seismic profile 1.—Seismic profile 1 extends from geographic reference point 1 to 24 and trends obliquely to the southern shore of Corpus Christi Bay in water depths ranging from 1 to 4 m. The profile illustrates a Pleistocene-Holocene unconformity that is characterized as a highly irregular surface that ranges in depth from 6.5 to 29 m below sea level. Conspicuous channeling occurs at the eastern end of the area profiled between reference points 1 and 7, showing 20 m of local relief. This area comprises the flank of a major channel (points 1–4), a small interfluve (point 4), and a minor channel (points 4–7). Further westward, the thalweg of another minor channel occurs at point 15 and has a local relief of 11 m. The interfluve between the areas of channeling is a broad terrace (points 7–14) near the northern terminus of the Encinal Peninsula structure.

Below the unconformity, the Pleistocene sequence is characterized by reflectors that indicate older episodes of channeling that took place during deposition of the Beaumont and underlying Lissie Formations in a fluvial-deltaic complex. The Pleistocene sequence is composed of both the muddy parallel- and subparallel-reflector facies and the sandy chaotic-reflector facies; the latter is more widespread, indicating a predominantly sandy section. The muddy parallel- and subparallel-reflector facies is best developed at a depth of 25–35 m within the interval between points 12 and 20. The overall facies pattern within the interval between points 10 and 24 suggests a general upward increase in the proportion of muddy sediments composing the Pleistocene sequence.

The overlying Holocene sequence is characterized mainly by the muddy parallel- and subparallel-reflector facies. A conspicuous channel structure occurs within the interval between points 3 and 7; between points 2 and 3, it appears to truncate strata concordantly overlying the Pleistocene-Holocene unconformity. This relationship indicates that this particular channel was cut sometime during the Holocene transgression, thus suggesting a sea-level stillstand or minor regressive phase. The channel-fill deposit, in turn,

is truncated by a strong onlapping reflector, which may represent the termination of local fluvial-deltaic deposition and the probable inception of bay-estuarine sedimentation. Local lithologic information from core C, which sampled part of the Holocene sequence near point 5, indicates that the uppermost channel-fill deposit consists of muddy sand and sandy mud and that the overlying truncating reflector consists of a clean fine sand. A radiocarbon date of 4,440±90 years B.P. (table 2) was obtained from the upper part of the truncating sand reflector, indicating that the local transition from fluvial-deltaic deposition to bay-estuarine sedimentation took place during the late Holocene transgression.

Seismic profile 2.—Seismic profile 2 extends from reference point 25 to 60 and trends along the southern shore of Corpus Christi Bay and across the northern entrance to Laguna Madre; the water depths range from 1 to 4 m. The Pleistocene-Holocene unconformity ranges in depth from 6 to 32 m below sea level, increasing in depth toward Mustang Island. As on profile 1, the unconformity is shown as a highly irregular erosional surface characterized by deep channeling. A minor channel occurs between points 33 and 36. Further eastward (points 36–44), the unconformity is manifested as a broad terrace, which occurs adjacent to the subaqueous terminus of the Encinal Peninsula structure and which correlates with the terrace of profile 1. Eastward of the terrace, the erosional surface is characterized by a minor channel (points 45–50), an interfluve (points 50–52), and a major channel (points 52–60); the thalweg of the major channel occurs at a depth of 32 m (points 54–55).

The Pleistocene sequence below the unconformity contains evidence of older channel structures, which are most apparent between points 26 and 42. The sequence is composed predominantly of the sandy chaotic-reflector seismic facies. The muddy parallel- and subparallel-reflector facies is localized mainly in the upper half of the sequence between points 26 and 42 where channel structures are most apparent.

The overlying Holocene sequence is composed predominantly of the muddy parallel- and subparallel-reflector facies. A noticeable channel-fill deposit is present between points 44 and 50 and is truncated by a strong horizontal reflector. The truncating reflector correlates with a similar truncating reflector on profile 1 (at corehole C) and apparently reflects the local transition from fluvial-deltaic deposition to bay-estuarine sedimentation. The seismic shadow zones on the profile (points 38 and 55) are of unknown origin. However, the shadow zone at point 55 appears to be associated with an acoustic-velocity reduction, possibly indicating the local presence of organic matter or gaseous sediments.

Seismic profile 3.—Seismic profile 3 extends from reference point 61 to 72 along a dredged navigation channel in northern Laguna Madre; the channel is approximately 50 m wide, and water depths range from 1 to 4 m. The Pleistocene-Holocene unconformity is a nearly featureless surface that gently dips gulfward; depths below sea level range from 14.5 m at its eastern terminus to 15 m at the western terminus. The underlying Pleistocene sequence is obscured by numerous seismic shadow zones, which could result from the presence of organic matter, gaseous sediment, or disturbed dredge spoil. The only strong reflection is from a jagged, high-relief horizon between points 64 and 67, which ranges in depth from 36 to 57 m. The reflector appears to cause reverberations within the overlying sediment column (point 66), suggesting the presence of an extremely hard surface having unusually high reflectivity that could result from local concentrations of oyster-shell beds. Alternately, the reflector could be an artifact resulting from diffraction along the sides of the navigation channel or from some phenomenon associated with the seismic instrumentation. The lower Holocene sequence also is partially obscured by shadow zones and reverberations. The upper half of the sequence, however, appears to be composed of the muddy parallel- and subparallel-reflector facies.

Seismic profile 4.—Seismic profile 4 (reference points 73–88) trends parallel to the western shore of Laguna Madre and contains an offset segment that has been tied into corehole D; water depths along the profile range from 0.6 to 3.0 m. The Pleistocene-Holocene unconformity is relatively featureless along this largely strike-oriented section and occurs within a depth range of 14.5 to 15.5 m below sea level. The underlying Pleistocene sequence is composed of both the sandy chaotic-reflector facies and the muddy parallel- and subparallel-reflector facies in approximately equal proportions, indicating a lithologically heterogeneous section. This heterogeneity is substantiated by core D, which shows interbedded sand and mud layers throughout the sequence. The overlying Holocene sequence is composed of sand and silty sand at corehole D but appears to be somewhat variable along the length of the profile.

Seismic profile 5.—Seismic profile 5 (reference points 89–104) trends diagonally across the southeastern corner of Corpus Christi Bay between the Encinal Peninsula and Mustang Island in water depths that range from 1.0 to 4.0 m. The Pleistocene-Holocene unconformity is a highly irregular surface that ranges in depth from 13.5 to 28.0 m below sea level. The deepest segment occurs along the thalweg (points 94–95) of a major channel. This channel has 14 m of local relief and is strongly asymmetrical, having a steeper northeastern margin. Further northeast, the erosional surface

consists of an interfluve (points 95–97), followed by a relatively broad valley (points 97–104) in which local relief is 9 m.

Below the unconformity, the Pleistocene sequence has several reflectors that indicate older episodes of channeling within a fluvial-deltaic complex. Both the sandy chaotic-reflector facies and muddy parallel- and subparallel-reflector facies are present; the latter is dominant. The seismic-facies distribution shows some correlation with the paleotopography of the boundary unconformity. The channel areas on both ends of the profile are underlain mainly by muddy parallel- and subparallel-reflector facies. In contrast, the interfluve area (points 95–97) is underlain mainly by the chaotic-reflector facies, indicating a more resistant sandy substrate.

The overlying Holocene sequence reflects multiple episodes of channeling; sequential channel structures are most apparent between points 99 and 104. This network of channels indicates a fluvial-deltaic complex and suggests that the Holocene transgression was not continuous but was associated with one or more sea-level stillstands or minor regressive phases. The uppermost channels are truncated by a persistent horizontal reflector at a depth of about 8 m, which correlates with similar truncating reflectors on profiles 1 and 2 and apparently represents the beginning of bay-estuarine deposition. The Holocene sequence is characterized mainly by the muddy parallel- and subparallel-reflector facies.

Seismic profile 6.—Profile 6 (reference points 105–111) is a dip section across most of the Mustang Island barrier. It was obtained along a dredged service-access channel in water depths of 1 to 1.5 m. The Pleistocene-Holocene unconformity dips gulfward beneath the barrier, and depths below sea level range from 15.5 m on the bayside to 26 m at a point approximately two-thirds of the way across the barrier. The underlying Pleistocene section is obscured by seismic shadow zones but appears to consist of both sandy chaotic-reflector and muddy parallel- and subparallel-reflector facies; the former is dominant in the upper part of the sequence, and the latter dominates the lower two-thirds of the sequence. The reflecting horizons, although obscured, seem to be concordant with the Pleistocene-Holocene unconformity. The overlying Holocene section, partially obscured by reverberations, appears to be composed mainly of the sandy chaotic-reflector facies.

Seismic profile 7.—Profile 7 (points 112-122) is a strike section oriented adjacent to the bayside margin of the Mustang Island barrier in water depths ranging from 0.6 to 2.5 m. The Pleistocene-Holocene unconformity is an irregular surface ranging in depth from 18 to 33 m below sea level. From north to south, the profile trends across a major channel (points 112–118). This channel shows maximum local relief of 15 m and is morphologically asymmetrical, having a steeper northern margin. Further southward (points 118–120), the unconformity is manifested as a flat interfluve.

The underlying Pleistocene sequence contains an older channel structure that is concordant with the channel along the Pleistocene-Holocene unconformity and has similar dimensions. This relationship indicates that a major fluvial channel was in the same approximate location during a substantial part of late Pleistocene time. The Pleistocene sequence is composed of both muddy parallel- and subparallel-reflector facies and sandy chaotic-reflector facies; the latter is somewhat more widespread.

Most of the overlying Holocene sequence is characterized by a network of cut-and-fill channel structures that indicates a fluvial-deltaic complex similar to that observed on profile 5. The uppermost persistent reflector, at a depth of about 13 m below sea level, appears to indicate the transition to bay-estuarine deposition during the latter part of the Holocene transgression. The section below this uppermost reflector is composed predominantly of the muddy parallel- and subparallel-reflector facies, whereas the section above the reflector is composed predominantly of the sandy chaotic-reflector facies. The upper sandy facies may have been deposited largely by overwash from an evolving Mustang Island barrier during late Holocene time.

Seismic profile 8.—Seismic profile 8 (points 123–140) is along a strike section in the middle of northern Laguna Madre, and it was obtained along the Intracoastal Waterway in water depths of 3.5 to 4 m. Here, the Pleistocene-Holocene erosional surface ranges in depth from 14 to 29 m below sea level. The greatest depths occur along the thalweg (points 123–126) of a major channel on the north end of the profile; the channel has a local relief of 14 m. The channel margin terminates near point 129, and further southward the unconformity is a relatively flat interfluve that underlies northern Laguna Madre. The underlying Pleistocene sequence suggests older episodes of channeling; channel structures are most apparent in the upper part of the section between points 131 and 138. Both the muddy parallel- and subparallel-reflector facies and the sandy chaotic-reflector facies are present in the Pleistocene sequence, and the latter appears to be dominant. The overlying Holocene section shows only minor evidence of internal channeling (points 124–125). Most reflectors are horizontal, and the sequence is composed almost entirely of the muddy parallel- and subparallel-reflector facies, suggesting bay-lagoonal deposits.

Seismic profile 9.—Profile 9 (points 143–147) is an oblique section across most of northern Padre Island. It was obtained along a former tidal inlet (Packery

Channel) in water depths between 0.6 and 3.6 m. The Pleistocene-Holocene unconformity is a relatively uniform surface that dips gulfward from 15 to 24 m below sea level. The underlying Pleistocene sequence is composed of strata that are largely concordant with the unconformity and show only minor evidence of channeling. The Pleistocene sequence is composed of both muddy parallel- and subparallel-reflector facies and sandy chaotic-reflector facies in approximately equal proportions, indicating a heterogeneous section. The overlying Holocene sequence contains mainly horizontal reflectors and is composed predominantly of the sandy chaotic-reflector facies. However, the parallel- and subparallel-reflector facies is locally present, especially in the lower part of the sequence near the gulfward end of the profile (points 146–147), suggesting the presence of a muddy lithosome beneath the barrier sand body.

Seismic profile 10.—Seismic profile 10 (points 148–150) is a dip section across the entire southern Mustang Island barrier. It was obtained along a dredged water-exchange pass in which water depths ranged from only 0.5 to 1.8 m. The Pleistocene-Holocene unconformity is an irregular surface having 13.5 m of relief and ranging in depth from 22 to 35.5 m below sea level; the surface is shallowest near point 149 and deepest at point 150 on the barrier's uppermost shoreface. An abrupt change in gradient occurs slightly shoreward of corehole F, apparently reflecting the descent from an interfluve into a channel.

The local correlation of lithologies with the acoustic signatures of specific seismic facies is well established on this profile because of detailed lithologic data from the adjacent corehole F, which penetrated most of the stratigraphic section. Core F contains an interval of Holocene homogeneous barrier sand from the surface to a core depth of 29 m; the acoustic signature of this interval is that of the chaotic-reflector facies. The barrier-sand interval is underlain by a mud interval from 29 to 36 m; this mud interval is composed of beds having varying proportions of silt and clay, and the associated acoustic signature is that of the parallel- and subparallel-reflector facies. The Pleistocene-Holocene unconformity occurs at the interface between an underlying bed of clayey silt that contains calcareous nodules and a thin overlying bed of fine sand. Subjacent to the unconformity, the upper Pleistocene sequence consists of a thin interval of interbedded sand and mud (parallel- and subparallel-reflector signature) to a depth of 39 m. Below this interval is a predominantly sandy interval (chaotic-reflector signature) to a depth of 48 m. From 48 to 52 m is a muddy interval (parallel- and subparallel-reflector signature), overlying another sandy interval (chaotic-reflector signature), which extends to a depth of 59 m. The local correlation of lithologies from core F with seismic signatures on profile 10 served as the basis for qualitatively establishing the chaotic-reflector facies as a predominantly sandy lithosome and the parallel- and subparallel-reflector facies as a predominantly muddy lithosome.

LATE PLEISTOCENE PALEOTOPOGRAPHY

The seismic profiles, in conjunction with supplemental depth information from the seven cores, were used to construct a paleotopographic contour map of the Pleistocene-Holocene unconformity (fig. 2). The paleotopographic surface mainly reflects pre-Holocene topography near the end of the Wisconsin glacial period (≈18,000 years ago), when sea level in the Gulf of Mexico was about 100 to 140 m (Curray, 1960) below present sea level, and the Gulf of Mexico shoreline was approximately 90 km seaward of its present position. During the late Wisconsinan regression, the study area was a coastal plain that experienced a major erosional episode, which resulted in the extensive dissection of older fluvial-deltaic deposits of the Beaumont Formation by the ancestral Nueces River system. Aside from some minor subsidence effects, the observed paleotopography is largely the upper erosional surface of the Beaumont Formation.

The erosional surface throughout the study area ranges from about 4.5 m above sea level along the Encinal Peninsula and Oso Bay margin, where Pleistocene deposits are subaerially exposed, to 35.5 m below sea level beneath southern Mustang Island. The erosional surface has several paleotopographic features, the most conspicuous of which are the incised valleys of the ancestral Nueces River system that dissected the area. The widest valley is beneath southern Mustang Island between the water-exchange pass and the service-access channel. This broad valley trends southeasterly, and its northern margin is steeper than the southern margin; it is interpreted as the main trunk-stream valley of the ancestral Nueces River system. Seismic coverage of the remainder of Corpus Christi Bay shows that this trunk-stream valley can be traced upstream toward the head of the bay (Wright, 1980), where it divides into two tributary valleys.

The trunk valley is bordered on the south by a prominent interfluvial ridge that results in about 13 m of local relief. The interfluve separates the trunk valley from a conspicuous tributary valley to the southwest, which trends southeasterly and is approximately parallel to the trunk valley. This tributary valley is relatively steep walled and well delineated; it crosses beneath Mustang Island just southwest of the water-exchange pass and joins the trunk valley on the present Continental Shelf. A seismic survey of post-Wisconsinan deposits on the adjacent Inner

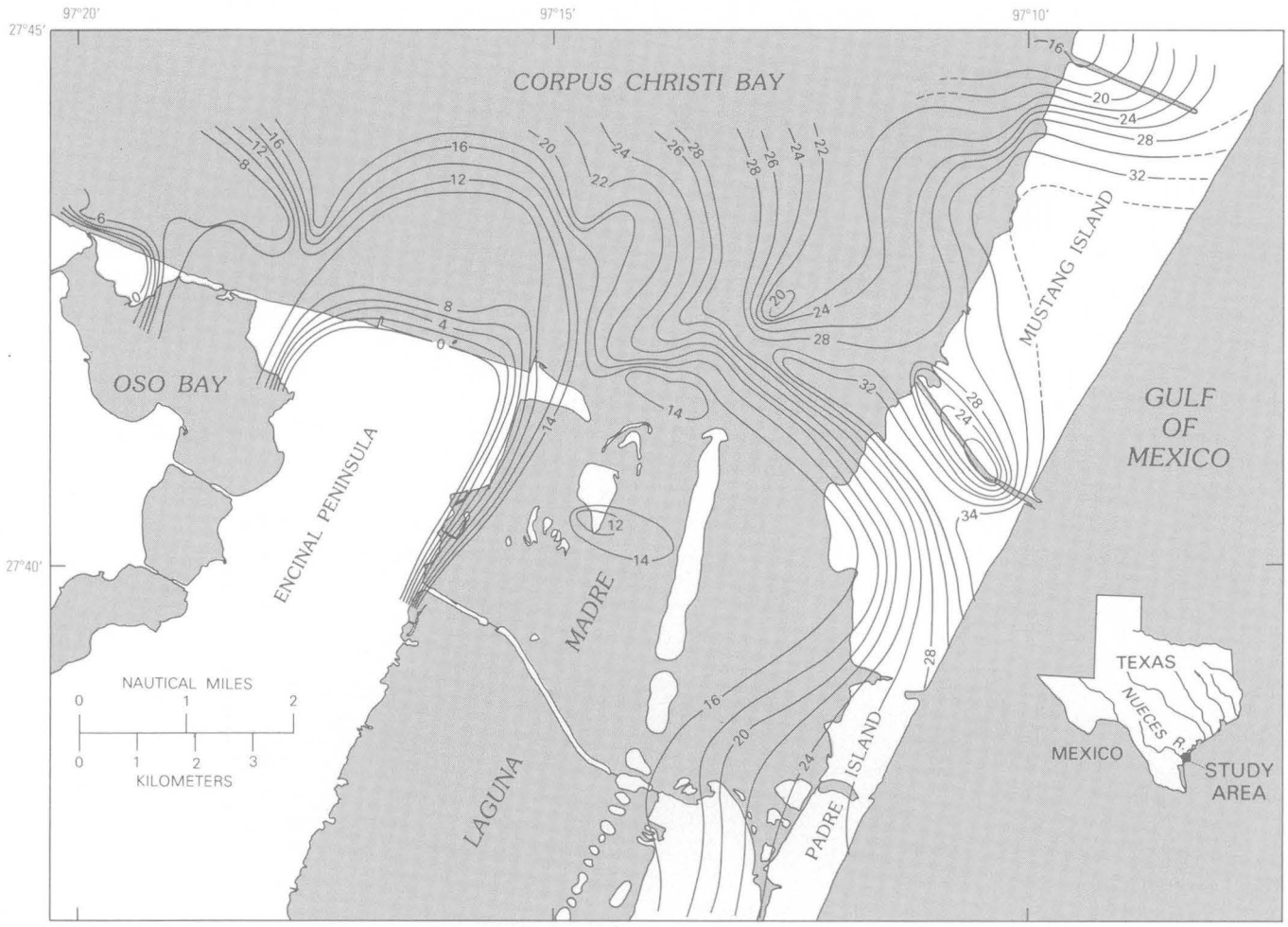

FIGURE 2.—Paleotopographic map of the southern Mustang Island–Corpus Christi Bay study area. Contours show depth to the Pleistocene-Holocene unconformity. Datum is sea level, and contour interval is 2 m.

Continental Shelf (Berryhill and Trippet, 1981) indicates the presence of both valleys. They appear to join approximately 10 to 15 km gulfward of the present shoreline. A paleogeographic reconstruction based on seismic data for the Continental Shelf adjacent to Corpus Christi Bay (Berryhill, 1981) further suggests that this valley system continues to trend southeasterly across the shelf to a distance of approximately 35 km from the present shoreline, where it then merges with another major valley and becomes reoriented into a southwest-flowing, coast-parallel drainage system.

In the study area, the major southeast-trending tributary valley is joined by two smaller secondary tributary valleys from the southwest. One of the secondary valleys emanates from Oso Bay; it was formed by the ancestral Oso Creek, the precursor of modern Oso Bay. The other secondary tributary valley emanates from along the lagoonal margin of the Encinal Peninsula. The orientation of both secondary tributary valleys relative to the Encinal Peninsula suggests that they were lithologically controlled subsequent valleys; the streams may have been localized in more easily eroded soft muddy deposits of the Beaumont Formation along the flanks of the more resistant Ingleside sand body that composes the Encinal Peninsula. A conspicuous terrace occurs along the northern terminus of the peninsula at a depth of 10 m below sea level. The terrace may have resulted from wave planation along the sandy peninsula during the Holocene transgression.

In addition to the valleys of the ancestral Nueces River system, the erosional surface also includes a low-gradient, interfluve area that dips gulfward beneath the northernmost part of Laguna Madre; the average gradient is approximately 0.36 m/km, which is close to the measured slope range of the subaerial Beaumont deltaic plain in the Corpus Christi region (Aronow, 1971). Along the lagoon-barrier margin, the low-gradient interfluve develops into a steeper gradient

homocline that dips gulfward beneath northern Padre Island; the average homoclinal gradient is 5 m/km, which probably reflects a combination of initial paleoslope and subsidence effects.

In general, the Pleistocene-Holocene unconformity in the study area is a highly dissected erosional surface. A cross section across northern Padre Island (prepared by Hunter and Dickinson, 1970) indicates that a short distance south of the study area, the Pleistocene-Holocene boundary is manifested as an undissected interfluve surface that occurs at a relatively uniform depth of about 19 m. However, Fisk (1959) indicated that still further southward, near central Padre Island (south of Baffin Bay), the Pleistocene-Holocene boundary beneath Laguna Madre and Padre Island is a highly channeled surface, similar to that underlying the present study area. Consequently, the nature of the Pleistocene-Holocene unconformity along the Mustang Island–Padre Island barrier chain is highly variable, and it depends upon the barrier's location relative to the position of coastal-plain fluvial systems during the late Wisconsinan lowstand of sea level.

HOLOCENE SEDIMENT DISTRIBUTION

The thickness distribution of Holocene deposits overlying the late Pleistocene erosional surface is illustrated by an isopach map prepared from the seismic profiles and cores (fig. 3). Holocene deposits attain a maximum thickness of 36.5 m at the shoreline of southern Mustang Island just south of the water-exchange pass. They are absent from most of the mainland areas (Encinal Peninsula and Oso Bay margin) where the Pleistocene Beaumont Formation crops out.

A comparison of Holocene sediment thickness with the paleotopographic contour map (fig. 2) of the Pleistocene-Holocene unconformity demonstrates a strong correlation, which indicates that Holocene

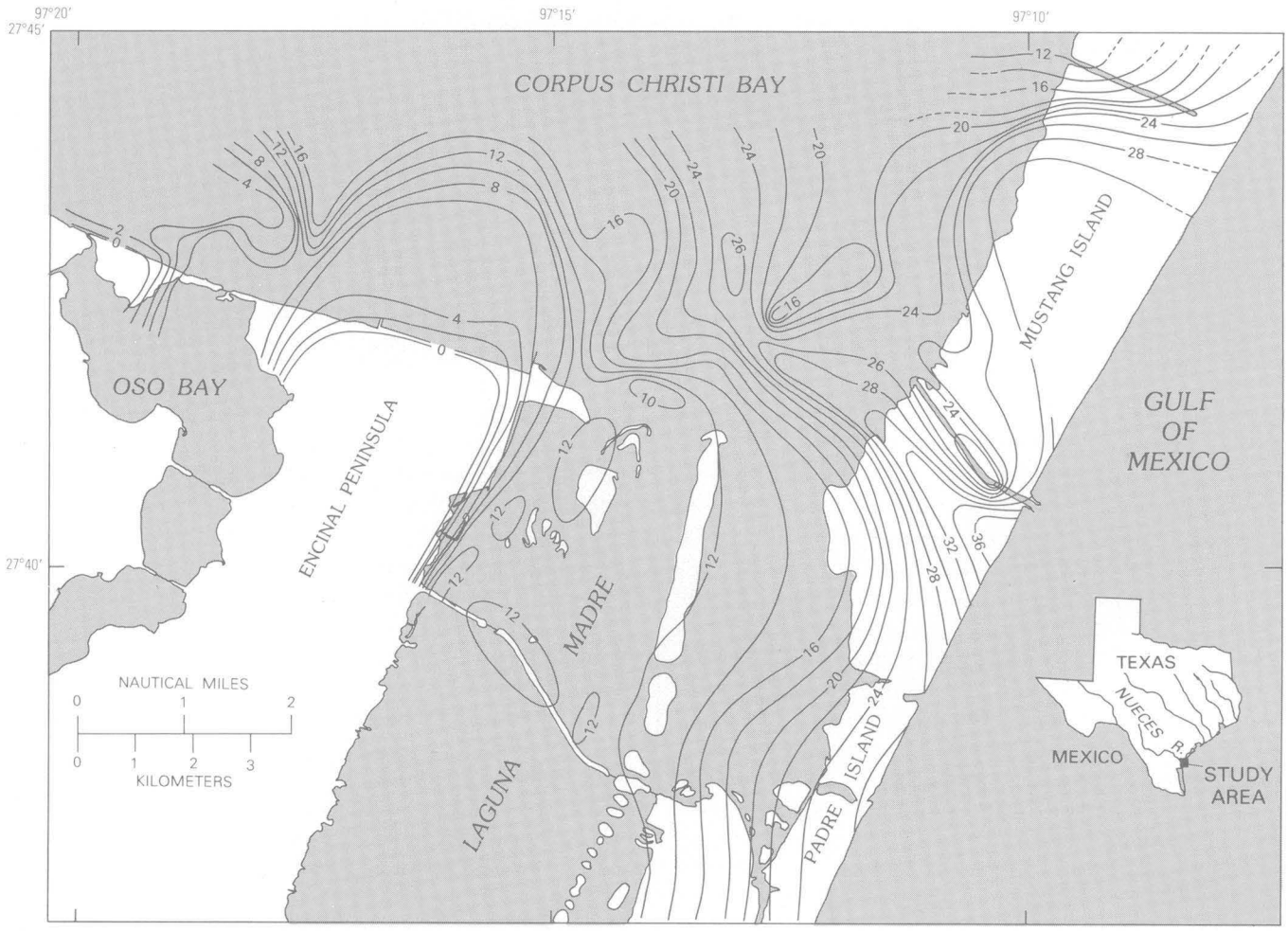

FIGURE 3.—Isopach map of the southern Mustang Island–Corpus Christi Bay study area showing the thickness of Holocene deposits. Contour interval is 2 m.

sedimentation was controlled mainly by late Pleistocene paleotopography. The thickest deposits occur within the incised valleys of the ancestral Nueces River system; the greatest thicknesses are within the trunk-stream valley and the adjacent major tributary valley. These valley-fill deposits most likely began accumulating during the early phases of the Holocene transgression when the rise in base level was sufficient to cause stream aggradation and valley filling. Consequently, the basal units of the trunk and tributary valley-fill deposits probably represent the oldest Holocene sediments within the area. In addition, the valley-fill deposits probably represent the most complete transgressive sequences accumulated during the Holocene because the adjacent interfluvial areas were still being eroded during the earlier phases of rising sea level.

In contrast to the valleys, the interfluvial areas are the sites of relatively thin Holocene deposits. These topographically higher areas were undergoing erosion during a greater part of Holocene time and were not inundated by the sea until the latter stages of the transgression. As transgression continued and valleys were filled in, the topographic relief of the area eventually became subdued, and sedimentation began within the interfluvial areas. Consequently, the interfluves are the sites of thinner sediment accumulations. The interfluvial sections also are probably less complete and consist mainly of younger Holocene deposits that accumulated during the latter stages of the Holocene transgression.

PHYSICAL STRATIGRAPHY

The stratigraphic sequences penetrated by the seven coreholes are illustrated in this report by lithologic logs and by supplementary logs of grain-size parameters (mode, mean, standard deviation) and of weight percentages of minor components (carbonate matter and gravel). The stratigraphic data presented in these logs (pls. 3–9), in conjunction with supportive seismic and radiocarbon-age data, as well as information on paleosalinities (Chap. C, this volume) and sand petrology (Chap. D, this volume), formed the basis for interpretations of sedimentary facies.

In the interpretation of paleoenvironments, the paleosalinity classification system presented by Cronin (Chap. C, this volume) was used. This system is based on ostracode death assemblages and consists of the following paleosalinity regimes: freshwater-fluvial (0 to 0.5 ppt), upper bay (> 0.5 to 5 ppt), mid-bay (> 5 to 18 ppt), lower bay-inlet (> 18 to 30 ppt), and sublittoral (> 30 to 36 ppt) regimes. Lithofacies and paleosalinity characteristics were used to infer sedimentary environments. In discussions of fluvial-deltaic depositional systems, the environmental terminology outlined by Coleman and Prior (1980) was used. The fluvial-deltaic system consists of the following gradational physiographic components, which are listed in the order they are encountered as one progresses downstream: (1) alluvial plain—the environment located upstream of the delta and characterized by exclusively riverine processes; (2) upper deltaic plain—subaerial delta environment located above the zone of significant tidal influence and dominated by riverine processes; (3) lower deltaic plain—subaerial delta environment located within the zone of tidal influence and characterized by the interaction of riverine and marine processes; and (4) subaqueous deltaic plain—submerged delta environment located seaward of the low-tide level and characterized by the interaction of riverine and marine processes (includes distributary-mouth-bar, delta-front, and prodelta subenvironments). Each of the foregoing physiographic components is characterized by a variety of depositional environments, as outlined by Coleman and Prior (1980). In relating these gradational components of a fluvial-deltaic system to paleosalinity regimes during the present study, the following associations were used: (1) the alluvial plain and upper deltaic plain were associated with freshwater-fluvial and upper bay regimes; (2) the lower deltaic plain was associated with mid-bay and lower bay-inlet regimes; and (3) the subaqueous deltaic plain was associated with lower bay-inlet and sublittoral marine regimes.

CORE A

LITHOSTRATIGRAPHY

Corehole A attained a depth of 61 m on the mainland, and it illustrates a heterogeneous stratigraphic section consisting of 38 lithologic units (fig. 1, pl. 3). In terms of composite thicknesses, sand units are dominant and compose 39 percent of the cored section. Next in abundance are silt units (30 percent), followed by clay units (19 percent), and then by mixed units composed of approximately equal proportions of sand, silt, and clay (12 percent). Primary bedding structures are mainly horizontal laminations, which are present in 32 percent of the section, and a few crossbeds (5 percent) present near the base of the section; no bedding structures are present in the remainder of the section. Other observed sedimentary structures include abundant calcareous nodules, occasional horizons of carbonaceous matter, and dispersed molluscan shell fragments. The degree of sediment bioturbation generally ranges from a trace to less than 30 percent throughout the section, except for uppermost unit 38, where modern plants and infauna have resulted in 30 to 60 percent bioturbation.

The grain-size measures of central tendency for the nongravel fraction show substantial variability. Modal diameters range from 1.60ϕ to 9.56ϕ, whereas mean diameters range from 1.77ϕ to 9.06ϕ. In terms of modal diameters, the section shows both short-period local variability, as well as longer period alternations of predominantly sandy intervals (units 1–6, 16–34) and predominantly muddy intervals (units 7–15, 35–38). The standard deviation values of the sediments range from 0.60ϕ to 3.12ϕ. The deposits range from moderately well sorted to very poorly sorted, and no sorting trend is apparent throughout the section. The carbonate content of the sediments ranges from 5.2 to 43.5 percent and shows no apparent trend. The content of gravel-size detritus (both shell fragments and inorganic clasts) within the sediments ranges from 0 to 33.1 percent but is generally less than 2 percent. The overall gravel content is relatively low and fairly consistent; it shows no apparent trend throughout the section.

The age of the section ranges from Pleistocene to Holocene. A single radiocarbon age of 25,410 ± 700 years B.P. was obtained at a core depth of 20.7 m (table 2). The Pleistocene-Holocene unconformity was established at a depth of 7.0 m, at the contact of the laminated, nodular, sand-silt-clay lithosome of unit 34 with the overlying structureless, silty-clay lithosome of unit 35. Evidence for an unconformable surface includes the first appearance of underlying calcareous nodules; sharp changes in lithology, structure, and color; and the presence of a strong seismic reflector at the same approximate depth on nearby profiles 1 and 2 (fig. 1, pl. 1), indicating a pronounced contrast in acoustic impedance. The penetrated Pleistocene section (units 1–34) is assigned to the Beaumont Formation and to the underlying Lissie Formation, thus implying a post-Aftonian age for the Pleistocene section. In the Corpus Christi Bay area, the average thickness of the Beaumont Formation is reported to be approximately 30 m and that of the Lissie Formation is approximately 60 m (Texas University Bureau of Economic Geology, 1975). Consequently, Pleistocene deposits below a core depth of about 37 m could represent units of the underlying Lissie Formation. However, no formal differentiation between the Beaumont and Lissie Formations was made during this study.

PALEOENVIRONMENTAL INTERPRETATION

The units within the cored Pleistocene section contain ostracode assemblages that reflect paleosalinities which range from freshwater to sublittoral conditions, thus indicating a wide spectrum of paleoenvironments. This section is interpreted as fluvial-deltaic deposits of the Beaumont and underlying Lissie Formations. The basal sandy interval (units 1–6) is barren of ostracodes except for an upper bay assemblage at its base (unit 1). The crossbedded fine- to medium-grained sands (units 3–5) within the interval have mainly fluvial petrologic characteristics indicative of a relatively high energy environment and are interpreted as channel-fill sands; the interval from unit 1 to unit 6 appears to reflect a lower alluvial-plain and upper deltaic-plain environment. The overlying muddy interval (units 7–15) contains ostracode assemblages ranging from freshwater to marine; brackish-water bay fauna are dominant. The predominance of well-laminated clays and the presence of carbonaceous matter indicate a marshy, low-energy interdistributary environment. The presence of a nearshore marine fauna at the top of the interval (unit 15) indicates a significant tidal influence, probably reflecting a lower deltaic-plain setting for the upper part of the interval; however, the remainder of the interval is more indicative of an upper deltaic plain. The entire interval from unit 1 to unit 15 appears to represent a transgressive sequence illustrating an environmental transition from a lower alluvial plain to a lower deltaic plain.

The interval from unit 16 to unit 26 shows a subsequent regressive phase back to nonmarine conditions, as evidenced by either the presence of freshwater ostracodes or the total absence of an ostracode fauna. These units may be largely overbank deposits of a lower alluvial-plain environment. From unit 26 to unit 31, the ostracode assemblages become progressively more marine; the sandy unit 31 contains a sublittoral assemblage, and it could represent a distributary-mouth bar deposit of a subaqueous deltaic plain. The interval from unit 26 to unit 31 appears to reflect a second transgressive sequence, indicating a transition from an alluvial-plain to a subaqueous deltaic-plain environment. The remainder of the Pleistocene section (units 32–34) contains a freshwater to upper bay ostracode fauna, indicating a regressive phase and the environmental transition back to a subaerial deltaic plain or lower alluvial plain. This regressive phase reflects the late Wisconsinan lowering of sea level.

The multiple transgressive and regressive sequences present within the fluvial-deltaic deposits of the Pleistocene section appear to be incomplete, having been partly obliterated by disconformities. However, at least two major transgressive phases and two regressive phases are indicated, which are attributed mainly to glacioeustatic fluctuations. However, the autocyclic nature of fluvial-deltaic depositional environments also could have contributed to the transgressive-regressive sequences. As noted by Coleman and Prior (1980), deltaic subsidence and the local shifting of distributaries and sites of sedimentation can result in frequent environmental transitions and the deposition of cyclic transgressive-regressive vertical sequences

within a deltaic complex. Consequently, the effects of this autocyclic process may have contributed to the observed environmental transitions.

The unconformably overlying Holocene section (units 35–38) is predominantly a structureless muddy section that becomes sandy toward the surface. Ostracode assemblages in unit 36 are representative of freshwater conditions, and those in unit 38 are representative of lower bay-inlet conditions. The section appears to be a transgressive fluvial-estuarine sequence; it reflects the progressive drowning of the Oso Creek tributary of the ancestral Nueces River system during the Holocene transgression that resulted in the formation of the present Corpus Christi Bay and Oso Bay estuaries.

CORE B

LITHOSTRATIGRAPHY

Corehole B, which attained a depth of 61.5 m, is located on the Encinal Peninsula of the mainland (fig. 1). The penetrated stratigraphic section is very heterogeneous, consisting of 57 lithologic units (pl. 4). The dominant lithology is sand, which constitutes 54 percent of the section. Next in abundance are silt units (20 percent), followed by units composed of sand, silt, and clay mixtures (12 percent), clay units (8 percent), and indurated sandstones and coquina units (6 percent). The only observed primary bedding structures are horizontal laminations, which are present in 31 percent of the section. Other observed structures are common calcareous nodules, molluscan shell layers, and occasional stringers of carbonaceous matter. Most of the section is characterized by only traces of sediment bioturbation, although a few horizons do show some pronounced effects.

Grain-size parameters for the nongravel fraction show substantial variability. Modal diameters range from -0.85ϕ to 9.67ϕ, and mean diameters range from 2.82ϕ to 8.61ϕ. These parameters show only local variations, and no trend is apparent throughout the section. The sediment standard-deviation values within the cored section range from 0.68ϕ to 3.2ϕ, indicating that the lithologic units range from moderately well sorted to very poorly sorted; no sorting trend is apparent throughout the section. The carbonate content of lithologic units ranges from 0.7 to 78.6 percent. The carbonate variations are mainly local, although there is some suggestion of a slight trend of increasing carbonate content with increasing core depth. The content of gravel-size detritus within the section ranges from 0 to 59.4 percent but is generally less than 2 percent. Except for a few local zones of high concentrations (largely shelly horizons), the gravel content is fairly constant throughout the section.

The cored section is entirely of Pleistocene age. A radiocarbon age of $29,260 \pm 630$ years B.P. was obtained at a core depth of 14 m; a second age of >37,030 years B.P. was obtained at a depth of 29.8 m (table 2). On the basis of reported local formational thicknesses, the penetrated section is assigned to the Beaumont Formation and to the underlying Lissie Formation, thus implying a post-Aftonian age for the section.

PALEOENVIRONMENTAL INTERPRETATION

The cored Pleistocene section contains ostracode faunal assemblages ranging from freshwater to sublittoral, and the section is interpreted as being composed of fluvial, deltaic, and barrier lithosomes. Most of the section (units 1–32) appears to represent a major transgressive sequence interrupted by minor regressive phases, as indicated by several environmental transitions. The basal interval (units 1–7) contains substantial carbonaceous matter and a freshwater to upper bay ostracode fauna, indicating a marshy lower alluvial plain or upper deltaic plain. The overlying interval (units 8–10) has mid-bay ostracodes, indicating a transgressive environmental transition to a lower deltaic plain, possibly representing an interdistributary bay deposit. Above this interval, the recurrence of freshwater to upper bay deposits (units 13–14) indicates a regressive transition back to a lower alluvial plain or upper deltaic plain. The overlying interval (units 15–32) contains a fauna indicating renewed transgression, and a transition back to a lower deltaic-plain environment, culminating with a sublittoral marine sand (unit 32). The unit 31–32 sandy interval may represent distributary-mouth bar deposits of a subaqueous deltaic plain.

Overlying the major transgressive sequence is a regressive sequence (units 33–49), as indicated by a transition from a marine fauna in underlying unit 32 to a freshwater fauna in unit 49. The sandy interval from unit 33 to unit 35 contains a lower bay-inlet fauna indicative of lower deltaic-plain environments, probably representing either distributary-channel-fill or crevasse-splay deposits. The interval from unit 36 to unit 49 contains a freshwater-upper bay fauna, common calcareous nodules, and some carbonaceous matter; a caliche-cemented sandstone (unit 48) having fluvial petrologic characteristics is also present. Collectively, these characteristics suggest a weathered alluvial plain or upper deltaic plain. All overlying deposits (units 50-57) are barren of ostracodes. However, the concretion-bearing sandy interval (units 50-54) appears to have affinities with underlying concretion-bearing deposits and is interpreted as the upper part of the regressive alluvial-plain and upper deltaic-plain assemblage.

The overlying interval (units 55-57) is interpreted as a second transgressive sequence. The uppermost sand deposit (unit 57) is a known surface exposure of the Pleistocene Ingleside sand body, a product of both marine and eolian processes. It has been mapped as a barrier island–beach facies of the Beaumont Formation (Texas University Bureau of Economic Geology, 1975). The Ingleside is locally 4.5 m thick and consists of homogeneous fine-grained sand that is petrologically similar to the modern barrier sands of Mustang Island. The exact age and origin of the Ingleside sand body have been a long-standing controversial issue. One hypothesis for its origin is that the Ingleside sand body formed as a transgressive offshore bar or barrier during the Sangamonian high stand of sea level, whereby it is interpreted as being essentially a late Pleistocene analog of the modern barrier-island system along the present Texas coast; this hypothesis was initially proposed by Price (1933) and has been accepted by many geologists. An alternate hypothesis has been proposed by Wilkinson and others (1975a), who interpreted the Ingleside as a regressive strandplain sheet sand that was deposited following the sea-level stillstand of the middle Wisconsin interstade. The present study supports a late Wisconsinan age for the Ingleside. Although this single core cannot conclusively resolve the origin controversy, the marine nature of the Ingleside (unit 57) indicates that the subjacent alluvial-plain and upper deltaic-plain complex must have been inundated. Consequently, the interval from unit 55 to unit 57 is interpreted as a transgressive sequence, although the upper part of the Ingleside may be partly composed of a nondistinguishable regressive sand member.

The Pleistocene section sampled by core B shows environmental transitions that indicate at least two major transgressive phases and a single major regressive phase, which are attributed to glacioeustatic fluctuations. In addition, minor regressive phases are indicated in the fluvial-deltaic deposits, resulting either from eustatic movements or from autocyclic processes associated with episodes of delta progradation.

CORE C

LITHOSTRATIGRAPHY

Corehole C was drilled in southeastern Corpus Christi Bay (fig. 1) and reached a depth of 10.5 m below the bay floor. The penetrated stratigraphic section consists of six lithologic units (pl. 5). The section is composed of sand units (56 percent), silt units (23 percent), and units composed of sand, silt, and clay mixtures (21 percent). The only primary bedding structures are horizontal laminations, which are present in 38 percent of the section. Dispersed molluscan shells are present mainly within the uppermost 3 m of sediment. Bioturbation also is most intense (>60 percent) within the uppermost 3 m, reflecting the effect of modern bay infauna; bioturbation is generally less than 30 percent at greater depths.

Grain-size parameters for the nongravel fraction show relatively minor variability. Modal diameters range from 2.63ϕ to 4.19ϕ; mean diameters range from 2.97ϕ to 5.92ϕ. No grain-size trends are apparent along the length of the core. Sediment standard-deviation values range from 0.65ϕ to 2.48ϕ, indicating moderately well sorted to very poorly sorted deposits; the best sorting occurs within a mid-depth fine sand (unit 4). The carbonate content of cored sediments ranges from 14.1 to 54.7 percent, and the highest content occurs within the uppermost bay-floor sediments (unit 6); carbonate percentages decrease to mid-depth, then increase again toward the base of the core. Gravel contents range from 0 to 9.6 percent; the highest content is in unit 4. However, they are consistently less than 1 percent throughout most of the core.

The cored section appears to be entirely of Holocene age. A single radiocarbon age of 4,440±90 years B.P. was obtained at a depth of 3.3 m (table 2). Corehole C is located along seismic profile 1 (pl. 1, fig. 1), which shows the base of the Holocene occurring locally at a depth of approximately 20 m.

PALEOENVIRONMENTAL INTERPRETATION

Corehole C is located along the margin of a buried tributary channel of the Pleistocene ancestral Nueces River system. The seismic stratigraphy at the site (profile 1, pl. 1) indicates that units 1–3 constitute the upper part of a channel-fill deposit, which is truncated by an onlapping deposit consisting of units 4–6. The penetrated Holocene section contains an ostracode fauna reflecting salinities that range from those typical of mid-bay environments to those typical of sublittoral environments. The section is interpreted as a transgressive sequence deposited during the drowning of present Corpus Christi Bay during approximately the last 10,000 years. The interval from unit 1 to unit 3 (upper channel-fill deposit) contains ostracodes that comprise a mid-bay fauna at the base and lower bay-inlet and sublittoral assemblages at the top of the interval, indicating the transition from a lower deltaic plain to a subaqueous deltaic plain. The onlapping interval (units 4–6) contains an ostracode fauna that progressively ranges from a sublittoral assemblage near the base (lower unit 4) to a mid-bay assemblage at the surface. This interval is interpreted as being a bay-estuarine facies; the basal fine sand (unit 4) probably represents, at least in part, subaqueous deltaic-plain deposits reworked during the transgression. The

interval appears to reflect the progressive restriction of Corpus Christi Bay, presumably by formation of the Mustang Island baymouth barrier during the latter stages of the Holocene transgression.

CORE D

LITHOSTRATIGRAPHY

Corehole D reached a depth of 62 m in northern Laguna Madre (fig. 1). The penetrated stratigraphic section consists of 63 lithologic units (pl. 6) and is the most heterogeneous section encountered among the seven coring sites. It is a predominantly sandy section; the composite thickness of sand units constitutes 63 percent of the total section. Second in abundance are silt units (22 percent), followed by units composed of mixed sand, silt, and clay (10 percent), clay units (3 percent), and indurated sandstone units (2 percent). Observed primary bedding structures are horizontal laminations, which are present in 28 percent of the section, and crossbedding, which is present in 14 percent of the section. The core also contains calcareous nodules, molluscan shell layers, and some carbonaceous matter. The degree of sediment bioturbation is pronounced in a few horizons; however, most of the section (81 percent) is characterized by only a trace of bioturbation.

Grain-size parameters for the nongravel fraction show that modal diameters range from 1.50ϕ to 9.62ϕ, and mean diameters range from 2.27ϕ to 8.36ϕ. Grain-size variations are local in nature and show no apparent trend along the length of the core. The standard-deviation values of the sediments range from 0.56ϕ to 3.53ϕ, indicating moderately well sorted to very poorly sorted deposits; no sorting trend is apparent throughout the section. The carbonate content of cored sediments ranges from 1.1 to 67.3 percent. The variations are of a local nature and show no apparent trend; the highest carbonate concentration is associated with a molluscan shell bed (unit 35). Gravel contents in the section range from 0 to 47.8 percent; the highest contents occur within molluscan shell beds in units 31–35. Except for a few local zones, the gravel content is relatively uniform throughout the section and is generally less than 3 percent.

The age of the cored section ranges from late Pleistocene to Holocene. Three radiocarbon ages were obtained (table 2): (1) 33,580±890 years B.P. at a 29.2-m depth; (2) 32,640±700 years B.P. at a 42.6-m depth; and (3) 32,090±880 years B.P. at a 44.2-m depth. These dates indicate a late Wisconsinan age for most of the Pleistocene section (units 1–53), which is assigned to the Beaumont Formation. However, the lower part of the section also could include some Sangamonian deposits of the underlying upper part of the Lissie Formation. The Pleistocene-Holocene unconformity was established at a depth of 10.8 m at the top of a nodular silty sand (unit 53) and the base of a relatively thick overlying shelly and laminated very fine sand (unit 54). Evidence for the erosional surface includes the first appearance of underlying calcareous nodules; sharp changes in lithology, structure, and color; and the presence of a strong seismic reflector at the same approximate depth, which is indicative of a pronounced acoustic-impedance contrast (see pl. 1, profile 4).

PALEOENVIRONMENTAL INTERPRETATION

The Pleistocene section (units 1–53) contains a spectrum of ostracode assemblages that represent freshwater to sublittoral marine conditions, reflecting fluvial-deltaic deposits of the Beaumont Formation. The interval from unit 1 to unit 37 represents a major transgressive sequence, possibly interrupted by minor regressive phases. Units 1–20 either contain a freshwater to upper bay ostracode fauna or are barren of ostracodes. This interval includes some fine- to medium-grained crossbedded sands that have fluvial petrologic characteristics (units 11–12), indicating relatively high energy channel-fill deposits. Some generally laminated carbonaceous muds (units 16, 18, 20) also are present and suggest low-energy, marshy floodplain or interdistributary deposits. The section from unit 1 to unit 20 appears to represent an alluvial-plain and upper deltaic-plain environment. The overlying interval from unit 21 to unit 36 contains an upper bay to mid-bay ostracode fauna and abundant oyster-shell layers, indicating the influence of marine waters and a transition toward a lower deltaic-plain environment. The upper part of the crossbedded sand unit 37 contains a sublittoral marine ostracode assemblage; this unit represents the culminating deposit of the transgressive sequence and probably formed as a distributary-mouth bar on a subaqueous deltaic plain. The overlying interval from unit 38 to unit 50 contains ostracodes that indicate a progressive reduction in salinity to upper bay conditions (unit 50), thus indicating a regressive transition back to an upper deltaic plain. Fauna in the remainder of the Pleistocene section (units 51–53) indicate increased saline conditions and a transgressive transition back to a lower deltaic-plain environment. The transgressive-regressive sequences of the Pleistocene section are attributed mainly to glacioeustatic fluctuations, although autocyclic deltaic processes may have had some minor influence.

The unconformably overlying Holocene section (units 54–63) is a sandy interval. It contains a basal sublittoral marine sand (unit 54), which is overlain by sands containing ostracodes that indicate decreasing salinities to mid-bay conditions (surface unit 63). This

sequence appears to consist of transgressive shallow-marine and lagoonal deposits that reflect the progressive restriction of coastal water circulation by the formation of the Mustang Island–Padre Island barrier structure during the Holocene rise in sea level.

CORE E

LITHOSTRATIGRAPHY

Corehole E was drilled on the backbarrier wind-tidal flat of southern Mustang Island (fig. 1) to a depth of 19.5 m before being abandoned because of unfavorable onsite drilling conditions. The penetrated section consists of 14 lithologic units (pl. 7). It is a predominantly sandy section (82 percent), containing minor occurrences of silt units (10 percent) and mixtures of sand, silt, and clay (8 percent). Primary bedding structures consist of horizontal laminations, present in 55 percent of the section, and crossbedding, present in 13 percent of the section. Mollusk shells are dispersed throughout the section. Bioturbation effects are variable, ranging from a trace to more than 60 percent in some horizons.

Grain-size parameters for the nongravel fraction show that modal diameters range from 2.19ϕ to 6.55ϕ, and mean diameters range from 2.19ϕ to 7.4ϕ. Grain-size variations are local and show no trend along the core. Sediment standard-deviation values range from 0.49ϕ to 2.28ϕ, indicating that the sediment is well sorted to very poorly sorted; sorting variations are local and have no apparent trend. Carbonate contents in the cored sediments range from 1.5 to 57.6 percent. In addition to varying locally, the carbonate content appears to increase with increasing core depth; this trend is attributed to increasing shell concentrations toward the bottom of the corehole. Gravel contents in the section range from 0 to 18.6 percent. Although the gravel content is consistently minimal (<0.5 percent) within the upper 11.5 m of the section, a notable increase occurs at greater depths. Like the carbonate-content increase, the gravel increase with depth is attributed to an increase in bioclastic shell layers within the lower section.

The age of the penetrated section ranges from late Pleistocene to Holocene. The Pleistocene deposits represent the top of the Beaumont Formation. The Pleistocene-Holocene unconformity was established at a depth of 17.4 m at the top of a laminated clayey silt (unit 1) and the base of a shelly and commonly crossbedded fine sand (unit 2) that contains a basal shell-gravel layer. This contact was established on the basis of pronounced contrasts in lithology, structure, and color, as well as the stratigraphic sequence observed at the nearby corehole EE, which had some radiocarbon age control.

PALEOENVIRONMENTAL INTERPRETATION

No microfaunal analyses were performed on samples from this core. In general, the observed megafauna are mainly shallow-marine to brackish-water mollusks, which are largely fragmented and commonly occur in shell-gravel layers. In the absence of diagnostic ostracodes, paleoenvironmental interpretations are based heavily on physical attributes.

The Pleistocene clayey silt (unit 1) contains only a few undiagnostic shell fragments and is probably a deltaic-plain deposit of the Beaumont Formation. The unconformably overlying Holocene section is a transgressive sequence. The basal fine sand (unit 2) of the Holocene section is commonly crossbedded, is highly burrowed, and contains an abundance of shell fragments that commonly occur as discrete shell-gravel layers. These attributes indicate a high-energy current regime, and the unit is interpreted as a littoral to shallow-sublittoral transgressive marine facies. The overlying interval (units 3–14) is commonly laminated and appears to represent largely lower energy backbarrier lagoon-fill deposits formed during the subsequent development and slight landward migration of the Mustang Island barrier. The sands were probably emplaced through the landward transport of barrier sediments as flood-tidal deltas,washover fans, and onshore-wind deposits. The silty units within the interval (units 6, 11, 12, 13) may represent lagoonal-estuarine muds derived from mainland sources and deposited from suspension after periods of storm-surge flooding during barrier evolution.

CORE EE

LITHOSTRATIGRAPHY

Corehole EE was drilled on the backbarrier wind-tidal flat of southern Mustang Island (fig. 1) to a depth of 61.0 m. The cored section consists of 43 lithologic units (pl. 8). It is a predominantly sandy section, as the composite thickness of sand units represents 54 percent of the section. Next in abundance are clay units (31 percent), followed by silt units (10 percent) and mixtures of sand, silt, and clay (5 percent). Primary bedding structures are horizontal laminations and crossbedding, which are present, respectively, in 21 percent and 7 percent of the section. The core also contains common mollusk shells, occasional concretions, and horizons of carbonaceous matter. Bioturbation effects are present only in trace quantities throughout most (81 percent) of the section but do exceed 60 percent in a few local horizons.

The grain-size parameters for the nongravel fraction show that modal diameters range from -0.86ϕ to 10.03ϕ and mean diameters range from 1.62ϕ to 8.80ϕ.

The grain-size parameters show pronounced short-interval local variations, as well as relatively long interval variability. The latter indicates a threefold division of the section into predominantly coarse textured basal (units 1–9) and upper (units 33–43) sandy intervals and an intervening, predominantly fine textured, muddy interval (units 10–32). Sediment standard-deviation values range from 0.47ϕ to 3.63ϕ, indicating the presence of well-sorted to very poorly sorted deposits. In addition to local variations, there also appears to be a slight trend of a reduction in sorting with increasing core depth. The carbonate content of cored sediments ranges from 2.1 to 66.8 percent. Carbonate variations appear to be of a local nature and show no apparent trend; highest carbonate contents are closely associated with shelly horizons. Gravel contents range locally from 0 to 65 percent, although most of the section contains less than 1 percent gravel-size detritus. The horizons of high gravel content are directly correlated with horizons of high carbonate content, indicating that the gravel-size detritus is composed mainly of bioclastic shell fragments.

The age of the penetrated section ranges from late Pleistocene to Holocene. The Pleistocene-Holocene boundary was established at the top of a silty clay (unit 32) and the base of a silty sand (unit 33), at a depth of 22.8 m. The boundary was established on the basis of a significant change in the ostracode fauna, a major lithologic change from a predominantly muddy interval to an overlying sandy interval, and radiocarbon dates. Six radiocarbon dates were obtained from the core at the depths indicated (table 2): 1,520±80 years B.P. at 4.0 m; 1,320±80 years B.P. at 12.3 m; 1,580±70 years B.P. at 15.0 m; 8,460±110 years B.P. at 18.8 m; 25,330±680 years B.P. at 44.8 m; and 34,900±850 years B.P. at 60.5 m. These dates are internally consistent and indicate a Wisconsinan age for the cored Pleistocene section, which is assigned to the Beaumont Formation. The age of basal Holocene deposits within this coastal zone was considered to be approximately 10,000 years B.P.; thus, the deposits represent the latter half of the late Wisconsinan-Holocene transgression, which is generally considered to have been initiated approximately 18,000 years B.P. following the last glacial maximum.

PALEOENVIRONMENTAL INTERPRETATION

The Pleistocene section (units 1–32) contains ostracode assemblages reflecting freshwater to mid-bay conditions. The section appears to indicate a single major transgressive-regressive cycle, possibly interrupted by a few minor fluctuations. Units 1–13 are either barren of ostracodes or contain freshwater assemblages only. This interval contains a lower sequence of sands (units 1–8), which are commonly crossbedded and have fluvial petrologic characteristics. Some of the sand units are relatively coarse textured and contain terrigenous gravel clasts. These attributes indicate relatively high energy conditions characteristic of channel-fill deposits. The overlying interval (units 9–13) is predominantly muddy and contains abundant carbonaceous matter, indicating lower energy, marshy overbank deposits. The entire interval from unit 1 to unit 13 is interpreted as an alluvial-plain and upper deltaic-plain deposit. The overlying muddy interval (units 14–25) contains a mid-bay fauna, indicating a transgressive transition to a lower deltaic-plain environment. The succeeding interval (units 26–32) contains predominantly upper bay fauna, indicating a regressive transition back to an upper deltaic plain. This transgressive-regressive sequence is interpreted as being mainly the result of glacioeustatic fluctuations, although the potential presence of autocyclic deposits in fluvial-deltaic sequences must certainly be recognized.

The overlying Holocene section (units 33–43) is composed entirely of sand units that contain an ostracode fauna distinctively different from those in the subjacent units. Here, the ostracodes are entirely lower bay-inlet to sublittoral marine assemblages that are essentially the same as present-day assemblages. This Holocene section is a transgressive sequence that formed during the latter half of the late Wisconsin-Holocene transgression (last 10,000 years) and during the evolution of the Mustang Island barrier. Sublittoral ostracode assemblages indicative of relatively unrestricted marine circulation are present only within some units of the lower sequence (interval from unit 33 to unit 37), probably indicating initial inundation of this coastal area. The remaining interval (units 38–43) contains lower bay-inlet assemblages, apparently reflecting barrier formation and slightly more restricted water circulation. This upper interval, like that in core E, is interpreted as being mainly a backbarrier lagoon-fill deposit that formed during the development and slight landward migration of the Mustang Island barrier. Most of the sand was probably derived from the barrier beach and dune field and was transported landward as flood-tidal deltas, washover fans, and onshore-wind deposits.

CORE F

LITHOSTRATIGRAPHY

Corehole F penetrated to a depth of 61.25 m and was drilled on the beach berm of southern Mustang Island (fig. 1). The cored stratigraphic section consists of 42 lithologic units (pl. 9). It is predominantly sandy, and sand units represent 76 percent of the total section

thickness. Next in abundance are silt units (14 percent), clay units (6 percent), and mixtures of sand, silt, and clay (4 percent). Primary bedding structures are horizontal laminations and crossbedding, which are present, respectively, in 25 percent and 9 percent of the section. Bioturbation effects are minimal and are present in only trace amounts throughout 94 percent of the section.

Modal diameters of the nongravel fraction range from 1.51ϕ to 9.57ϕ, and mean diameters range from 1.42ϕ to 8.59ϕ. Grain size is very consistent from the boring surface to a depth of about 29 m, below which substantial local variability occurs; no overall trend is apparent throughout the section. Sediment standard-deviation values range from 0.49ϕ to 2.61ϕ, indicating the presence of well-sorted to very poorly sorted deposits. In addition to local variations, a trend exists of a reduction in sorting with increasing core depth. The carbonate content of the sediments ranges from 3.0 to 44.6 percent. The carbonate variations are local and show no apparent trend; high carbonate contents tend to be associated with concentrations of shell material. The gravel content of cored sediments ranges from 0 to 35.7 percent. Most of the section has a consistently small gravel content (<2 percent). The horizons of high gravel content are directly related to horizons of high carbonate content, indicating that bioclastic shell fragments are the main gravel component.

The cored section ranges in age from late Pleistocene to Holocene. The Pleistocene-Holocene unconformity was established at the top of a nodular clayey silt (unit 25) and at the base of an overlying structureless fine sand (unit 26), at a depth of 36.5 m. Evidence for this unconformity includes the first appearance of underlying calcareous nodules, changes in lithology and color, a strong seismic reflector (high acoustic-impedance contrast) along nearby profile 10 (pl. 2, fig. 1) at almost the same depth as the changes observed in the corehole, and radiocarbon dates. Five dates were obtained from this core at the following depths (table 2): 4,620±130 years B.P. at 8.5 m; 6,460±100 years B.P. at 14.5 m; 6,640±120 years B.P. at 22.3 m; 9,840±110 years B.P. at 34.0 m; and 24,640±1,580 years B.P. at 51.8 m. The dates are internally consistent and indicate a Wisconsinan age for the Pleistocene section, which is assigned to the Beaumont Formation. The age of overlying basal Holocene deposits is established at about 10,000 years B.P., indicating a relatively thick local Holocene section.

PALEOENVIRONMENTAL INTERPRETATION

Corehole F is in an area that has been deeply eroded by channels of the ancestral Nueces River system; consequently, Pleistocene deposits were penetrated at a greater depth than at all other coreholes in this study. The basal part of the Pleistocene section (units 1–3) contains a mid-bay to lower bay ostracode fauna, suggesting a lower deltaic-plain environment. The remainder of the Pleistocene section (units 4–25) is barren of ostracodes except for the upper part (unit 24), which contains a freshwater assemblage. This interval contains an abundance of relatively coarse textured sand units, several of which contain admixtures of terrigenous gravel clasts; the sands also are commonly crossbedded. Petrologic studies were conducted on most sand units within this interval, and all were found to have fluvial characteristics. Collectively, these attributes indicate that the sands are mainly high-energy channel-fill deposits; some lower energy marshy overbank deposits also are indicated by the presence of carbonaceous muds (units 10, 11). The entire interval from unit 4 to unit 25 appears to represent upper deltaic-plain deposits toward the base, grading upward into higher energy alluvial-plain deposits. This interpretation is supported by the upward coarsening of sand units, which indicates a transition from relatively low gradient deltaic distributaries to higher gradient streams of an alluvial-plain environment. The association of similar changes in sand texture with alluvial-deltaic environmental transitions has been commonly observed in Quaternary deposits of the Gulf Coast (Bernard and LeBlanc, 1965). The Pleistocene section, therefore, is inferred to be a major regressive sequence, apparently deposited during a lowering of sea level that followed the mid-Wisconsin interstade.

The overlying Holocene deposits (units 26–42) at this corehole site were formed within a deeply channeled area of the Pleistocene substrate; consequently, this boring shows the thickest and most complete Holocene section observed among the seven coreholes. Thus, the section provides the most complete local documentation of the Holocene transgression. The lower part of the section (units 26–33) is a predominantly laminated muddy interval above a thin basal sand. This interval contains ostracode assemblages that show a progressive upward increase in salinity; a freshwater assemblage is near the base of the interval, and a lower bay-inlet assemblage is near the top. In addition, the radiocarbon date of 9,840 ± 110 years B.P. was obtained from an oyster shell (*Crassostrea virginica*) contained within unit 29 (table 2, pl. 9). These attributes indicate that the interval from unit 26 to unit 33 represents a transgressive fluvial-estuarine-lagoonal deposit that formed along the route of a major tributary channel during the drowning of the ancestral Nueces River system. The lower part of the interval (units 26–29) contains a fauna indicating upward-increasing salinities within the range from 0 to 18 ppt, thus reflecting a transition from a fluvial to an estuarine

environment. However, the upper part of the interval reflects higher salinities (18–30 ppt) and has a higher sand content, possibly indicating a transgressive phase characterized by more extensive inundation and the incipient development of a barrier-lagoonal system.

The remaining Holocene section (units 34–42) that overlies the basal fluvial-estuarine-lagoonal assemblage is a thick and fairly homogeneous sand sequence. The sands contain some zones of crossbedding and some shell-gravel layers. Petrologic studies of most sand units within this interval indicate that they are all petrologically similar to modern Mustang Island barrier-beach sands and that they are very distinct from the underlying Pleistocene fluvial sands. The basal part of the interval (units 34–37) contains an ostracode fauna indicating mid-bay–inlet salinities (5–30 ppt). These basal sand units appear to be back-barrier lagoon-fill deposits that resulted from the landward transport of barrier sand by wind, overwash, and tidal processes; the sands reflect the early growth and landward migration of the primordial Mustang Island barrier, which originated somewhat seaward of corehole F. In origin, these basal sand deposits are probably similar to the younger Holocene lagoon-fill sands within the upper parts of cores E and EE; however, the basal sands were deposited at a much earlier stage of barrier and lagoonal evolution approximately 8,500 years ago. The remaining Holocene sands (units 38–42) contain almost entirely sublittoral (30–36 ppt) marine ostracodes; the only exceptions are a few horizons bearing lower bay-inlet (18–30 ppt) ostracodes. This thick sand interval is a barrier-beach and dune assemblage that originated through the continued vertical accretion and concurrent landward retrogression of the Mustang Island barrier during the latter stages of the Holocene transgression.

SUMMARY DISCUSSION

STRATIGRAPHIC FRAMEWORK

The seismic profiles and continuous cores from this study illustrate that the late Quaternary stratigraphy of the Corpus Christi coastal zone is characterized by highly complex vertical and lateral facies relationships. Lithologically, the observed stratigraphic section is an extremely heterogeneous sequence of unconsolidated to poorly consolidated clastic deposits consisting mainly of alternating sand and mud lithosomes. Structurally, the stratigraphic section is characterized by evidence of multiple episodes of stream channeling and valley infilling. Paleoenvironmental transitions indicate multiple transgressions and regressions resulting primarily from glacioeustatic movements and possibly showing some secondary effects from autocyclic processes. The resulting section is characterized by a general absence of persistent horizons for correlation. The only correlative horizon throughout the area is the Pleistocene-Holocene unconformity, which is locally manifested as a highly dissected erosional surface having a maximum relief of approximately 36 m.

As noted by Beard and others (1982), the Pleistocene marine depositional record within the Gulf of Mexico contains eight eustatic cycles that closely correlate with the nonmarine midcontinent glacial-interglacial record. Consequently, the conceptual usage of midcontinent chronostratigraphic terminology for Pleistocene deposits of the Texas Gulf Coast appears to be justified. Within the present study area, the age of the studied stratigraphic section ranges from Pleistocene (post-Aftonian) to Holocene.

The chronostratigraphic framework of the study area was based upon 18 radiocarbon dates (table 2) and upon the recognition of the Pleistocene-Holocene unconformity in cores and seismic profiles. As noted by Thom (1973), the older finite radiocarbon dates (>20,000 years B.P.) based on shell materials must be viewed cautiously because of possible contamination effects from younger carbon that could have resulted in erroneously young dates for the Pleistocene section. Although the possibility of contamination does exist, the Pleistocene dates are believed to be essentially valid for the following reasons: (1) substantial care was taken during sample processing, including a surface acid leach, to avoid contamination by younger carbon; (2) the dates (corrected by stable-isotope ratios) are based on both wood fragments and a variety of mollusk shells and are internally consistent along individual cores, and (3) the dates are compatible with the known stratigraphic framework. Consequently, with no evidence to the contrary, the dates are presently accepted as valid, and the bulk of the studied Pleistocene section is tentatively assigned a Wisconsinan age. However, no age information is available for the lower part of the mainland sections (cores A and B), which probably contains older Pleistocene deposits of post-Aftonian age. More extensive future dating of the local section may refine the time-stratigraphic framework established in the present study.

The stratigraphic evolution of the Corpus Christi coastal area was controlled mainly by late Quaternary glacioeustatic changes that resulted in multiple transgressive-regressive episodes. Paleoenvironmental analyses indicate that the local sea-level fluctuations resulted in complex facies relationships that reflect transitions among alluvial-plain, upper and lower deltaic-plain, subaqueous deltaic-plain, barrier-strandplain, and estuarine-lagoonal environments. The stratigraphic history and facies relationships of

the study area are illustrated in a generalized summary cross section (fig. 4).

PLEISTOCENE HISTORY

The Pleistocene history of the area appears to encompass at least two major glacioeustatic transgressions and two regressions. However, several abrupt paleoenvironmental transitions, as well as pronounced channeling and truncation throughout the section, indicate that a substantial amount of the stratigraphic record has been destroyed by erosion. Consequently, evidence for other transgressive-regressive sequences may have been obliterated, and the present stratigraphic record may reflect only partial sequences. In addition, the stratigraphic record is further complicated by the fact that the bulk of the Pleistocene units were deposited in fluvial-deltaic environments where sedimentation often is strongly influenced by autocyclic processes. The actual contributions of autocyclic processes to the observed transgressive-regressive sequences are largely unknown, but they are assumed to be of a local nature and highly subordinate to the effects of glacioeustatic fluctuations.

The first transgression appears to have taken place more than 35,000 years ago, as indicated by the presence of paleoenvironmental sequences that range from freshwater to lower bay-inlet and sublittoral units within the older parts of the mainland sections (cores A and B). These sequences are inferred to represent deposits formed during the sea-level rise associated with the Sangamon interglacial stage. Vestiges of a subsequent regressive sequence are indicated by some paleoenvironmental transitions and by pronounced channeling, probably reflecting a lowering of sea level associated with the early Wisconsin glacial stage. A second transgressive sequence is indicated within the Pleistocene section (cores A, B, D) during the last 35,000 years; it probably was deposited during a sea-level rise associated with the mid-Wisconsin (Farmdalian) interstade.

The Ingleside barrier-strandplain sand body that now composes the Encinal Peninsula of the mainland may have begun forming locally during the latter part of the mid-Wisconsinan transgression when sea level was near its present position. It could have been manifested either as an offshore barrier island or as a mainland beach, depending upon local paleogradients. During the subsequent fall in sea level associated with the late Wisconsin glacial stage, the Ingleside sand body may have been partially reworked and extended gulfward as a regressive strandplain sheet sand. Consequently, the Ingleside may be a composite sand body that consists of both basal transgressive deposits and younger overlying regressive deposits. It could be somewhat analogous to the Holocene sand complex on the western coast of Mexico described by Curray and others (1969), where transgressive littoral sands are overlain by regressive littoral sands.

Nearby evidence for a mid-Wisconsinan interstadial high stand of sea level consists of radiocarbon dates from relict shoreline deposits on the Inner Continental Shelf approximately 100 nautical miles northeast of the present study area (Curray, 1960, 1961). Dates of 26,900±1,800 years B.P. and 32,500±3,500 years B.P. were obtained from specimens (*Crassostrea virginica* and *Rangia cuneata*) incorporated in a beachrock-coquina at a depth of 14 m. On the basis of these dates, Curray (1960, 1961) concluded that an interstadial beachline occurred at this depth approximately 30,000 years ago. This time framework would be compatible with the age of the Ingleside sand body determined in the present study. If one allows for minor continued transgression, the Ingleside beach could represent the interstadial high stand of sea level that existed approximately 25,000 years ago. Additional evidence for a mid-Wisconsinan high stand of sea level in the Gulf Coast about 25,000 years ago was presented by Beard and others (1982), who described Pleistocene eustatic cycles indicated in the marine depositional record of the Gulf of Mexico.

During the subsequent late Wisconsinan regression, the Ingleside structure and subjacent Beaumont fluvial-deltaic plain were highly dissected by streams of the ancestral Nueces River system (which flowed to the southeast beneath the present southern Mustang Island), and the dissection resulted in an erosional surface of considerable relief. At the end of late Wisconsin glaciation (Woodfordian substage) approximately 18,000 to 20,000 years ago, sea level in the Gulf of Mexico may have been about 120 m below present mean sea level (Curray, 1960, 1961). If so, the paleoshoreline would have been approximately 45–50 nautical miles seaward of the present shoreline, and the study area would have been a coastal plain undergoing extensive weathering and erosion, resulting in the development of a prominent unconformity on the Beaumont Formation.

HOLOCENE HISTORY

The glacioeustatic late Wisconsinan-Holocene transgression began approximately 18,000 to 20,000 years ago after the Woodfordian glaciation. The Holocene history of the study area is recorded within a single major transgressive sequence, which also reflects either episodic stillstands of sea level or minor regressive phases. The Pleistocene-Holocene unconformity is

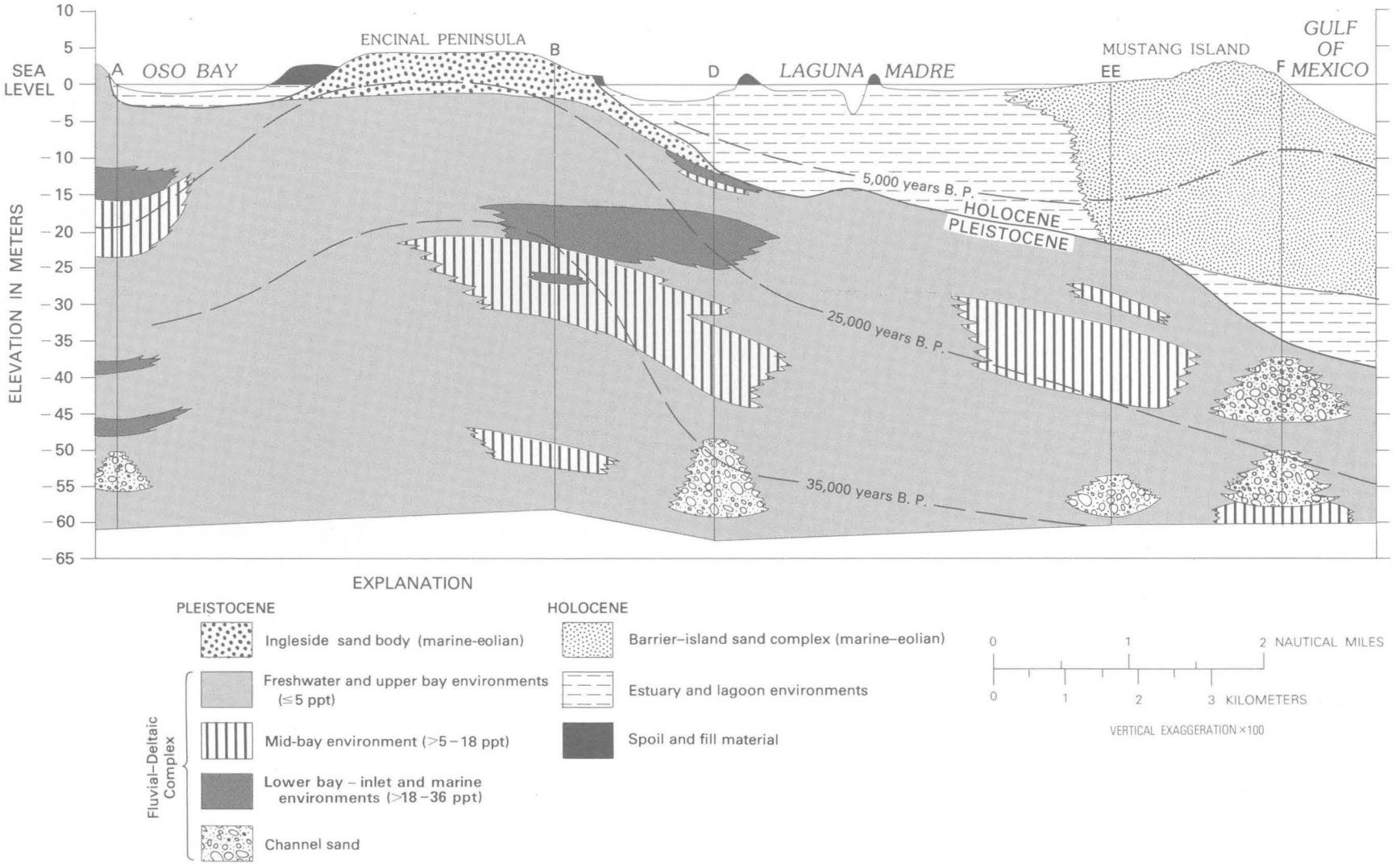

FIGURE 4.—Generalized summary stratigraphic cross section A–F showing facies relationships in the southern Mustang Island–Corpus Christi Bay study area (fig. 1). Isochrons are based on radiocarbon dates; see table 2 and plates 3, 4, 6, 8, and 9 for depths of dated samples.

a time-transgressive surface, reflecting a progressively longer hiatus in an onshore direction. In the study area, the most complete observed Holocene section was penetrated by corehole F at the southern Mustang Island shoreline (fig. 1). At this locality, the oldest Holocene deposits are about 10,000 years old and record the latter half of the late Wisconsinan-Holocene transgression when local sea level had reached approximately 35–40 m below its present position. In the present study, a date of 10,000 years B.P. is considered to be the Pleistocene-Holocene boundary; therefore, deposits penetrated by corehole F represent essentially all of Holocene time. The local evidence of multiple episodes of channel dissection and infilling by the ancestral Nueces River system indicates that the Holocene transgression was not continuous but included one or more sea-level stillstands or minor regressive phases. This situation would be compatible with Gulf of Mexico sea-level curves presented by Curray (1960), Nelson and Bray (1970), and Frazier (1974).

During the Holocene transgression, sedimentation was controlled largely by late Pleistocene paleotopography. The thickest Holocene deposits, which attain a maximum thickness of 36.5 m, accumulated within incised valleys of the ancestral Nueces River system; consequently, the valleys contain the oldest and most complete Holocene sections. In contrast, the topographically higher ancestral interfluve areas, which were not inundated by the sea until the latter stages of the transgression, received the thinnest and least complete Holocene sections.

The oldest observed basal Holocene deposits occur along the flank of a major tributary channel beneath southern Mustang Island at corehole F, and they represent a transgressive fluvial-estuarine facies deposited during the drowning of the ancestral Nueces River system. Somewhat older Holocene fluvial-estuarine deposits may be present within the deeper main trunk channel of the fluvial system just north of corehole F. The basal fluvial-estuarine facies in core F grades upward into lagoonal deposits, indicating progressive inundation and the formation of a primordial Mustang Island barrier, which was somewhat seaward of its present position and which partially restricted water circulation. As transgression continued, the barrier retrograded landward to its present location. The first accretion of barrier sand along the present Gulf of Mexico shoreline at corehole F began approximately 8,500 years ago when sea level was about 25–30 m below present mean sea level; the initial barrier sands were backbarrier lagoon-margin deposits formed when the primordial barrier was a short distance seaward of the present barrier. As sea level continued to rise during the latter stages of the Holocene transgression, vertical accretion and landward migration of the Mustang Island barrier resulted in the accumulation of a thick barrier-beach and dune sand complex. Barrier growth, in turn, caused the progressive restriction of Corpus Christi Bay and Laguna Madre, allowing the accumulation of backbarrier estuarine-lagoonal deposits.

Radiocarbon dates indicate that average barrier sedimentation rates during the past 5,000 years have been substantially higher in the backbarrier environment (0.33 cm/year at corehole EE) than in the barrier-beach environment (0.19 cm/year at corehole F). These differential rates indicate that the landward migration of Mustang Island has continued into modern time. Nearby evidence for the ongoing landward migration of the barrier can be seen on northern Padre Island a few kilometers south of the study area, where backbarrier dune fields are encroaching into Laguna Madre. Here, Padre Island has advanced westward into Laguna Madre an average of 213 m during the 1948–67 period alone (Hunter and Dickinson, 1970). Similar barrier migration and lagoon infilling caused by the landward transport of sand by wind, tides, and overwash processes appear to have taken place throughout much of the Holocene transgression, resulting in the Holocene stratigraphic relationships observed within the present study area.

REFERENCES CITED

Aronow, Saul, 1971, Nueces River delta plain of Pleistocene Beaumont Formation, Corpus Christi region, Texas: American Association of Petroleum Geologists Bulletin, v. 55, no. 8, p. 1231–1248.

Beard, J. H., Sangree, J. B., and Smith, L. A., 1982, Quaternary chronology, paleoclimate, depositional sequences, and eustatic cycles: American Association of Petroleum Geologists Bulletin, v. 66, no. 2, p. 158–169.

Bernard, H. A., and LeBlanc, R. J., 1965, Résumé of the Quaternary geology of the northwestern Gulf of Mexico province, *in* Wright, H. E., Jr., and Frey, D. G., eds., The Quaternary of the United States: Princeton, N. J., Princeton University Press, p. 137–185.

Berryhill, H. L., Jr., 1981, Map showing paleogeography of the continental shelf during the low stand of sea level, Wisconsin glaciation, Corpus Christi 1° × 2° quadrangle, Texas: U.S. Geological Survey Miscellaneous Investigations Map I–1287–E.

Berryhill, H. L., Jr., and Trippet, A. R., compilers, 1981, Map showing post-Wisconsin sedimentation patterns and faulting in the Corpus Christi 1° × 2° quadrangle, Texas: U.S. Geological Survey Miscellaneous Investigations Map I–1287–D.

Coleman, J. M., and Prior, D. B., 1980, Deltaic sand bodies: American Association of Petroleum Geologists Continuing Education Course Note Series, no. 15, 171 p.

Curray, J. R., 1960, Sediments and history of Holocene transgression, continental shelf, northwest Gulf of Mexico, *in* Shepard, F. P., Phleger, F. B., and Van Andel, T. H., eds., Recent sediments, northwest Gulf of Mexico: Tulsa, Okla., American Association of Petroleum Geologists, p. 221–266.

———1961, Late Quaternary sea level—A discussion: Geological Society of America Bulletin, v. 72, no. 11, p. 1707–1712.

Curray, J. R., Emmel, F. J., and Crampton, P. J. S., 1969, Holocene history of a strand plain, lagoonal coast, Nayarit, Mexico, *in* Ayala Castañares, Agustín, and Phleger, F. B., eds., Coastal lagoons, a symposium—UNAM–UNESCO, México, D. F., 1967: México, D. F., Universidad Nacional Autónoma de México, p. 63–100.

Fisk, H. N., 1959, Padre Island and the Laguna Madre flats, coastal south Texas, *in* Russell, R. J., ed., Coastal Geography Conference, Coastal Studies Institute, Louisiana State University, 1959: Washington, D.C., U.S. Office of Naval Research, Geography Branch, p. 103–152.

Frazier, D. E., 1974, Depositional episodes—Their relationship to the Quaternary stratigraphic framework in the northwestern portion of the Gulf Basin: Texas University Bureau of Economic Geology Geological Circular 74–1, 28 p.

Goddard, E. N., and others, 1948, Rock-color chart: Washington, D.C., National Research Council, 6 p. (Republished by Geological Society of America, 1951; reprinted 1963, 1970.)

Hunter, R. E., and Dickinson, K. A., 1970, Map showing landforms and sedimentary deposits of the Padre Island portion of the South Bird Island 7.5-minute quadrangle, Texas: U.S. Geological Survey Miscellaneous Geologic Investigations Map I–659, scale 1:24,000.

Mitchum, R. M., Jr., Vail, P. R., and Sangree, J. B., 1977, Seismic stratigraphy and global changes of sea level. Part 6, Stratigraphic interpretation of seismic reflection patterns in depositional sequences, *in* Payton, C. E., ed., Seismic stratigraphy—Applications to hydrocarbon exploration: American Association of Petroleum Geologists Memoir 26, p. 117–133.

Nelson, H. F., and Bray, E. E., 1970, Stratigraphy and history of the Holocene sediments in the Sabine–High Island area, Gulf of Mexico, *in* Morgan, J. P., ed., Deltaic sedimentation, modern and ancient: Society of Economic Paleontologists and Mineralogists Special Publication 15, p. 48–77.

Otvos, E. G., Jr., 1975, Ingleside strandplain sand of central Texas coast—Discussion: American Association of Petroleum Geologists Bulletin, v. 59, no. 12, p. 2324–2325.

Price, W. A. 1933, Role of diastrophism in topography of Corpus Christi area, south Texas: American Association of Petroleum Geologists Bulletin, v. 17, no. 8, p. 907–962.

———1958, Sedimentology and Quaternary geomorphology of south Texas; Gulf Coast Association of Geological Societies Transactions, v. 8, p. 41–75.

Schlee, John, 1966, A modified Woods Hole rapid sediment analyzer: Journal of Sedimentary Petrology, v. 36, no. 2, p. 403–413.

Shepard, F. P., 1954, Nomenclature based on sand-silt-clay ratios: Journal of Sedimentary Petrology, v. 24, no. 3, p. 151–158.

Shideler, G. L., 1976, A comparison of electronic particle counting and pipette techniques in routine mud analysis: Journal of Sedimentary Petrology, v. 46, no. 4, p. 1017–1025.

———1982, Lithologic descriptions of late Quaternary core borings from the Corpus Christi area, Nueces County, Texas: U.S. Geological Survey Open-File Report 82–471, 32 p.

Texas University Bureau of Economic Geology, 1975, Geologic atlas of Texas, Corpus Christi sheet: Austin, scale 1:250,000.

Thom, B. G., 1973, The dilemma of high interstadial sea levels during the last glaciation: Progress in Geography, v. 5, p. 167–246.

Wentworth, C. K., 1922, A scale of grade and class terms for clastic sediments: Journal of Geology, v. 30, no. 5, p. 377–392.

Wilkinson, B. H., McGowen, J. H., and Lewis, C. R., 1975a, Ingleside strandplain sand of central Texas coast: American Association of Petroleum Geologists Bulletin, v. 59, no. 2, p. 347–352.

———1975b, Ingleside strandplain sand of central Texas coast—Reply: American Association of Petroleum Geologists Bulletin, v. 59, no. 12, p. 2326–2327.

Wright, S. S., 1980, Seismic stratigraphy and depositional history of Holocene sediments in the central Texas Gulf Coast: Austin, Texas University, unpublished M.S. thesis, 123 p.

Ostracodes from Late Quaternary Deposits, South Texas Coastal Complex

By THOMAS M. CRONIN

STRATIGRAPHIC STUDIES OF A
LATE QUATERNARY BARRIER-TYPE COASTAL COMPLEX,
MUSTANG ISLAND–CORPUS CHRISTI BAY AREA,
SOUTH TEXAS GULF COAST

U.S. GEOLOGICAL SURVEY PROFESSIONAL PAPER 1328–C

CONTENTS

ILLUSTRATIONS

TABLES

STRATIGRAPHIC STUDIES OF A LATE QUATERNARY BARRIER-TYPE COASTAL COMPLEX, MUSTANG ISLAND–CORPUS CHRISTI BAY AREA, SOUTH TEXAS GULF COAST

OSTRACODES FROM LATE QUATERNARY DEPOSITS, SOUTH TEXAS COASTAL COMPLEX

By THOMAS M. CRONIN

ABSTRACT

Ostracodes from Quaternary deposits penetrated by six coreholes in the southern Mustang Island–Corpus Christi Bay area, South Texas Gulf Coast, provided evidence of significant paleoenvironmental fluctuations during the Quaternary. Freshwater-fluvial, upper bay, mid-bay, lower bay-inlet, and sublittoral (Inner Continental Shelf) assemblages were found at various levels within the cores, documenting a gradation from freshwater to normal marine paleosalinities. Ostracode assemblages representing bay environments are virtually identical with those assemblages inhabiting the modern Texas estuarine-lagoonal system.

When correlated with the lithostratigraphic and radiocarbon evidence from the cores, the ostracode assemblages indicate at least three distinct high stands of sea level during the Quaternary, each of which signifies relatively warm interglacial conditions. The Holocene is represented by a thick section in one of the cores, which contains an excellent sequence of bay and marine ostracode assemblages. Periods of nonmarine deposition characterized by freshwater forms are believed to represent glacial periods when eustatic sea level was lower than it is at present.

INTRODUCTION

Approximately 17 percent of the North American coastline consists of barrier-lagoonal environments in which shallow coastal lagoons are separated from the Continental Shelf by elongate barrier islands. North America has more than one-third of the world's lagoonal coastlines. An understanding of how these complexes are formed is important because of the clues they hold (1) to the trend and rate of the Holocene sea-level rise and (2) to the probable effects on barriers of future sea-level fluctuations.

Although lithologic and sedimentologic studies of Atlantic and Gulf of Mexico barrier islands are plentiful, few have incorporated micropaleontologic analyses into the reconstruction of paleoenvironments of deposition. Yet, to understand the geologic history of barrier islands requires a knowlege of the history of the adjacent estuarine-lagoonal complex and the inner sublittoral zone of the Continental Shelf. The study of the Inner Atlantic Continental Shelf and the evolution of barrier islands by Field and Duane (1976) indicates the continuum of diverse environments of deposition that are often very transient during a rapid sea-level rise such as that which took place during the Holocene. An ideal way to augment investigations of the depositional history of these coastal complexes is through paleoenvironmental reconstructions of the Quaternary sediments underlying modern barrier-lagoonal systems. As part of a detailed study of the southern part of Corpus Christi Bay and adjacent Mustang Island, South Texas, benthic microfossils were analyzed from six cores (fig. 1). Emphasis was placed on the ostracode fauna because these microscopic crustaceans were abundant in the cores, and because the modern distributions of ostracode species in Texas coastal environments are well known. Ostracodes are particularly useful for paleoenvironmental and biofacies analyses in coastal sediments because different taxonomic groups inhabit fresh, brackish, and marine waters. This report describes the distribution of ostracodes in the six cores and provides an interpretation of the paleoenvironments they indicate. Most species are illustrated by scanning-electron photomicrographs in plates 1–10.

ACKNOWLEDGMENTS

Thanks go to G. L. Shideler and J. E. Hazel, U.S. Geological Survey (USGS), and Dr. Paul Krutak, Atlantic Richfield Co., for helpful suggestions on the

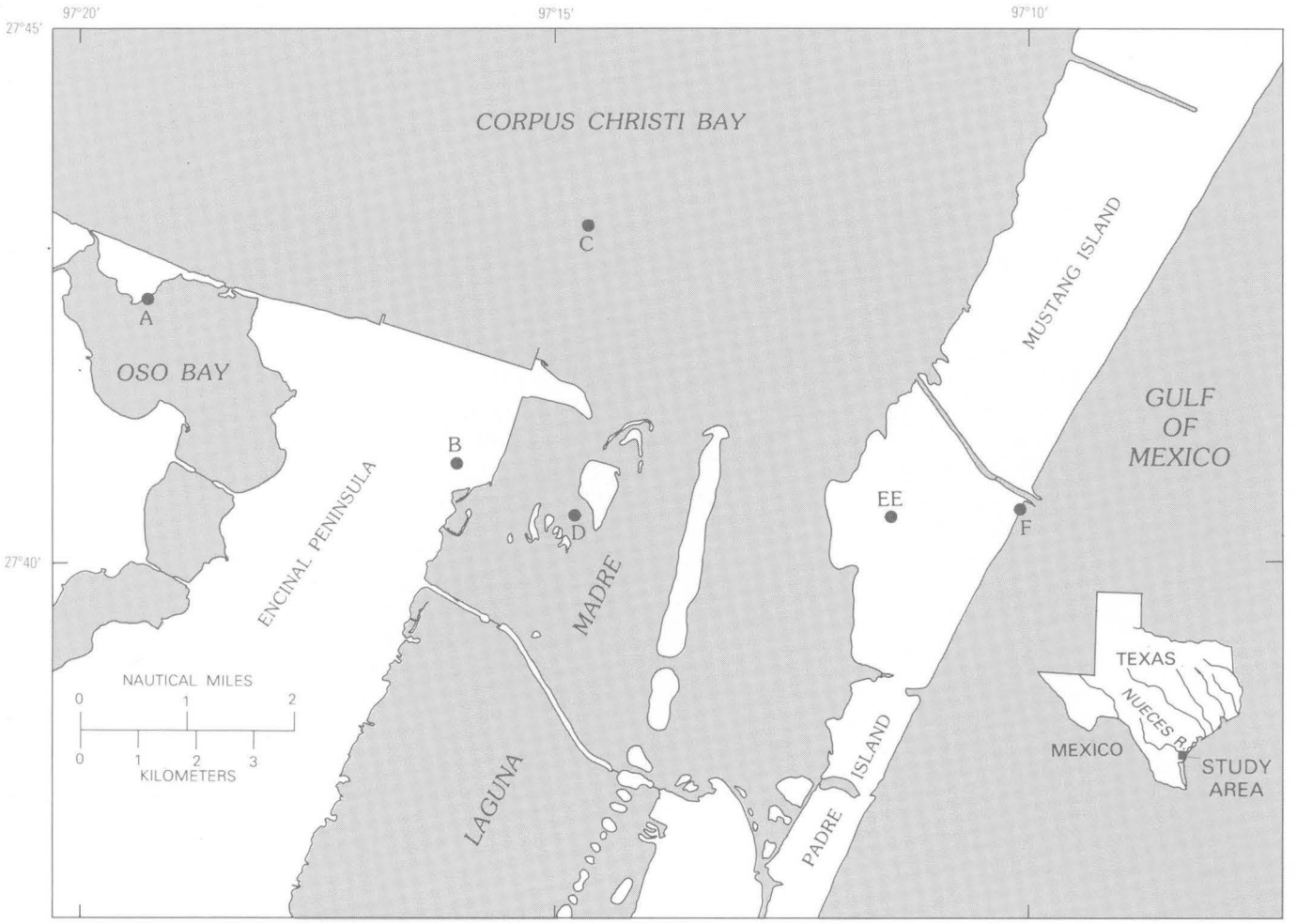

FIGURE 1.—Map of the southern Mustang Island–Corpus Christi Bay study area on the South Texas Gulf Coast showing locations of coreholes A–D, EE, and F.

manuscript. Meyer Rubin, USGS, and G. L. Shideler provided helpful discussions of the radiocarbon dates and sea-level data. R. M. Forester, USGS, identified some of the nonmarine ostracodes. I thank M. Quinones and E. E. Compton, USGS, for help in preparing samples and paleoenvironmental logs for the cores, and E. G. Shaw, USGS, for help with the electron photomicrographs.

METHODS

Ostracodes were recovered from six cores that were collected in the southern Mustang Island–Corpus Christi Bay study area (fig. 1). Coreholes A, B, D, EE, and F penetrated about 60–62 m of deposits; C penetrated only 10.75 m. The lithostratigraphy and geologic history are described in detail in companion chapters of this volume. The density of sampling (table 1) ranged from 1 sample per 0.85 m in core C to 1 sample per 2.2 m in core A. Of the 220 samples analyzed for micro-

TABLE 1.—*Ostracode sample data*

Core	Density of sampling[1]	No. of samples analyzed for microfossils	No. of analyzed samples containing ostracodes	Total No. of ostracode specimens	Average No. of ostracode specimens per sample
A	2.2	28	15	592	39.5
B	1.5	40	23	1,507	65.5
C	.85	12	12	1,329	111
D	1.3	48	21	1,718	81.8
EE	1.7	37	24	1,386	57.8
F	1.1	55	34	1,725	50.7
Total		220	129	8,257	——

[1]Average distance between analyzed samples within the core, in meters.

fossils, 129 contained ostracodes. A total of 8,257 ostracode specimens were recovered from the 129 fossiliferous samples.

Samples analyzed for microfossils weighed about 50 g each. They were soaked overnight in water. Then they were washed through standard U.S. sieves, and the residue between the 230- and 20-mesh sieves (that is, particles 6.25–850 μm in diameter) was examined for microfossils. Ostracodes were picked and sorted on standard micropaleontologic slides. The variable preservation throughout the cores and the resulting variation in sample size precluded rigorous quantitative analyses of the microfossil data; however, this limitation did not diminish the overall paleoenvironmental utility of the ostracodes.

Ostracode valves and carapaces were usually well preserved and could be identified by using the published literature, USGS collections of shallow-water and marginal marine ostracodes from the Atlantic Coast (Cronin, 1979), and collections housed at the U.S. National Museum of Natural History, Washington, D.C. The recent study by Garbett and Maddocks (1979) was particularly useful in identifying marine and lagoonal species. This work provides an updated taxonomy and excellent scanning-electron photomicrographs of most species found in the six cores, and hence, it was used as a primary source for species identification. Other studies that were useful in identifying species were by Swain (1955), Kontrovitz (1976), Morales (1966), Valentine (1971), and Benson and Coleman (1963).

Freshwater ostracodes are poorly known from this region, and little is published on them. Further, some taxa such as *Candona* were generally fragile, and adults of these taxa were commonly rare or broken. These preservation problems, as well as the lack of literature, made species-level identification of freshwater taxa not feasible. Because many genera are restricted to either fresh, brackish, or marine environments, generic-level identifications were adequate for some paleoenvironmental reconstructions.

Specimens in a few samples from marine facies in core F had a slight degree of recrystallization of calcite. Reworked older Cenozoic ostracodes were not found, and most taxa found are currently extant in parts of the Gulf of Mexico. However, in some parts of the cores, possible transport was suspected when very rare specimens of planktic foraminifers were found in medium to coarse fluvial sands barren of other calcareous microfossils.

Table 2 gives presence-absence data for 64 ostracode taxa found throughout the cores, and plate 11 illustrates logs of the cores, showing the paleoenvironments inferred from the ostracode assemblages and showing the abundance of ostracodes in each sample. The microfossil data in plate 11 and table 2 show that the distribution of microfossils was irregular. Some cores contained thick barren intervals, whereas other parts of the cores were rich in ostracodes. This irregular distribution is believed to be primarily the result of shifting depositional environments and sedimentation rates.

Representative ostracode specimens were coated with a gold-palladium alloy and were photographed by use of a JEOL 35C[1] scanning-electron microscope. These photomicrographs are shown in plates 1–10.

OSTRACODES IN MODERN TEXAS ESTUARINE-LAGOONAL-MARINE ENVIRONMENTS

Many microfaunal samples from the cores indicated lagoonal environments similar to those that are common along the modern Texas coast. Lagoons throughout the world vary widely in size, depth, substrate, fauna, and water chemistry. For this study, we were concerned primarily with very shallow coastal lagoons separated from the Continental Shelf by elongate barrier islands and receiving freshwater from rivers draining a broad Coastal Plain. Most Texas lagoons average less than 1 m in depth, and they are commonly fringed by oyster reefs. The substrate is usually muddy and contains variable amounts of sand. Salinities can be extremely low, approaching less than a few parts per thousand (ppt) near the mouth of the river, but they can also reach nearly normal marine levels at the inlet entrance where marine water mixes with lagoonal water. Hypersaline conditions exist in isolated parts of some Texas lagoons where evaporation takes place, but these conditions are more common in arid tropical areas. Salinities also vary temporally because of increasing or decreasing freshwater influx, tidal effects, evaporation, and precipitation.

Water temperatures in Texas lagoons range annually from about 10° to 33°C. The region is in a subhumid to semiarid, subtropical climatic zone, and the ostracode faunas are considered characteristic of subtropical marine climates (van den Bold, 1977). Water temperature has a significant effect on the reproduction and survival of many ostracode taxa and is considered a major factor limiting the broad-scale distribution of many species.

Another factor controlling the abundance of ostracodes is food. Coastal lagoons generally contain abundant food supplies, including vegetation, diatoms, algae, and other microscopic organisms, which serve as sources of nutrients. Because this was not a detailed

[1]Any use of trade names in this report is for descriptive purposes only and does not constitute endorsement by the U.S. Geological Survey.

ecological investigation, the control of ostracode species by the availability of food was not considered. King and Kornicker (1970) provided the most detailed study of ostracode ecology in Texas lagoons and concluded that ostracode abundances were controlled by food supply and salinity and that ostracodes were more abundant in oyster reefs and on lagoonal muds than on sandy substrates.

QUATERNARY OSTRACODE ASSEMBLAGES

Cronin (1979) reviewed the methodology used by previous workers in classifying ostracode assemblages and biofacies and environments along the Atlantic and Gulf Coasts and discussed the approach to biofacies that is used in the present paper. In this study, biofacies were recognized by particular species assemblages living in a particular area; therefore, biofacies helped to define particular paleoenvironments, which were also inferred from the lithofacies characteristics and the seismic evidence.

In their comprehensive study of ostracodes from Texas bays, Garbett and Maddocks (1979) recently found five ostracode biofacies corresponding to upper bay, mid-bay, lower bay, tidal-inlet, and oyster-reef environments. The delineation of discrete ostracode assemblages in the present study is shown in table 3 and generally conforms to those groups of species recognized by Garbett and Maddocks (1979) with the following exceptions: (1) Assemblages believed to signify polyhaline salinity conditions in the lower bays and near inlets are lumped into one category, and (2) Garbett and Maddocks (1979) did not study sublittoral or limnic environments, whereas ostracode assemblages indicating these environments were found in the present study.

The semiquantitative classification of biofacies shown in table 3 is based on the fossil assemblages found in the six cores and is augmented by the modern distribution data. Although several factors control ostracode species distribution, the assemblage data indicate that salinity was the predominant factor in determining species assemblages in this material. Thus, this classification essentially represents a nonmarine to marine gradation, a transition from freshwater-fluvial environments that fed into the lagoons to an inner continental shelf environment that had normal marine salinities. Although discrete groups are identified, the data represent a continuum of death assemblages, most of which are indigenous. However, some valves and carapaces may have been transported from the life habitat.

The depositional model adopted for the present study is the fluvial-deltaic model discussed by Brown and Fisher (1977), which is applicable to river-dominated nearshore Gulf Coast Tertiary and Quaternary stratigraphic sequences. According to the model, interfingering of fluvial, deltaic, lagoonal, and marine lithofacies reflects patterns of sedimentation controlled by complex interactions of sea-level changes and changing patterns of fluvial deposition. Many of the depositional environments in evidence from the microfaunal data fit within the region termed the "delta plain" in the fluvial-deltaic model. The biofacies equivalents of the delta plain are shallow muddy lagoons and estuaries inhabited by distinctive ostracode assemblages. Some ostracode assemblages indicate inner shelf marine environments, which correspond in part to the delta-front–barrier-bar and prodelta-shelf facies of the fluvial-deltaic model.

The most significant implication revealed by faunal changes in the cores is that they document fluctuations

TABLE 3.—*Quaternary ostracode assemblages used in this study to identify environments of deposition*

Depositional environment	Salinity (ppt)	Ostracode death assemblage
Freshwater-fluvial	Limnic (0–0.5)	Marine and bay taxa absent; nonmarine taxa present include *Candona, Limnocythere, Physocypria, Ilyocypris.*
Upper bay	Oligohaline (> 0.5–5)	Mixture of bay and freshwater taxa, including *Limnocythere, Candona, Perissocytheridea, Cyprideis salebrosa, Cytherura.*
Mid-bay	Mesohaline (> 5–18)	Bay species only, including *Perissocytheridea, Cytherura, Megacythere repexa, Loxoconcha moralesi.*
Lower bay-inlet	Polyhaline (> 18–30)	Mixture of bay and marine taxa, including *Actinocythereis subquadrata, Peratocytheridea bradyi, Proteoconcha* spp., *Cytherura* spp., *Hulingsina* spp., *Malzella littorala.*
Sublittoral	Euhaline (> 30–36)	Marine taxa only, including *Actinocythereis, Malzella, Pellucistoma, Puriana, Reticulocythereis, Hulingsina, Protocytheretta.*

in sea level—transgressions and regressions that primarily reflect glacioeustatic fluctuations. Although a continuous sea-level curve could not be drawn because the record is incomplete, the paleoenvironmental data give evidence for the timing and rate of sea-level change when they are interpreted in light of the lithologic data and the radiocarbon dates. All fossil ostracode assemblages indicated that deposition took place in water less than 20 or 30 m deep. Most fossiliferous samples indicate shallow inner shelf or lagoonal environments, or periods of nonmarine deposition when sea level was relatively low. A discussion of possible sea-level fluctuations follows the next section.

PALEOENVIRONMENTS INDICATED BY CORE OSTRACODE ASSEMBLAGES

In this section, the paleoenvironments indicated by ostracode assemblages are discussed in ascending order for each core, beginning with core A. The general trends in environments of deposition, as shown in plate 11, are emphasized, although specific ostracode occurrences used to infer these environments are also mentioned where appropriate. The detailed presence-absence data for each of the 129 samples are given in table 2 along with the sample numbers and depths.

CORE A

The bottom of core A, from 60.3 m below sea level, contains an upper bay assemblage, above which is a barren interval of about 13 m. From 46.6 to 37.6 m, a lower bay to nonmarine sequence of environments predominates. *Cyprideis salebrosa* characterizes this interval and is often found with nonmarine taxa. This species is a euryhaline species and is extremely widespread (Sandberg, 1964). It is known from three inland bodies of water in North America (Stout, 1981) and is able to survive salinities at least as low as a few parts per thousand; its regular occurrence with nonmarine taxa in the study-area cores supports interpretations on its environmental tolerance.

A noteworthy peak in salinity at 38.9 m is indicated by a relatively diverse marine assemblage of more than 25 species. This assemblage is one of the more diverse found in the study, and because the radiocarbon dates indicate a pre-Holocene age for this interval, this fauna may signify a Pleistocene interglacial period (see "Discussion" section).

At 37.6 m, a shift toward nonmarine environments is indicated by the increase in numbers of *Candona* and *Limnocythere*. The absence of ostracodes between 37.6 and 25.3 m and the presence of freshwater taxa at 37.6 and 25.3 m probably indicate a nonmarine interval.

An increase in salinity is indicated by the ostracode assemblages beginning at 25.3 m and culminating in a nearly normal marine assemblage at 14.5 m. A rapid drop in salinity is indicated by fossils between 14.5 and 0.5 m below the top of the core. An increase in salinity in the uppermost 0.5 m is in evidence from the presence of lower bay-inlet ostracode assemblages.

In summary, core A is characterized by extreme variability in the preservation and abundance of ostracodes, by the predominance of upper bay to freshwater environments, and by the presence of two distinct marine intervals, which were sampled at 38.9 and 14.5 m.

CORE B

At the bottom of core B is a mixed assemblage of nonmarine and brackish-water taxa. The presence of *Radimella* c.f. *R. wantlandi*, *Aurila* sp., *Limnocythere floridensis*, *Cyprideis gelica*, and *Candona* spp. at 61.1 m (sample B–49–2P) distinguishes this assemblage from younger lagoonal and sublittoral assemblages in the area. The occurrence of these species possibly represents a middle Pleistocene interglacial period. *Radimella* is a thermophilic genus common in tropical climatic zones (Pokorný, 1968) and regions transitional from tropical to subtropical such as southern Florida.

The nonmarine genera *Candona, Ilyocypris, Physocypria*, and *Limnocythere* also occur in this core and predominate from 60.2 to 57.3 m. Salinities during the time these animals lived were less than 3 or 4 ppt. This interval of core B also contains a few benthic foraminifers that are probably detrital.

Mid-bay and upper bay assemblages predominate from 54.8 to 47.0 m, but the sample from 47.0 m contains specimens of the nonmarine genus *Candona*, indicating a proximity to freshwater. Ostracodes are rare from 45.7 to 41.1 m, but occasional specimens of *Candona* and *Limnocythere* indicate nonmarine conditions.

From 33.4 to 27.4 m, ostracodes are fairly common, and assemblages consist primarily of typical mid-bay forms; a lower bay-inlet assemblage is present at 29.3 m. Predominant taxa at 29.3 m include abundant *Cytherura sandbergi, Perissocytheridea brachyforma, P. troglodyta,* and *Loxoconcha*. At 21.8 m, a nearly normal marine salinity environment is indicated by the presence of the ostracodes *Puriana, Malzella, Proteoconcha*, and *Actinocythereis*. A similar assemblage occurs at 17.8 m, but it also contains specimens of *Limnocythere* and *Candona* and, thus, indicates an upper bay environment. Except for a few specimens of nonmarine ostracodes at 12.3 m, the uppermost 17 m of core B is unfossiliferous.

In general, the sequence of paleoenvironments indicated by ostracodes in core B parallels that in core A.

Nonmarine to very brackish upper bay to mid-bay assemblages, and occasional inlet assemblages, characterize the lower 35 m. Marine intervals at 14.5 m in core A and at 21.8 m in core B overlie these more brackish intervals.

CORE C

Corehole C, located in Corpus Christi Bay, penetrated only about 10 m of very fossiliferous sediments. Well-preserved mid-bay to sublittoral ostracode assemblages characterize the core, which was deposited during approximately the last 10,000 years. Most samples have 15–22 species, and, therefore, this core yielded some of the most diverse ostracode assemblages found in this study. Garbett and Maddocks (1979) found that the modern ostracode fauna of Corpus Christi Bay is also relatively diverse and contains a total of about 30 species. Salinities ranging from 25 to 30 ppt are probably responsible for this diversity because many sublittoral marine species inhabit Corpus Christi Bay.

CORE D

Core D is barren of ostracodes from 62 to 52.5 m, whereas from 52.5 to 47.0 m, rare nonmarine taxa occur. Evidence for increasing salinity and the beginning of a mid-bay environment is present between 47.0 and 41.7 m. No ostracodes were found between 41.7 and 31.7 m; however, well-preserved mid-bay and upper bay assemblages occur between 31.7 and 24.0 m. At 22.9 m, a sublittoral assemblage contains very abundant ostracode specimens, which show relatively poor preservation. Valves and carapaces are recrystallized, and in some specimens, the recrystallized material partially obscures the surface ornament; however, the cause or significance of the recrystallization is not known. If the radiocarbon dates for adjacent samples are accurate, then this marine interval might signify a middle Wisconsin interstadial period (see "Discussion" section). Paleoenvironments for the uppermost 22 m of core D fluctuated from upper bay to lower bay-inlet. Especially noteworthy is the presence of *Actinocythereis* aff. *A. bahamensis* (pl. 7, fig. 3) at a depth of 11.4 m. This species, which does not occur in modern Texas bays and lagoons, also occurs in core C, in sample C–8–2P, at 10.2 m and resembles a species illustrated by Howe and van den Bold (1975, pl. 1, figs. 1a, b) in their study of mudlump ostracodes from the Mississippi Delta area.

CORE EE

Corehole EE was drilled on the landward side of Mustang Island near the juncture of Laguna Madre and Corpus Christi Bay. Its sequence of paleoenvironments is generally similar to that indicated by ostracodes from corehole F, which was drilled on the seaward side of Mustang Island. Both cores contain detailed, usually well preserved faunal records for the region during the late Wisconsinan-Holocene sea-level rise from the level at about 10,000 years B.P. to the present level. From 53.6 to 44.4 m, core EE contains sparse but distinctive freshwater to upper bay ostracode assemblages, which include *Candona, Limnocythere*, and *Physocypria*. An increase in salinity is in evidence from the occurrence of mid-bay and upper bay assemblages between 44.4 and 25.0 m. At 22.4 m, a significant and lasting faunal change is marked by the appearance of lower bay-inlet to sublittoral ostracode assemblages containing 10 to as many as 33 species (sample E–12–1P). This marine incursion represents the Holocene transgression that was also recognized in the limited section of core C. Significantly, the ostracodes in these samples consist of essentially the same subtropical assemblages that today inhabit the region. Typical species of *Cytherura, Perissocytheridea, Hulingsina, Proteoconcha, Paracytheroma,* and *Pellucistoma* are the dominant taxa.

CORE F

At the bottom of core F (at 60.5 and 61.1 m), a brackish-water ostracode assemblage occurs that is different from modern assemblages, from the typical Holocene assemblages found in the other cores, and from those in the upper part of this core. Because of the scarcity of specimens for many species, analysis of the assemblage and identification of most of the species were difficult. However, many species seem to be unique to this interval, and some represent morphological forms of species that are different from their modern counterparts. Among the several taxa that characterize this sample are *Tanella, Sahnia, Cytheromorpha* aff. *C. apheles, Cytherura* aff. *C. nucis, Puriana* aff. *P. carolinensis*, and *Perissocytheridea* n. sp. Specimens of *Loxoconcha moralesi* have slightly different morphology than do those from other samples, particularly in the presence of a postventral spine. *Cytheromorpha curta*, a species very common along the Atlantic Coast in Pliocene and Pleistocene estuarine deposits (Cronin, 1979), also occurs in this sample.

Two genera whose species have a great deal of intraspecific morphologic variation are *Proteoconcha* and *Hulingsina*. The latter is common at 60.5 m and has morphologies atypical of the species living in the region. Additional study of these forms is required in order to determine whether these represent new species that are now extinct in the region.

Between 59.3 and 38.1 m in core F, ostracodes are absent, although occasional detrital foraminiferal tests were found. The absence of ostracodes and the lithologies in this interval suggest fluvial conditions. This suggestion is supported by the rare occurrence of nonmarine ostracodes immediately overlying this section in samples at 38.1 m and 35.8 m. From 35.5 to 22.7 m, a pronounced environmental shift is recorded as midbay to lower bay ostracode assemblages appear. From 22.7 m to the top of the core, inlet and lower bay ostracode assemblages containing substantial numbers of marine species predominate. Occasional specimens of nonmarine species are mixed in with the typical lower bay and inlet assemblages, indicating the proximity of freshwater to the region. Therefore, beginning at 35.5 m, the ostracode assemblages appear to be recording the Holocene marine transgression, an event for which evidence was also recognized in core EE.

DISCUSSION

That the ostracode data of the present study do not reveal evidence for cooler water temperatures during the time studied is significant, because the Corpus Christi region now provides an important Holocene reference section for correlating climatic changes during the last 10,000 years around North America. The data indicate that, in contrast to many areas along the Atlantic Coast that were locally cooler during the late Wisconsinan and early Holocene and during deglaciation about 18,000 to 6,000 years ago (Hazel, 1968; Cronin, 1983; Cronin and others, 1981), this region remained relatively mild. Unfortunately, samples confidently dated at about 17,000 to 18,000 years B.P., when glaciation reached a maximum, were not found in the Corpus Christi area, although Berryhill (1981) did map late Wisconsinan paleogeography for the shelf and slope adjacent to Corpus Christi Bay.

Ostracode assemblages provided evidence for fluctuations in the positions of the marine shoreline. The presence of sublittoral or lower bay ostracode assemblages is strong evidence of depositional environments near a paleoshoreline, although neither assemblage is a precise indicator of former sea-level positions. The local sea-level record inferred from ostracode data can be interpreted in light of the stratigraphic and radiometric data (Shideler, Chap. B, this volume) and compared to records from other areas. Cores A–D, EE, and F document at least three separate marine transgressive events, probably all of which were Quaternary in age.

Fossiliferous marine and bay deposits below 37 m in core A, below 47 m in core B, and below 57 m in core F are all considered to be the remains of Pleistocene interglacial deposits. The evidence for a Pleistocene age assignment is based on: (1) their stratigraphic position below the Holocene deposits, (2) the occurrence in cores B and F of ostracode taxa that do not live in the region today (discussed above), and (3) the presence of many extant ostracode species. The precise ages of these units remain unknown. Furthermore, these units are not necessarily correlative with one another, and each may represent a separate transgression of which only patches remain. Whether these deposits represent the last interglacial period, which is believed to correspond to the Sangamon of Illinois (Follmer, 1979) and deep-sea oxygen-isotope stage 5, hinges on the age of the stratigraphically higher marine sediments found in cores A, B, D, and EE. These pre-Holocene deposits were dated by radiocarbon analyses on shells and wood as reported by Shideler (Chap. B, this volume), and because some dates were finite, they raise the prospect of a possible middle Wisconsinan high stand of sea level.

The existence of a middle Wisconsinan high stand has long been debated in the literature (Mörner, 1971). Thom (1973) presented the most detailed discussion of the topic, and his critical review of the literature is the most definitive and the most objective discussion yet available.

Along the Atlantic Coast, some formations that may have been deposited during a middle Wisconsinan high stand are deposits at Port Washington, N.Y. (Sirkin and Stuckenrath, 1980), the Sinepuxent Formation of Delaware (Owens and Denny, 1978), the Diamond City Clay of North Carolina (Moslow and Heron, 1979; Snyder and others, 1982), the Anastasia Formation of Florida, and the Silver Bluff Formation of Georgia (Hoyt and Hails, 1974). Belknap (1982) studied amino-acid racemization in mollusks from these formations and concluded that the ^{14}C ages were inaccurate because of contamination with young carbon; he suggested ages ranging from 80,000 to 700,000 years for these deposits.

Stratigraphic units in the Texas Gulf Coast area also have contributed to the controversy. Curray (1961) dated carbonates from the shelf off Texas that suggested that sea level reached within 15 m of its present level but later urged caution in accepting the existence of a middle Wisconsinan high stand of sea level based on these dates (Shepard and Curray, 1967). Whereas Wilkinson and others (1975) suggested that the Ingleside sand barrier system of South Texas represents a middle Wisconsin interstadial period, Otvos (1975a) disputed this interpretation and concluded that the Ingleside formed during a Sangamonian high stand of sea level. Further, Otvos (1975b) considered the Ingleside correlative with the Biloxi and Gulfport Formations of coastal Mississippi that have produced

numerous radiocarbon dates he considered to be inaccurate because of contamination (Otvos, 1972, p. 246).

The ^{14}C ages from the Mustang Island–Corpus Christi Bay area also present the same recurring equivocal results so often encountered in coastal studies of lagoonal-barrier island systems. Shideler (Chap. B, this volume) lists the ^{14}C dates produced by Beta Analytical, Inc. The shell dates documenting the Holocene transgression are internally consistent, fit the stratigraphic and paleontologic record, and pose no problems. The shell and wood dates between 25,000 and 37,000 years B.P. require scrutiny in light of the implications for Wisconsinan sea level if they are accurate. The dates in this group obtained on shells could possibly reflect contamination by young carbon and, if so, are too young. Olsson (1968) stated that 1-percent contamination of a 44,000-year-old sample would yield an apparent radiocarbon age of 34,000 years B.P. The extent to which the Mustang Island–Corpus Christi Bay material might be contaminated with young carbon cannot be estimated because the amount of groundwater contamination is unknown.

Two wood dates of 24,640±1,580 years B.P. from core F and 32,090±880 years B.P. from core D are more reliable age estimates. The dated material from core F came from nonmarine sediments that are overlain by Holocene marine deposits; therefore, this date yields no direct information on Wisconsinan marine deposits and sea levels. The dated material from core D came from nonmarine deposits underlying a thick sequence of lagoonal and marine sediments that yielded two shell dates of about 32,000–33,000 years B.P. If the wood date of 32,090±880 years B.P. is relatively accurate, then the following implications are evident. First, the overlying pre-Holocene lagoonal-marine sequence in core D must be considered middle Wisconsinan in age and provides evidence for a marine transgression at least as high as 12 m below present sea level. Second, if these subsurface lagoonal-marine deposits are correlative with those in cores A, B, and EE as suspected, then the level of marine deposits in core A indicates that the transgression reached 11 m below present sea level. If the Encinal Peninsula, consisting of the Ingleside sand body, is part of this transgression, as suggested by Shideler (Chap. B, this volume), then this marine event reached near present-day sea level. Finally, if this date is correct, then the lowermost marine deposits in cores A, B, and F are pre-middle Wisconsinan and probably represent the Sangamon interglacial period and oxygen-isotope stage 5e.

An alternate hypothesis is to reject the radiocarbon ages as too young and to infer a Sangamonian age of between 140,000 and 80,000 years B.P. for the major subsurface marine unit and a probable middle Pleistocene age (more than 140,000 years B.P.) for the lowermost marine deposits in cores A, B, and F. The following evidence would favor this view. First, Otvos (1972, p. 246) discussed false finite radiocarbon dates on shells and wood in the Biloxi Formation of Mississippi and concluded that this unit and its correlative Ingleside beach ridge are Sangamonian in age. Second, many studies from other areas indicate that radiocarbon dates on materials from clastic coasts are too young (Belknap, 1982). Other studies provide direct evidence for a sea-level position 40 m below present sea level at about 30,000 years B.P. (Chappell and Veeh, 1978). The most accepted current eustatic sea-level model also calls for middle Wisconsinan sea level below −40 m (Bloom and others, 1974). These eustatic sea-level curves for the late Pleistocene come from two main sources: (1) the ages and elevations of emerged flights of coral reef tracts in New Guinea, Barbados, and elsewhere (Bloom and others, 1974) and (2) deep-sea oxygen-isotope curves that are believed to represent changes in global ice volume (Shackleton and Opdyke, 1973). Proponents of the Barbados model contend that the last time sea level reached its modern level was during the last interglacial interval between 140,000 and 120,000 years B.P. Finally, the substantial differences between the ostracode assemblages in the lowermost marine facies in cores B and F and the overlying assemblages suggest that these units are older than the last interglacial interval. Unfortunately, this evidence must be considered as equivocal because Pliocene and Pleistocene ostracode biostratigraphy for this region is poorly known.

At present, the major subsurface marine unit in the Corpus Christi area cannot be assigned an age with certainty because, although the stratigraphy is well documented and the paleontologic evidence for a major marine unit is not disputable, radiocarbon dates of the middle Wisconsinan must be viewed cautiously. These dates should not, however, be rejected outright, because evidence is accumulating that Wisconsin ice sheets were very dynamic and that the Laurentide ice sheet may not have been as extensive as previously believed (Shilts and others, 1979; Andrews and Miller, 1979). These new studies cast doubt on the precision of some current ideas on eustatic sea level, and a review of the topic of eustatic sea levels indicates a wide range of sea-level estimates for many times during the last 200,000 years (Cronin, 1983). At present, the radiocarbon-dated marine sediments in the Mustang Island–Corpus Christi Bay area represent a possible middle Wisconsinan sea level; obtaining additional dates by other techniques (including amino-acid racemization and determinations of $^{230}Th/^{234}U$ ratios of corals or mollusks) in the future might refine ideas about the age of these pre-Holocene units.

In conclusion, the existence of at least three Quaternary marine transgressions has been documented in the Mustang Island–Corpus Christi Bay area, but the precise ages of all but the Holocene transgression remain uncertain.

REFERENCES CITED

Andrews, J. T., and Miller, G. H., 1979, Glacial erosion and ice sheet divides, northeastern Laurentide Ice Sheet, on the basis of the distribution of limestone erratics: Geology, v. 7, no. 12, p. 592–596.

Belknap, D. F., 1982, Amino acid racemization from C-14 dated "mid-Wisconsin" mollusks of the Atlantic Coastal Plain [abs.]: Geological Society of America Abstracts with Programs, v. 14, nos. 1–2, p. 4.

Benson, R. H., and Coleman, G. L., 2d, 1963, Recent marine ostracodes from the eastern Gulf of Mexico: Kansas University Paleontological Contributions 31, Arthropoda, art. 2, 52 p.

Berryhill, H. L., Jr., 1981, Map showing paleogeography of the continental shelf during the low stand of sea level, Wisconsin glaciation, Corpus Christi 1° × 2° quadrangle, Texas: U.S. Geological Survey Miscellaneous Investigations Map I–1287–E.

Bloom, A. L., Broecker, W. S., Chappell, J. M. A., Matthews, R. K., and Mesolella, K. J., 1974, Quaternary sea level fluctuations on a tectonic coast—New $^{230}Th/^{234}U$ dates from the Huon Peninsula, New Guinea: Quaternary Research, v. 4, no. 2, p. 185–205.

Bold, W. A. van den, 1977, Distribution of marine podocopid Ostracoda in the Gulf of Mexico and the Caribbean, *in* Löffler, Heinz, and Danielopol, Dan, eds., Aspects of ecology and zoogeography of Recent and fossil Ostracoda—Proceedings of the 6th International Symposium on Ostracoda, Saalfelden (Salzburg), 1976: The Hague, W. Junk, p. 175–186.

Brown, L. F., Jr., and Fisher, W. L., 1977, Seismic-stratigraphic interpretation of depositional systems—Examples from Brazilian rift and pull-apart basins, *in* Payton, C. E., ed., Seismic stratigraphy—Applications to hydrocarbon exploration: American Association of Petroleum Geologists Memoir 26, p. 213–248.

Chappell, J., and Veeh, H. H., 1978, $^{230}Th/^{234}U$ age support of an interstadial sea level of −40 m at 30,000 yr BP: Nature, v. 276, no. 5866, p. 602–604.

Cronin, T. M., 1979, Late Pleistocene marginal marine ostracodes from the southeastern Atlantic Coastal Plain and their paleoenvironmental implications: Géographie Physique et Quaternaire, v. 33, no. 2, p. 121–173.

———1981, Paleoclimatic implications of late Pleistocene marine ostracodes from the St. Lawrence Lowlands: Micropaleontology, v. 27, no. 4, p. 384–418.

———1983, Rapid sea level and climate change—Evidence from continental and island margins: Quaternary Science Reviews, v. 1, p. 177–214.

Cronin, T. M., Szabo, B. J., Ager, T. A., Hazel, J. E., and Owens, J. P., 1981, Quaternary climates and sea levels of the U. S. Atlantic Coastal Plain: Science, v. 211, no. 4479, p. 233–240.

Curray, J. R., 1961, Late Quaternary sea level—A discussion: Geological Society of America Bulletin, v. 72, no. 11, p. 1707–1712.

Field, M. E., and Duane, D. B., 1976, Post-Pleistocene history of the United States Inner Continental Shelf—Significance to origin of barrier islands: Geological Society of America Bulletin, v. 87, no. 5, p. 691–702.

Follmer, L. R., 1979, A historical review of the Sangamon soil, *in* Wisconsinan, Sangamonian, and Illinoian stratigraphy in central Illinois [—Midwest Friends of the Pleistocene 26th Field Conference, May 4–6, 1979]: Illinois State Geological Survey Guidebook Series, no. 13, p. 79–91.

Garbett, E. C., and Maddocks, R. F., 1979, Zoogeography of Holocene cytheracean ostracodes in the bays of Texas: Journal of Paleontology, v. 53, no. 4, p. 841–919.

Hazel, J. E., 1968, Pleistocene ostracode zoogeography in Atlantic Coast submarine canyons: Journal of Paleontology, v. 42, no. 5, p. 1264–1271.

Howe, H. V., and Bold, W. A. van den, 1975, Mudlump Ostracoda: Bulletins of American Paleontology, v. 65, no. 282, p. 303–315.

Hoyt, J. H., and Hails, J. R., 1974, Pleistocene stratigraphy of southeastern Georgia, *in* Oaks, R. Q., Jr., and DuBar, J. R., eds., Post-Miocene stratigraphy, central and southern Atlantic Coastal Plain: Logan, Utah, Utah State University Press, p. 191–205.

King, C. E., and Kornicker, L. S., 1970, Ostracoda in Texas bays and lagoons—An ecologic study: Smithsonian Contributions to Zoology 24, 92 p.

Kontrovitz, Mervin, 1976, Ostracoda from the Louisiana Continental Shelf: Tulane Studies in Geology and Paleontology, v. 12, no. 2, p. 49–100.

Morales, G. A., 1966, Ecology, distribution, and taxonomy of Recent Ostracoda of the Laguna de Términos, Campeche, Mexico: Mexico Universidad Nacional Autónoma Instituto de Geología Boletin 81, 103 p.

Mörner, N.-A., 1971, The position of the ocean level during the interstadial at about 30 000 B.P.—A discussion from a climatic-glaciologic point of view: Canadian Journal of Earth Sciences, v. 8, no. 1, p. 132–143.

Moslow, T. F., and Heron, S. D., Jr., 1979, Quaternary evolution of Core Banks, North Carolina; Cape Lookout to New Drum Inlet, *in* Leatherman, S. P., ed., Barrier islands from the Gulf of St. Lawrence to the Gulf of Mexico: New York, Academic Press, p. 211–236.

Olsson, I. U., 1968, C^{14}/C^{12} ratio during the last several thousand years and the reliability of C^{14} dates, *in* Morrison, R. B., and Wright, H. E., Jr., eds., Means of correlation of Quaternary successions: Salt Lake City, Utah, University of Utah Press, p. 241–252.

Otvos, E. G., Jr., 1972, Mississippi Gulf Coast Pleistocene beach barriers and the age problem of the Atlantic–Gulf Coast "Pamlico"-"Ingleside" beach ridge system: Southeastern Geology, v. 14, no. 4, p. 241–250.

———1975a, Ingleside strandplain sand of central Texas coast—Discussion: American Association of Petroleum Geologists Bulletin, v. 59, no. 12, p. 2324–2325.

———1975b, Late Pleistocene transgressive unit (Biloxi Formation), northern Gulf Coast: American Association of Petroleum Geologists Bulletin, v. 59, no. 1, p. 148–154.

Owens, J. P., and Denny, C. S., 1978, Geologic map of Worcester County: Baltimore, Maryland Geological Survey, scale 1:62,500.

Pokorný, Vladimír, 1968, *Radimella* gen. n., a new genus of the Hemicytherinae (Ostracoda, Crust.): Acta Universitatis Carolinae Geologica, 1968, no. 4, p. 359–373.

Sandberg, P. A., 1964, The ostracod genus *Cyprideis* in the Americas: Stockholm Contributions in Geology, v. 12, 178 p.

Shackelton, N. J., and Opdyke, N. D., 1973, Oxygen isotope and paleomagnetic stratigraphy of equatorial Pacific core V28–238—Oxygen isotope temperatures and ice volumes on a 10^5 year and 10^6 year scale: Quaternary Research, v. 3, no. 1, p. 39–55.

Shepard, F. P., and Curray, J. R., 1967, Carbon-14 determinations of sea level changes in stable areas: Progress in Oceanography, v. 4, p. 283–291.

Shilts, W. W., Cunningham, C. M., and Kaszycki, C. A., 1979, Keewatin ice sheet—Reevaluation of the traditional concept of the Laurentide ice sheet: Geology, v. 7, no. 11, p. 537–541.

Sirkin, L., and Stuckenrath, R., 1980, The Portwashingtonian warm interval in the northern Atlantic Coastal Plain: Geological Society of America Bulletin, v. 91, no. 6, p. 332–336.

Snyder, S. W., Belknap, D. F., Hine, A. C., and Steele, A. G., 1982, Seismic stratigraphy, lithostratigraphy, and amino acid racemization of the Diamond City Fm.—Reinterpretation of a reported "mid-Wisconsin high" sea-level indicator from the North Carolina Coastal Plain [abs.]: Geological Society of America Abstracts with Programs, v. 14, nos. 1–2, p. 84.

Stout, L. N., 1981, An unusual occurrence of the brackish-water ostracode *Cyprideis salebrosa* in central Missouri: Journal of Paleontology, v. 55, no. 4, p. 898–900.

Swain, F. M., 1955, Ostracoda of San Antonio Bay, Texas: Journal of Paleontology, v. 29, no. 4, p. 561–646.

Thom, B. G., 1973, The dilemma of high interstadial sea levels during the last glaciation: Progress in Geography, v. 5, p. 167–246.

Valentine, P. C., 1971, Climatic implication of a late Pleistocene ostracode assemblage from southeastern Virginia: U.S. Geological Survey Professional Paper 683–D, 28 p.

Wilkinson, B. H., McGowen, J. H., and Lewis, C. R., 1975, Ingleside strandplain sand of central Texas coast: American Association of Petroleum Geologists Bulletin, v. 59, no. 2, p. 347–352.

PLATES 1–10

USNM, U.S. National Museum, Washington, D.C. Contact photographs of plates 1–10 are available, at cost, from the U.S. Geological Survey Library, Federal Center, Denver, CO 80225.

PLATE 1

FIGURE 1. *Physocypria*?, left valve, × 120, sample B–46–2P, USNM 380894.
2. *Cypridopsis* sp., left valve, × 100, sample F–26–2P, USNM 380895.
3. *Candona* sp., left valve, female, × 66, sample B–46–2P, USNM 380896.
4. *Ilyocypris* sp., left valve, female, × 100, F–52–1P, USNM 380897.
5–6. *Limnocythere floridensis* Keyser, 1975.
5. Left valve, female, × 150, sample A–30–1P, USNM 380898.
6. Right valve, female, × 150, sample A–30–1P, USNM 380899.
7. *Peratocytheridea bradyi* (Stephenson, 1938), left valve, female, × 110, sample F–7–1P, USNM 380900.
8. *Peratocytheridea setipunctata* (Brady, 1869), left valve, female, × 72, sample F–10–1P, USNM 380901.

DEPARTMENT OF THE INTERIOR
U.S. GEOLOGICAL SURVEY

PROFESSIONAL PAPER 1328—C
PLATE 1

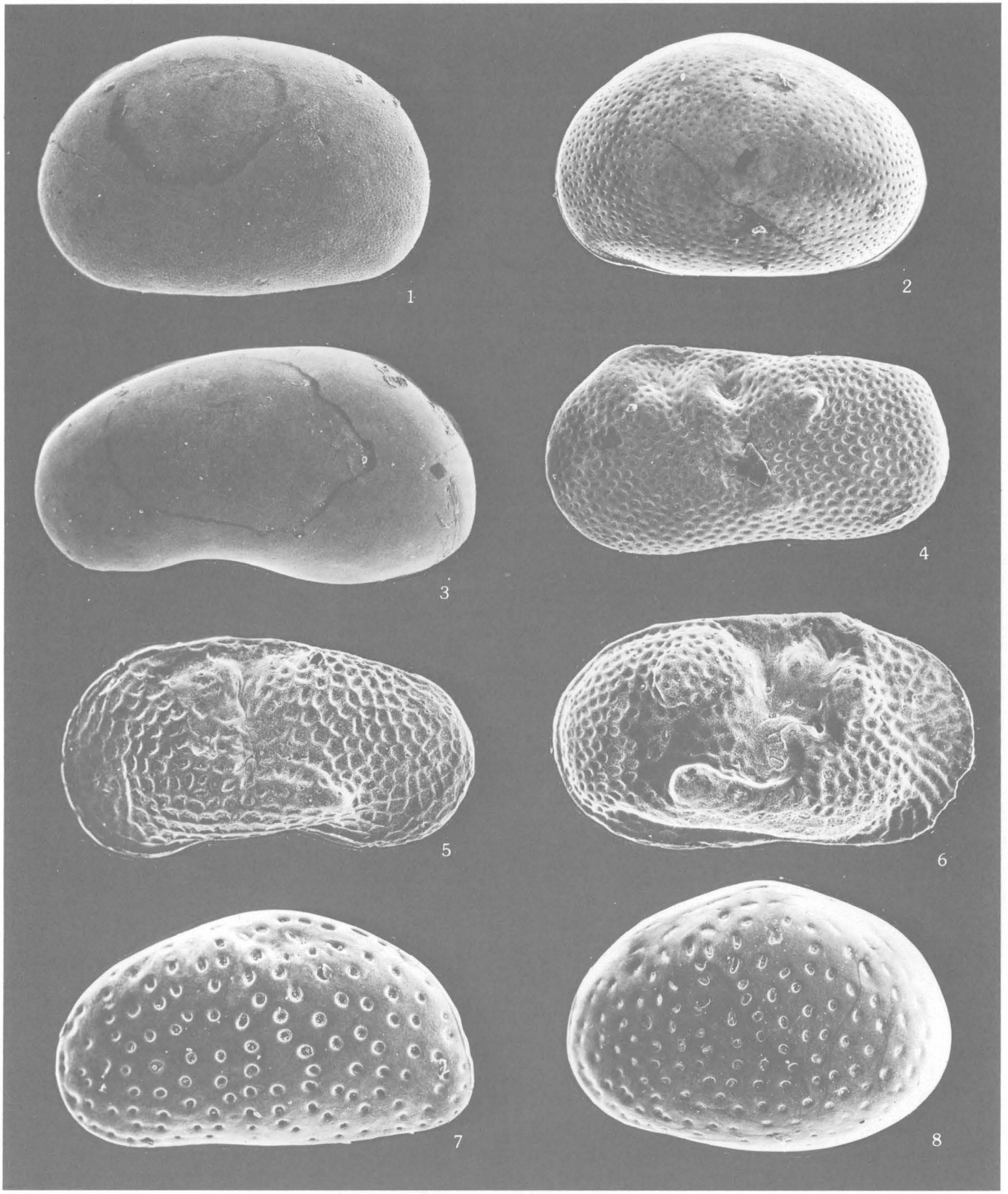

PHYSOCYPRIA?, CYPRIDOPSIS, CANDONA, ILYOCYPRIS, LIMNOCYTHERE, AND *PERATOCYTHERIDEA*

PLATE 2

FIGURE 1. *Pellucistoma magniventra* Edwards, 1944, left valve, female, × 110, sample F–4–2P, USNM 380902.

2. *Pellucistoma* cf. *P. howei* (Coryell and Fields, 1937), left valve, male?, × 150, sample EE–12–1P, USNM 380903.

3. *Paracytheroma stephensoni* (Puri, 1960), left valve, female, × 130, sample EE–12–1P, USNM 380904.

4. *Paracytheroma texana* Garbett and Maddocks, 1979, left lateral view, female carapace, × 160, sample C–2–1P, USNM 380905.

5–7. *Megacythere repexa* Garbett and Maddocks, 1979.

5. Left lateral view, female carapace, × 160, sample C–1–1P, USNM 380906.

6. Right valve, female, × 180, sample F–52–1P, USNM 380907.

7. Left valve, male, × 150, sample F–52–1P, USNM 380908.

8. *Hulingsina* sp., right valve, male, × 130, sample EE–3–1P, USNM 380909.

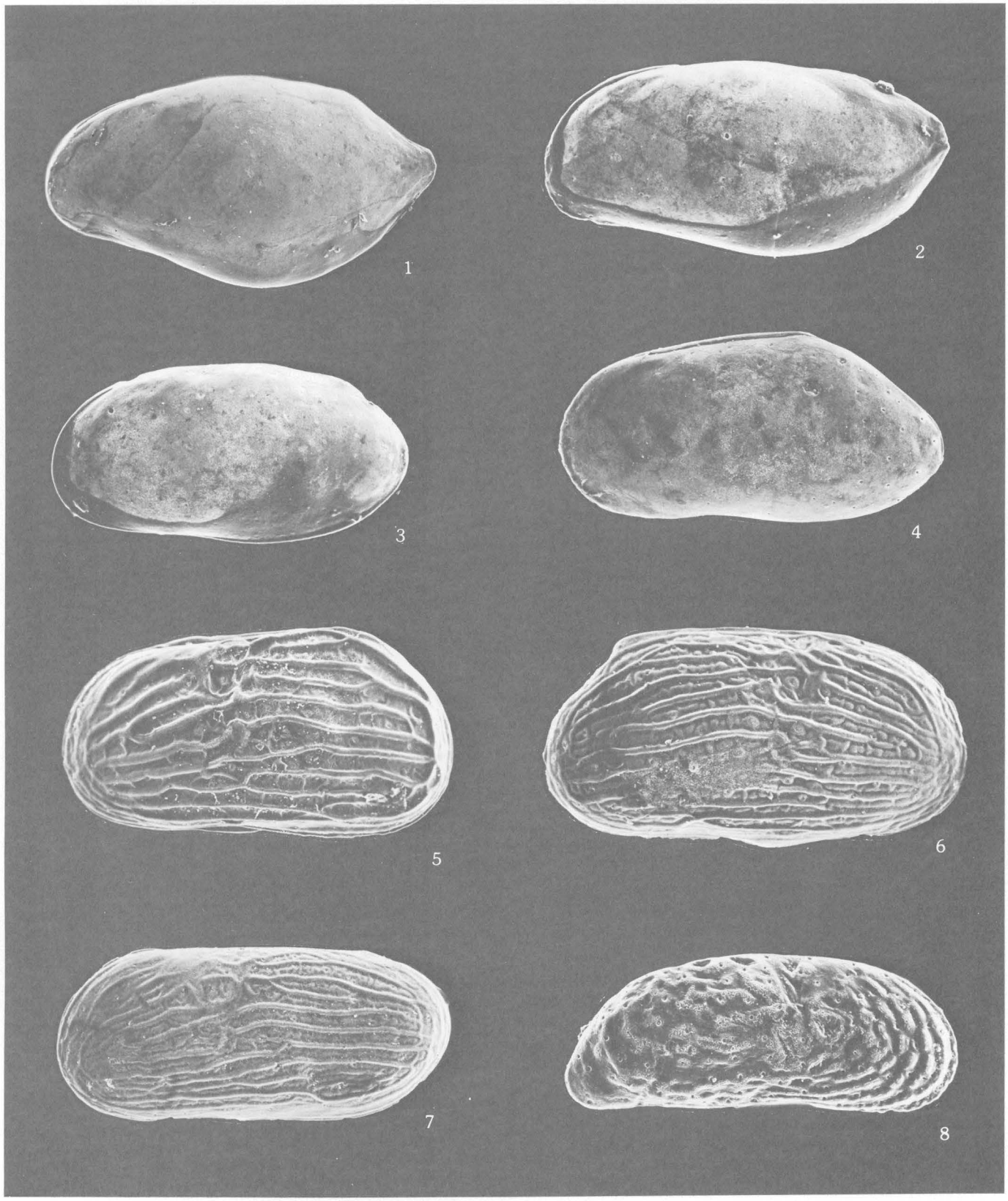

PELLUCISTOMA, PARACYTHEROMA, MEGACYTHERE, AND *HULINGSINA*

PLATE 3

FIGURES 1–2. *Cytheromorpha* cf. *C. apheles* van den Bold, 1963.
1. Left valve, female, × 150, sample F–52–1P, USNM 380910.
2. Right valve, female, × 150, sample F–52–1P, USNM 380911.

3–4. *Cytheromorpha paracastanea* (Swain, 1955).
3. Left lateral view, female carapace, × 160, sample C–3–2P, USNM 380912.
4. Left lateral view, male carapace, × 150, sample C–3–2P, USNM 380913.

5. *Cytheromorpha curta* Edwards, 1944, left valve, female?, × 180, sample F–52–1P, USNM 380914.
6. *Leptocythere nikraveshae* Morales, 1966, left lateral view, female carapace, × 150, sample F–52–1P, USNM 380915.
7. *Tanella* sp., left valve, female, × 200, sample F–52–1P, USNM 380916.
8. *Sahnia* sp., right valve, × 130, sample F–52–1P, USNM 380917.

DEPARTMENT OF THE INTERIOR
U.S. GEOLOGICAL SURVEY

PROFESSIONAL PAPER 1328—C
PLATE 3

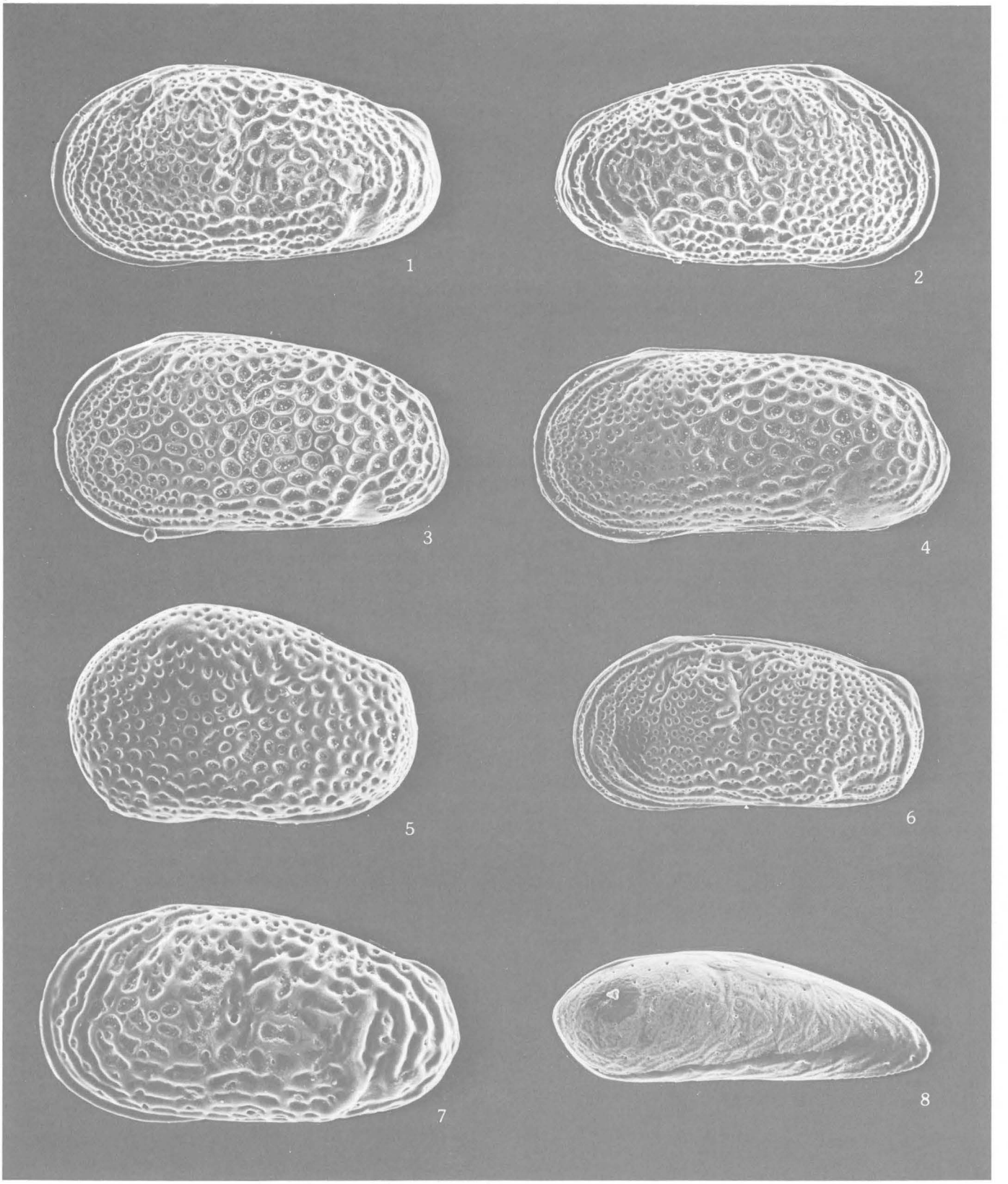

CYTHEROMORPHA, LEPTOCYTHERE, TANELLA, AND *SAHNIA*

PLATE 4

FIGURE 1. *Cytherura scissa* Garbett and Maddocks, 1979, left valve, female, × 180, sample EE–3–1P, USNM 380918.

2, 4, 6. *Cytherura radialirata* Swain, 1955.

2. Left valve, female, × 160, sample F–52–1P, USNM 380919.
4. Left valve, female, × 160, sample B–13–1P, USNM 380921.
6. Left valve, male, × 160, sample B–13–1P, USNM 380923.

3. *Cytherura cybaea* Garbett and Maddocks, 1979, left valve, female, × 160, sample C–1–1P, USNM 380920.
5. *Cytherura sandbergi* Morales, 1966, left valve, female, × 180, sample C–1–1P, USNM 380922.
7. *Cytherura fiscina* Garbett and Maddocks, 1979, left valve, female, × 160, sample C–1–1P, USNM 380924.
8. *Cytherura* aff. *C. nucis* Garbett and Maddocks, 1979, left valve, female, × 160, sample F–51–2P, USNM 380925.

DEPARTMENT OF THE INTERIOR
U.S. GEOLOGICAL SURVEY

PROFESSIONAL PAPER 1328—C
PLATE 4

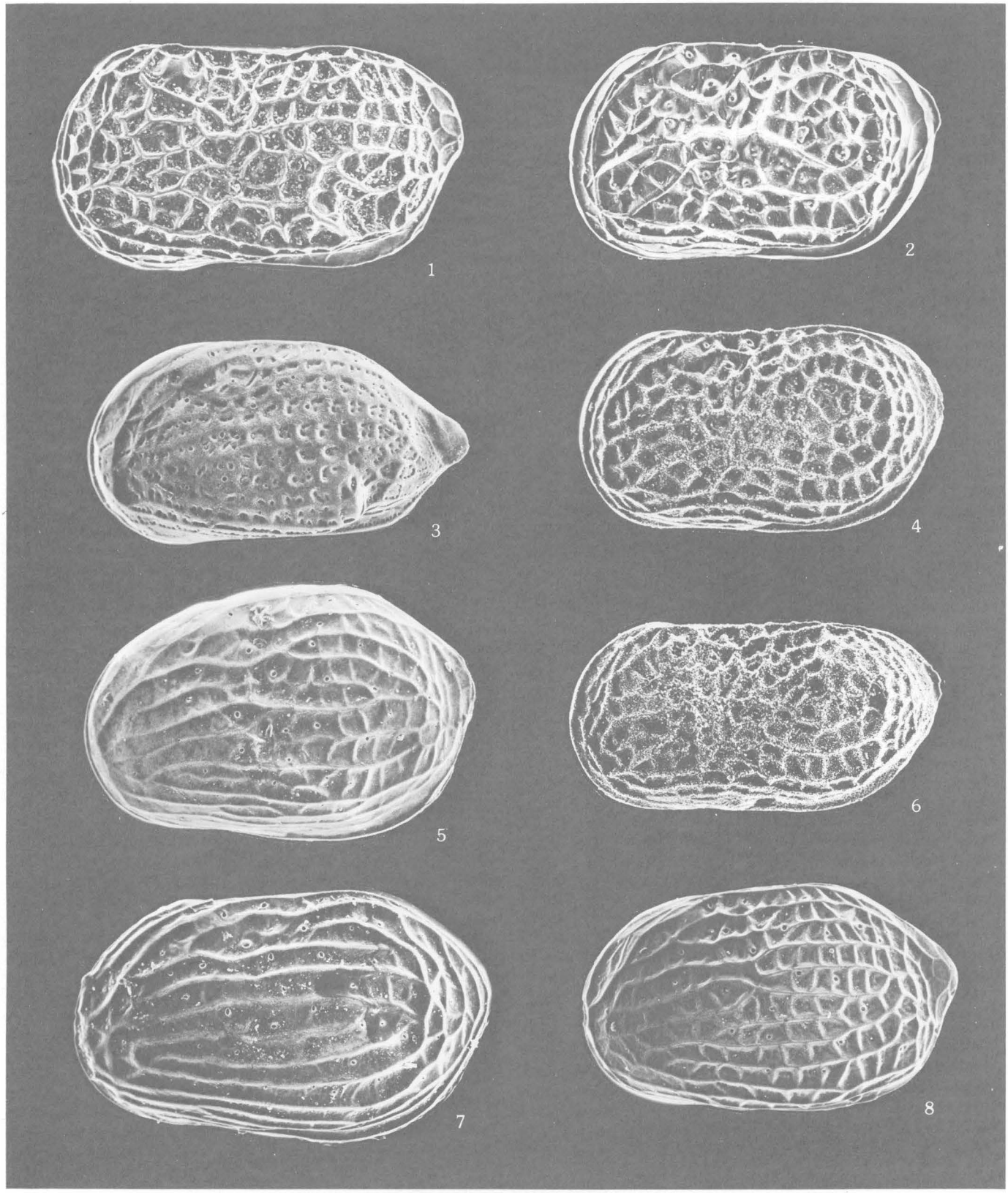

CYTHERURA

PLATE 5

FIGURES 1–2. *Perissocytheridea rugata* Swain, 1955.

1. Left valve, male, × 120, sample B–22–1P, USNM 380926.
2. Left valve, female, × 150, sample B–22–1P, USNM 380927.
3. *Perissocytheridea troglodyta* Swain, 1955, left valve, male, × 160, sample B–46–2P, USNM 380928.
4. *Perissocytheridea brachyforma* Swain, 1955, left valve, male, × 150, sample C–1–1P, USNM 380929.
5. *Perissocytheridea* aff. *P. bicelliforma* Swain, 1955, left valve, female, × 150, sample B–47–2P, USNM 380930.
6. *Perissocytheridea* n. sp., left valve, female, × 150, sample F–52–1P, USNM 380931.
7. *Perissocytheridea excavata* Swain, 1955, left valve, female, × 200, sample D–26–1P, USNM 380932.
8. *Cyprideis gelica* Plusquellec and Sandberg, 1974, internal view of right valve, female, × 110, sample EE–25–2P, USNM 380933.

DEPARTMENT OF THE INTERIOR
U.S. GEOLOGICAL SURVEY

PROFESSIONAL PAPER 1328—C
PLATE 5

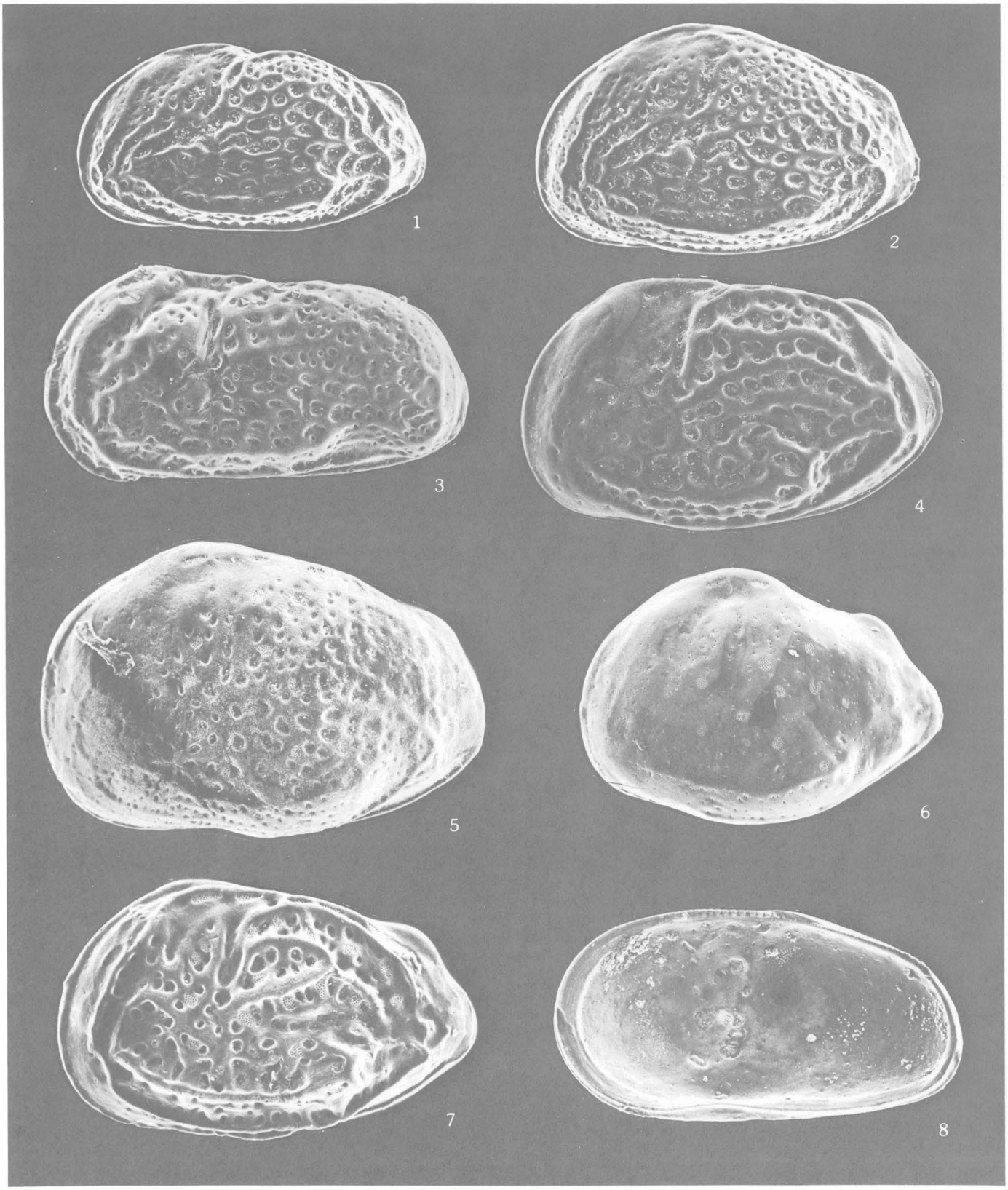

PERISSOCYTHERIDEA AND *CYPRIDEIS*

PLATE 6

FIGURES 1–3. *Cyprideis gelica* Plusquellec and Sandberg, 1974.
1. Left valve, female, × 100, sample EE–25–2P, USNM 380934.
2. Right valve, male?, × 100, sample EE–25–2P, USNM 380935.
3. Right valve, female (pitted form), × 110, sample B–46–2P, USNM 380936.

4. *Cyprideis salebrosa* van den Bold, 1963, left valve, female, × 86, sample B–46–2P, USNM 380937.

5–6. *Cyprideis* cf. *C. bensoni* Sandberg, 1966.
5. Left valve, male?, × 94, sample EE–25–2P, USNM 380938.
6. Right valve, male?, × 94, sample EE–25–2P, USNM 380939.

7–8. *Cyprideis* n. sp. A.
7. Left valve, female, × 110, sample B–47–1P, USNM 380940.
8. Right valve, female, × 100, sample B–47–1P, USNM 380941.

DEPARTMENT OF THE INTERIOR
U.S. GEOLOGICAL SURVEY

PROFESSIONAL PAPER 1328—C
PLATE 6

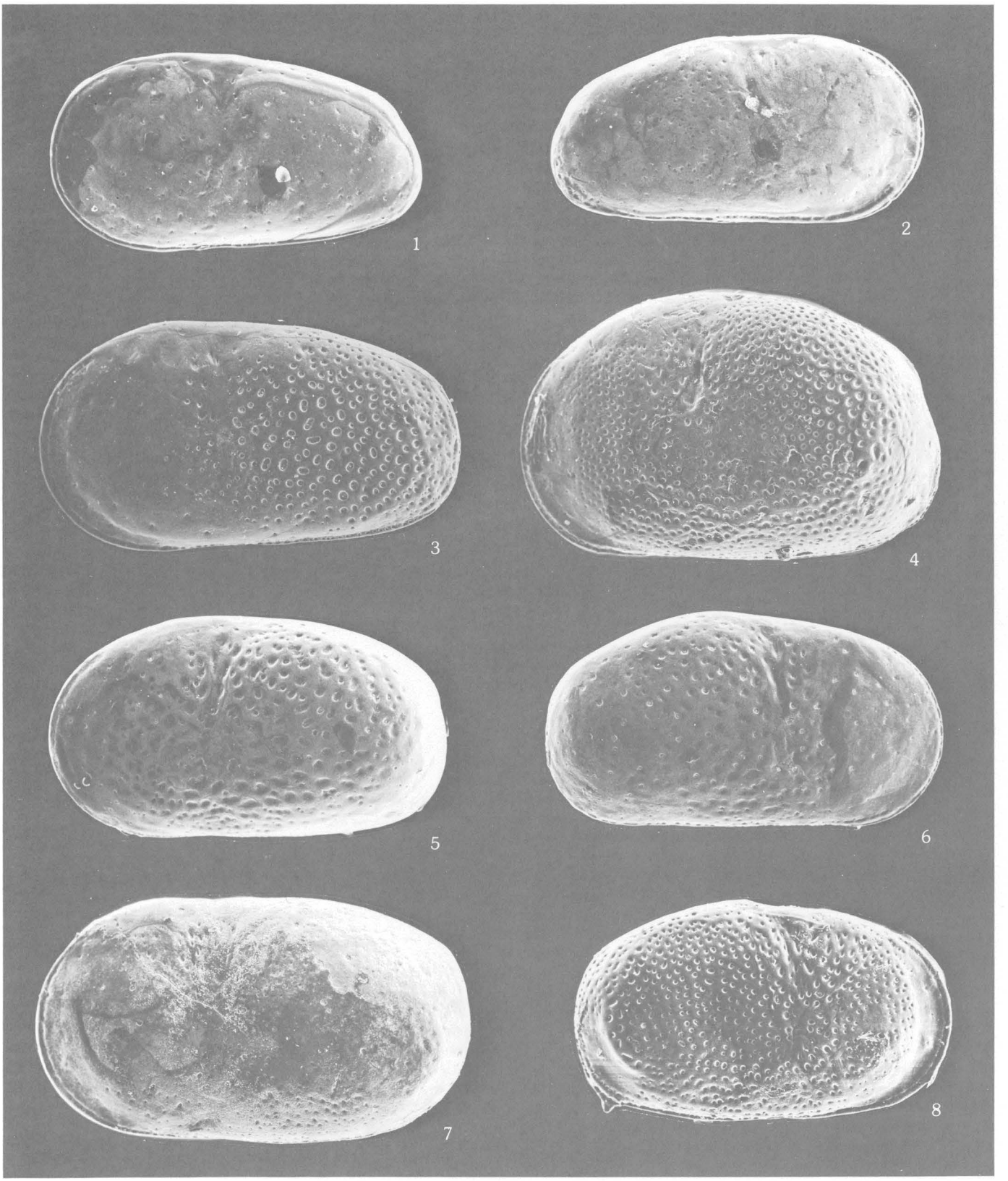

CYPRIDEIS

PLATE 7

FIGURES 1–2. *Actinocythereis subquadrata* Puri, 1960.
1. Left valve, female, × 130, sample C–1–1P, USNM 380942.
2. Left valve, male, × 130, sample C–1–1P, USNM 380943.
3. *Actinocythereis* aff. *A. bahamensis* (Brady, 1870) as illustrated by Howe and van den Bold (1975), right valve, female, × 120, sample D–9–1P, USNM 380944.
4. *Protocytheretta louisianensis* Kontrovitz, 1976, left lateral view, female carapace, × 100, sample C–2–1P, USNM 380945.

5–6. *Protocytheretta litorea* Garbett and Maddocks, 1979.
5. Left valve, female × 100, sample F–10–1P, USNM 380946.
6. Left lateral view, male carapace, × 94, sample F–15–2P, USNM 380947.
7. *Hulingsina sulcata* (Puri, 1960), right valve, female, × 120, sample C–7–1P, USNM 380948.
8. *Hulingsina sandersi* (Puri, 1958), right lateral view, male carapace, × 110, sample A–1–1P, USNM 380949.

DEPARTMENT OF THE INTERIOR
U.S. GEOLOGICAL SURVEY

PROFESSIONAL PAPER 1328—C
PLATE 7

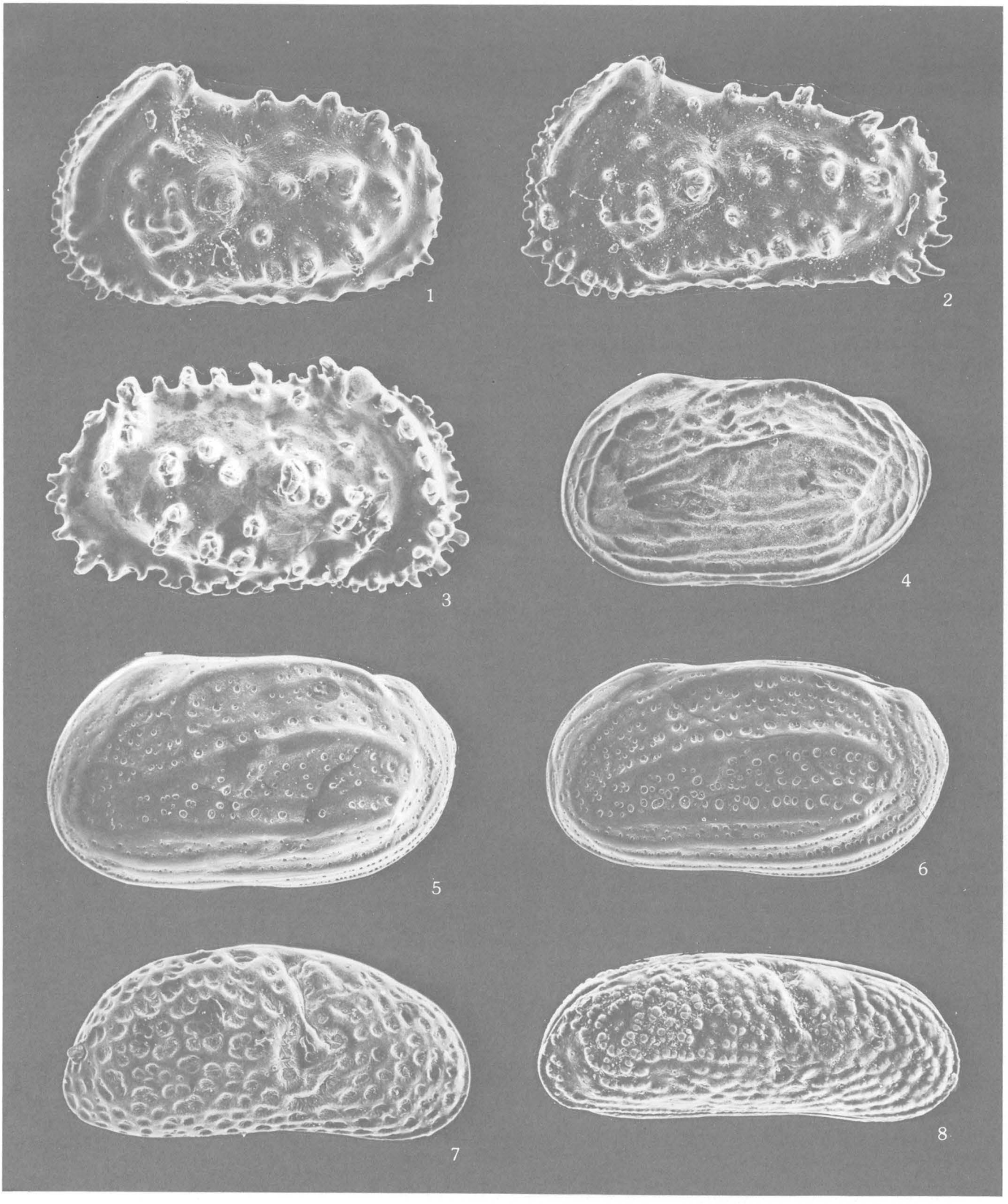

ACTINOCYTHEREIS, PROTOCYTHERETTA, AND *HULINGSINA*

PLATE 8

FIGURE 1. *Proteoconcha* cf. *P. tuberculata* (Puri, 1960), left lateral view, male carapace, × 130, sample F–7–1P, USNM 380950.

2. *Proteoconcha* aff. *P. nelsonensis* (Grossman, 1967), right valve, female?, × 130, sample F–17–3P, USNM 380951.
3. *Proteoconcha edwardsi* Plusquellec and Sandberg, 1969, left valve, female, × 130, sample EE–3–1P, USNM 380952.
4. *Proteoconcha* cf. *P. concinnoidea* (Swain, 1955), left lateral view, female carapace, × 130, sample C–3–2P, USNM 380953.
5. *Campylocythere laeva* Edwards, 1944, right valve, female, × 94, sample F–20–1P, USNM 380954.
6. *Proteoconcha gigantica* (Edwards, 1944), left valve, male, × 100, sample F–10–1P, USNM 380955.
7. *Reticulocythereis* n. sp., left valve, female, × 120, sample F–5–2P, USNM 380956.
8. *Reticulocythereis multicarinata* (Swain, 1955), left lateral view, female carapace, × 120, sample C–3–2P, USNM 380957.

DEPARTMENT OF THE INTERIOR
U.S. GEOLOGICAL SURVEY

PROFESSIONAL PAPER 1328—C
PLATE 8

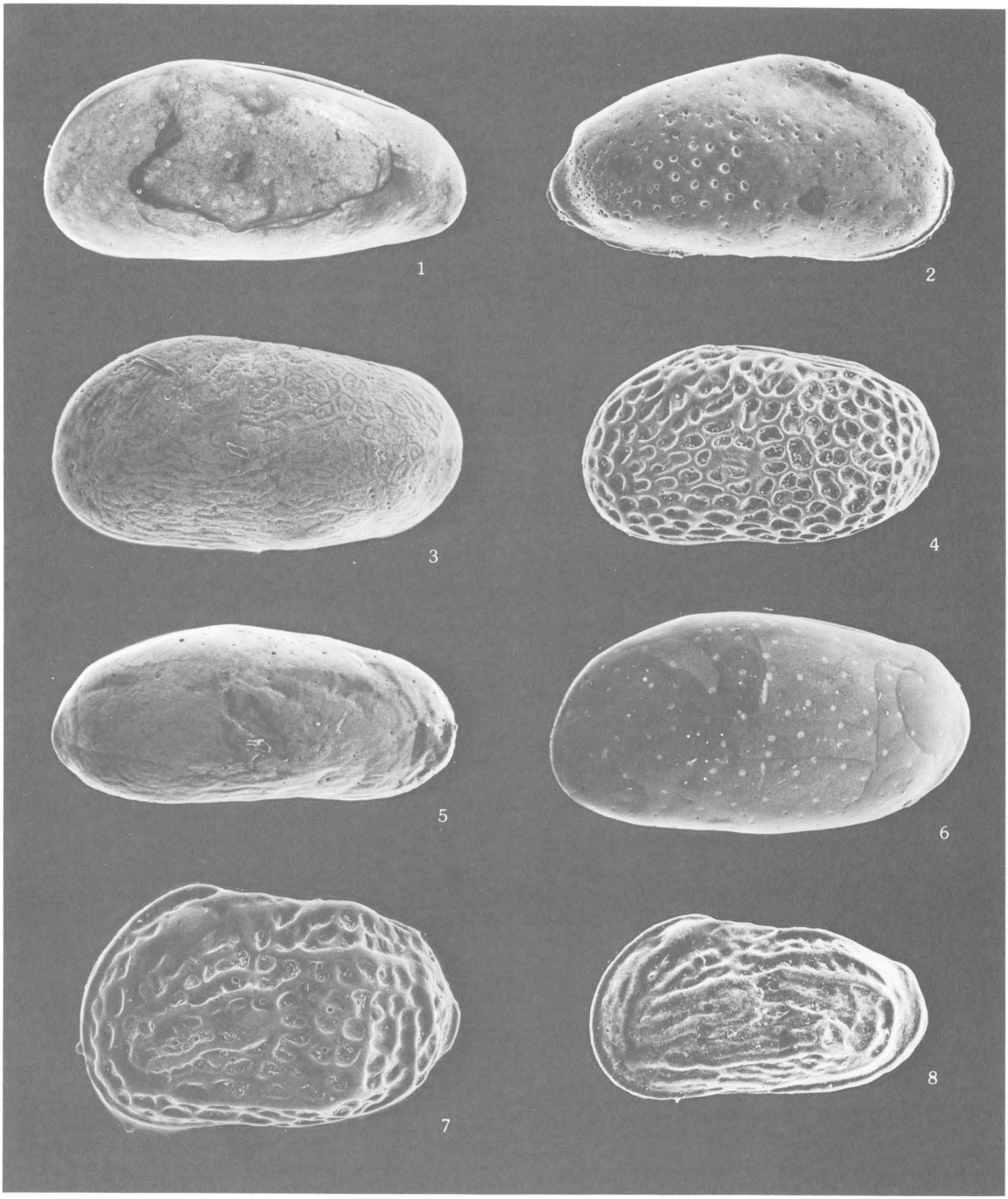

PROTEOCONCHA, CAMPYLOCYTHERE, AND *RETICULOCYTHEREIS*

PLATE 9

FIGURE

1. *Puriana* aff. *P. carolinensis* Hazel, 1983, left valve, female, × 150, sample F–52–2P, USNM 380958.
2. *Puriana* sp., left valve, female × 120, sample EE–13–2P, USNM 380959.
3. *Puriana* aff. *P. mesacostalis* (Edwards, 1944), left valve, female, × 110, sample D–9–1P, USNM 380960.

4–6. *Puriana krutaki* Kontrovitz, 1976.

4. Right valve, female, × 130, sample D–9–1P, USNM 380961.
5. Left valve, female, × 120, sample EE–13–2P, USNM 380962.
6. Left valve, male?, × 120, sample A–31–1P, USNM 380963.

7. *Pterygocythereis* cf. *P. alophia* Hazel, 1983, left valve, female, × 94, sample C–3–2P, USNM 380964.
8. *Paracytheridea* cf. *P. washingtonensis* Puri, 1953, right valve, female, × 120, sample F–19–2P, USNM 380965.

DEPARTMENT OF THE INTERIOR
U.S. GEOLOGICAL SURVEY

PROFESSIONAL PAPER 1328—C
PLATE 9

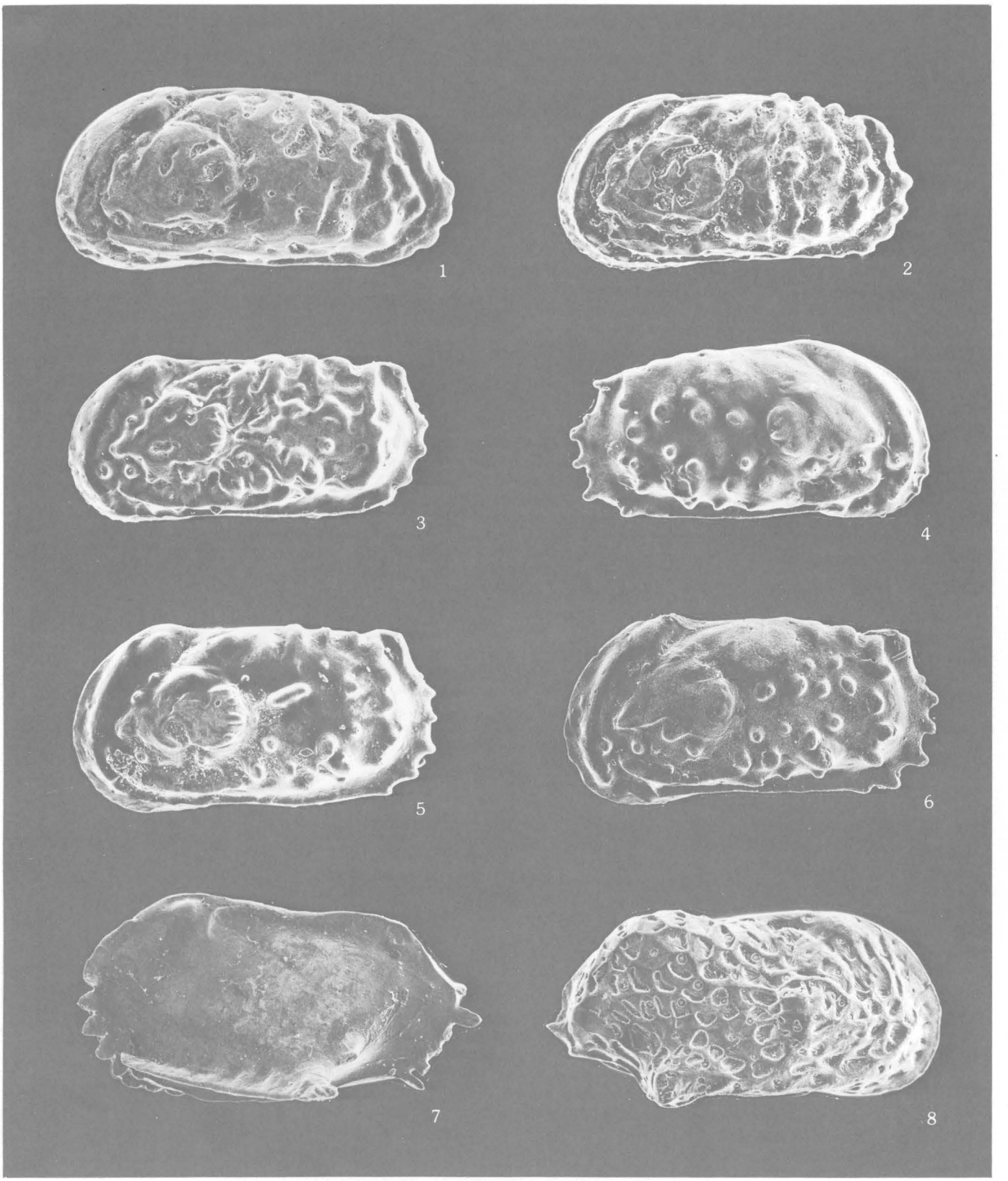

PURIANA, PTERYGOCYTHEREIS, AND *PARACYTHERIDEA*

PLATE 10

FIGURE 1. *Aurila laevicula* (Edwards, 1944), left valve, female, × 130, sample F–20–1P, USNM 380966.

2. *Aurila* aff. *A. laevicula* (Edwards, 1944), left valve, male?, × 130, sample B–49–2P, USNM 380967.
3. *Malzella littorala* (Grossman, 1967), left valve, female, × 130, sample B–22–2P, USNM 380968.
4. *Radimella* cf. *R. wantlandi* Teeter, 1975, left lateral view, male carapace, × 130, sample B–49–2P, USNM 380969.
5. *Loxoconcha* cf. *L. wilberti* Puri, 1960, left valve, male, × 130, sample EE–27–1P, USNM 380973.
6. *Loxoconcha* aff. *L. purisubrhomboidea* Edwards, 1944, left valve, female, × 160, sample B–23–1P, USNM 380971.
7. *Loxoconcha matagordensis* Swain, 1955, left valve, female, × 130, sample F–20–1P, USNM 380972.
8. *Loxoconcha moralesi* Kontrovitz, 1976, left valve, male, × 110, sample B–21–1P, USNM 380970.

DEPARTMENT OF THE INTERIOR
U.S. GEOLOGICAL SURVEY

PROFESSIONAL PAPER 1328—C
PLATE 10

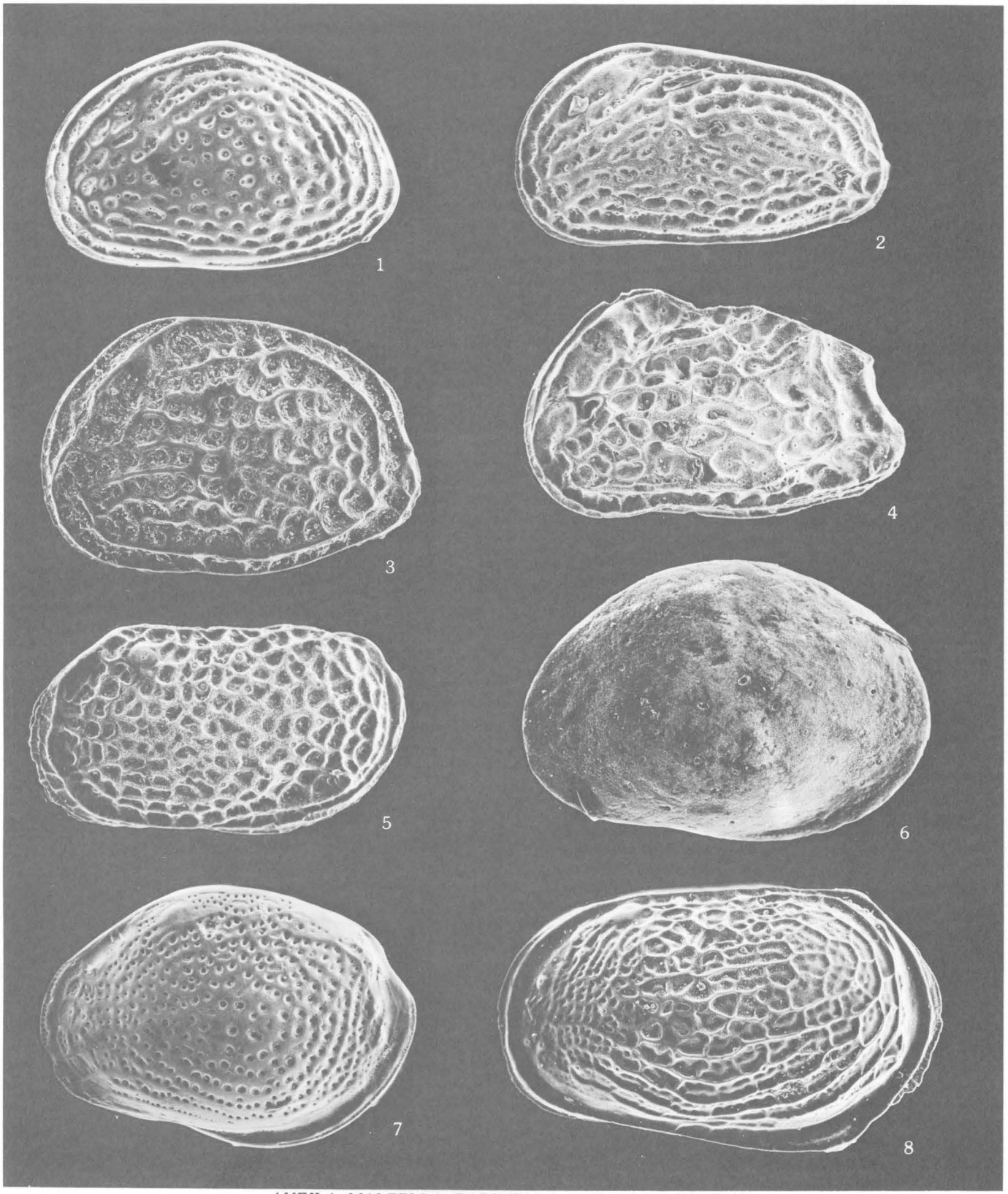

AURILA, MALZELLA, RADIMELLA, AND *LOXOCONCHA*

Petrology and Diagenesis of Late Quaternary Sands, South Texas Coastal Complex

By ROMEO M. FLORES *and* C. WILLIAM KEIGHIN

STRATIGRAPHIC STUDIES OF A
LATE QUATERNARY BARRIER-TYPE COASTAL COMPLEX,
MUSTANG ISLAND–CORPUS CHRISTI BAY AREA,
SOUTH TEXAS GULF COAST

U.S. GEOLOGICAL SURVEY PROFESSIONAL PAPER 1328–D

CONTENTS

ILLUSTRATIONS

TABLES

STRATIGRAPHIC STUDIES OF A LATE QUATERNARY BARRIER-TYPE COASTAL COMPLEX, MUSTANG ISLAND–CORPUS CHRISTI BAY AREA, SOUTH TEXAS GULF COAST

PETROLOGY AND DIAGENESIS OF LATE QUATERNARY SANDS, SOUTH TEXAS COASTAL COMPLEX

By ROMEO M. FLORES and C. WILLIAM KEIGHIN

ABSTRACT

Late Quaternary sand deposits of southern Mustang Island, northern Laguna Madre, southern Corpus Christi Bay, and the adjacent mainland, Texas, consist of arenites and subordinate wackes. Petrographic analyses, in conjunction with stratigraphic and paleontological studies, suggest that mature sands are typified by barrier-strandplain-type deposits and that immature sands are exemplified by fluvial-type deposits. A third, hybrid, sand type is mineralogically and texturally different from both these sand types. Statistical analyses show that the framework-grain compositions and matrix contents of all three sand types differ significantly from each other. However, only quartz, rock-fragment, and matrix contents are sufficiently environmentally sensitive to statistically differentiate barrier-strandplain, fluvial, and hybrid sand types. The barrier-strandplain sand type, which contains large amounts of quartz and subordinate amounts of rock fragments and matrix, represents recycled older coastal-plain deposits that were mechanically reworked by coastal processes during marine transgressions from late Pleistocene to modern time. The fluvial sand type, which contains significant amounts of rock fragments and matrix, represents first-cycle detritus derived mainly from a sedimentary terrane that was incised by the ancestral Nueces River system. The sedimentary rock fragments in the fluvial sands served as a source of matrix, which formed at the site of deposition by fragmentation due to compaction and which mechanically infiltrated voids in the sands.

Diagenetic features include effects of chemical diagenesis and subordinate physical diagenesis. Physical diagenesis consisted of fracturing and disaggregation of labile grains by compaction. Chemical diagenesis included cementation by sparry and micritic calcite and selective dissolution of feldspar and chert. Calcite cementation is the most common diagenetic feature that is pervasive in all sand types. Authigenic feldspar is a rare intergranular cement. Clay coats are common and probably formed by mechanical infiltration. Neogenetic mineralization, which took place after the cores were collected, consisted of precipitation of gypsum and halite from trapped saline pore water.

INTRODUCTION

The history of deposition on the coastal plain during the Pleistocene and Holocene in the northwestern Gulf of Mexico province is best described by Bernard and LeBlanc (1965). These workers indicated that the Pleistocene coastal plains consisted of four progressively older depositional surfaces representing interglacial stages. Each depositional surface was underlain by similar alluvial, deltaic, coastal interdeltaic (barrier-strandplain), and marine sequences. Each progressively younger Pleistocene coastal-plain sequence was underlain by deposits that formed the preceding coastal-plain sequence. These Pleistocene coastal-plain deposits in the Texas Gulf Coast were initially reported by Deussen (1924) and Barton (1930); their origin was explained by LeBlanc and Hodgson (1959). Most of the Pleistocene coastal-plain deposits of the South Texas Gulf Coast were described by Price (1958). In the study area (fig. 1), the Pleistocene and Holocene coastal-plain deposits were mapped in detail by the University of Texas Bureau of Economic Geology (Texas University Bureau of Economic Geology, 1974, 1975). Here, the coastal-plain deposits of late Pleistocene to Holocene age represent coalesced fluvial, deltaic, bay, and barrier-strandplain sediments.

Continuous cores of coastal-plain sediments were recovered from seven coreholes drilled on southern Mustang Island, in northern Laguna Madre, in southern Corpus Christi Bay, and on the adjacent mainland, Texas (fig. 1). As a part of the overall stratigraphic and

FIGURE 1.—Map showing locations of coreholes A–E, EE, and F in the southern Mustang Island–Corpus Christi Bay study area on the South Texas Gulf Coast.

paleontological study of these cores, a detailed petrographic investigation of six of the cores was performed in order to differentiate genetic sand types. In addition, diagenetic overprints and controlling conditions in diagenesis were studied to determine what relationships exist between sedimentary processes and the sand characteristics. Although energy conditions during sediment deposition vary within each environment, the differences in these energy conditions between the fluvial and barrier-strandplain environments have long been known to result in intrinsic differences in the mineral composition of the sedimentary deposits. Distinctive mineral compositions of these sediment types were taken as distinguishing characteristics of modern and ancient fluvial and barrier-strandplain deposits by Gibbons (1967) and Davies and Ethridge (1975). These authors suggested that the barrier-strandplain sands are more mature mineralogically than the fluvial deposits. That is, stable minerals such as quartz are concentrated in the barrier-strandplain deposits, and labile minerals are relatively more abundant in the fluvial deposits. This hypothesis was tested in this study of the Pleistocene and Holocene coastal-plain deposits of the study area.

METHODS

The unconsolidated sands required special handling in the laboratory analyses. In order to collect samples from the longitudinal core halves for thin-section analysis, a special cylindrical aluminum tube sampler, 3.8 cm in diameter and 12.7 cm in length, was constructed from a cake-icing dispenser. The cylinder was carefully inserted into the sand in order to minimize mechanical compaction. The sand samples were dried in a warm oven and impregnated with blue epoxy. One major difficulty in impregnating the samples was caused by the

lack of cohesiveness due to evaporation of trapped pore water between the sand grains and lack of cementation. Some samples required several impregnations; however, a few samples were not usable for analysis because of unsuccessful impregnation. Samples were collected from the top, middle, and base of each sand unit in cores A–D, EE, and F. From these samples, a total of 138 thin sections were prepared for petrographic analysis.

In order to standardize operator's bias, the thin sections were point counted by one person. Point counts were made after initial petrographic investigation showed that the mineral composition of the sands is mainly quartz (monocrystalline and polycrystalline), feldspars (microcline, orthoclase, and plagioclase), and rock fragments (sandstone, siltstone, mudstone, chert, chalcedony, limestone, and igneous and metamorphic rock fragments). Minor amounts of ostracode and foraminiferal tests and pelecypod fragments are present.

Two point counts were made on each thin section. One hundred points were counted for framework grains consisting of the varieties of quartz, feldspars, and rock fragments. An additional one hundred points were counted and included all framework grains, matrix, and cement. Points that fell on interstitial voids, ostracode and foraminiferal tests, and pelecypod fragments were not counted, although the presence of the fossils was noted.

Separate sand samples for scanning-electron microscopy (SEM) and X-ray diffraction (XRD) analysis were collected from the same stratigraphic intervals in the cores from which the petrographic samples were acquired. Relatively undisturbed samples for SEM and XRD work were collected in shallow aluminum caps 2.5 cm in diameter and 0.6 cm in depth. The SEM samples were coated with gold and palladium and examined by use of a Cambridge 180[1] scanning-electron microscope. The 10-g samples of each sand unit collected for XRD analysis were dried, powdered, pressed into cellulose-backed pellets, and analyzed for mineralogy.

Statistical analyses were performed on the point-count data in order to establish a meaningful quantitative differentiation of the mineral contents of the sand types. One-way analysis of variance (Snedecor, 1956) was used to differentiate the framework-grain compositions and matrix contents of the sand types. An additional statistical test, a t-test, provided specific differentiation of the quartz, rock-fragment, and matrix contents of the sand types.

[1]Any use of trade names in this report is for descriptive purposes only and does not constitute endorsement by the U.S. Geological Survey.

PETROLOGY

FRAMEWORK MINERALS

The framework grains (fig. 2) of the sands in the study area consist of, in descending order of abundance, quartz, rock fragments, and feldspar. These framework-grain categories and their mineral varieties are described below.

Quartz.—Quartz grains are elongate, are rounded to subangular, and display straight to strongly undulose extinction. Both monocrystalline and polycrystalline quartz grains are present. As indicated by the terminology, a monocrystalline grain consists of a single quartz crystal, and a polycrystalline grain contains microscopic aggregates of quartz crystals. The polycrystalline aggregates show sutured intercrystalline boundaries and unimodal to polymodal size distributions. The polycrystalline-quartz variety does not include chert and chalcedony. Monocrystalline quartz, which is the more abundant of the two varieties, contains traces of randomly scattered vacuoles and rutile needles. A few monocrystalline quartz grains contain local embayments. The point counts show that quartz makes up 57–92 percent of the framework grains.

Feldspar.—Feldspar grains are somewhat elongate, subrounded to angular, and twinned; they consist of microcline, orthoclase, and plagioclase. The microcline has the common grid structure, and the plagioclase displays albite and pericline twinning. The plagioclase grains are commonly altered, whereas the microcline and orthoclase grains are typically fresh or slightly

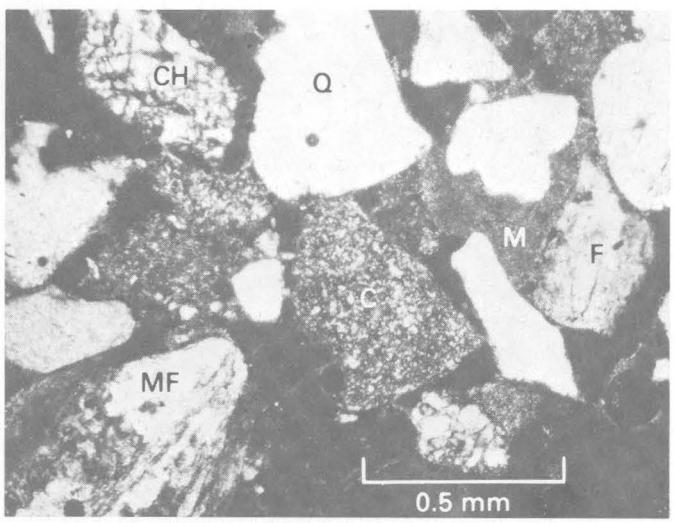

FIGURE 2.—Photomicrograph showing framework grains common in sands from the study area. Q, quartz; F, orthoclase; C, chert; CH, chalcedony; and MF, metamorphic rock fragment. Matrix (M) partially fills voids between the framework grains.

altered. The orthoclase grains are more common than both the microcline and plagioclase grains. The point counts show that feldspar makes up 0–22 percent of the framework grains.

Rock fragments.—Rock fragments are elongate and rounded to angular and are variable in composition. Most abundant are sedimentary rock fragments that include grains of sandstone, siltstone, mudstone, chert, chalcedony, and limestone. Of these, chert is the most abundant grain. The sandstone grains consist of aggregates of very fine grains of rounded to subangular quartz cemented by silica overgrowth and calcite and partly surrounded by clay matrix; particles in the clay matrix have diameters of less than 2 μm. The siltstone fragments are made up of aggregates of silt-sized grains of subrounded to angular quartz supported by micaceous particles 2–50 μm in diameter and clay particles less than 2 μm in diameter. The mudstone grains are rounded to angular fragments that consist of a few coarse clay-sized particles floating in an organic-matter-rich micaceous and clayey paste. Chert grains are rounded to subangular and contain microcrystalline quartz and chalcedony spherules. A few microcrystalline dolomite rhombs occur as inclusions in some of the chert grains. Chalcedony grains are subrounded to subangular and consist of microscopic, fibrous quartz that occurs in concentric lamellae. Limestone grains are rounded to angular fragments and consist of sparry to micritic calcite. The point counts show that sedimentary rock fragments make up 0–36 percent of the framework grains.

Traces of subrounded to subangular metamorphic and igneous rock fragments are present in the sands. The metamorphic variety, which is the more common of the two, is composed of schist, gneiss, and quartz-mica aggregates. The igneous rock fragments consist of aggregates of (1) intergrown lath-shaped feldspars; (2) quartz, feldspar, and mica; and (3) quartz and feldspar. Metamorphic and igneous rock fragments make up 0–6 percent of the framework grains.

MATRIX MINERALS

Matrix is present in about 50 percent of the total number of sand units. Where matrix is present, it is as much as 32 percent. The matrix includes clay- and silt-sized quartz, allogenic sparry and micritic calcite, clay minerals, and micaceous minerals. Some matrix contains abundant organic matter and behaves as isotropic material. The quartz matrix was derived mainly from aggregates of fragmented sandstone and siltstone grains during compaction. However, some quartz matrix may have been transported and primarily derived from the source area. The origin of the sparry and micritic calcite may have been similar to the origin of the quartz matrix. The clay minerals, which were identified by both petrographic and XRD analysis, include kaolinite, illite, and mixed-layer illite-smectite. In samples analyzed by XRD, kaolinite is the most common clay mineral. Diffractograms showing the peak distributions of these various clay minerals and other minerals are shown in figure 3. The micaceous minerals in the matrix are sericite, chlorite, and muscovite. These minerals occur as masses of interlocking crystals and books of flakes or platelets that fill intergranular voids.

The matrix minerals occur either as local patches (fig. 4) or as widespread void fillings (fig. 5) between framework grains. The intergranular debris is of both primary and secondary origin. That is, some of the quartz, calcite, and other grains composing the matrix were transported along with the framework grains from the source area, and some were derived at the site of deposition from mechanical fragmentation of sedimentary rock fragments such as siltstone, mudstone, and limestone. The common occurrence of sedimentary rock fragments that show various degrees of deformation and breakage (figs. 6, 7) and the mineralogical similarity of broken and unbroken fragments indicate that the most common origin of the matrix in the sands was mechanical fragmentation of detrital grains. The mechanism of crushing and fragmentation of soft detrital grains was probably compaction; the resulting matrix material mechanically infiltrated intergranular voids. Squeezing between grains during compaction and movement by interstitial waters are means by which the matrix material may have been transported within the sediments. Another method of forming matrix in place was leaching of feldspar (fig. 8) and chert grains. Disaggregation by leaching of feldspar and chert grains produced silt-sized grains that contributed to the intergranular matrix.

DIAGENETIC MINERALS

Although some of the sands show clear evidence of modification, diagenesis has not been a major factor. This lack of significant diagenesis is probably a result of the shallow burial and youth of the sediments, which preclude high confining pressure, high temperature, and a long duration of interstitial fluid movement. However, the sands that were buried to about 60 m may have been compacted somewhat and exposed to interstitial waters; they contain some minerals that may be early diagenetic chemical precipitates like those described by Pettijohn and others (1972). Some compaction of the sands is indicated by deformed or disaggregated labile grains, strained or fractured grains, and sutured contacts (see preceding section, "Matrix Minerals," and figs. 6 and 7). Evidence for

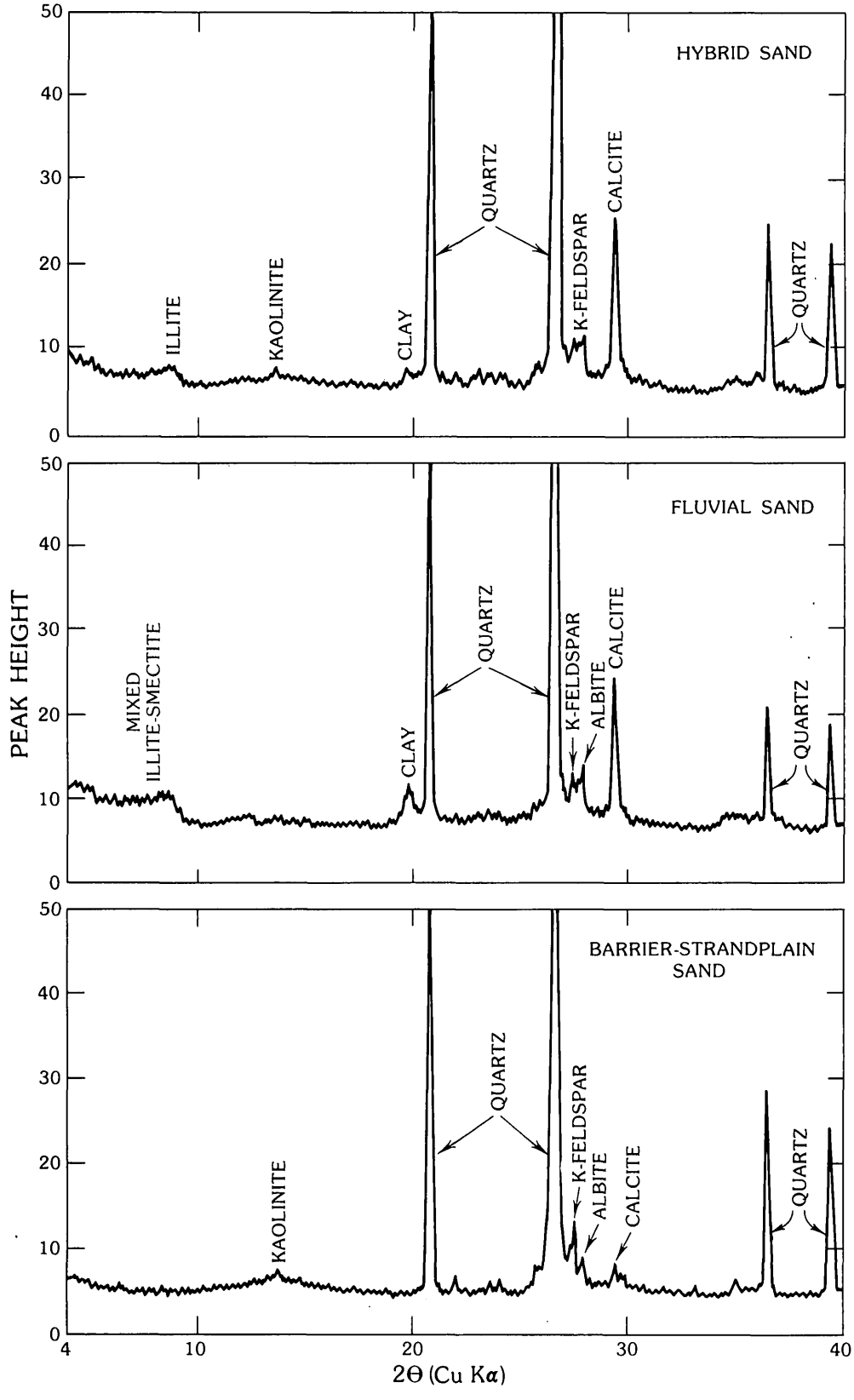

FIGURE 3.—X-ray diffraction patterns of the hybrid, fluvial, and barrier-strandplain sand types.

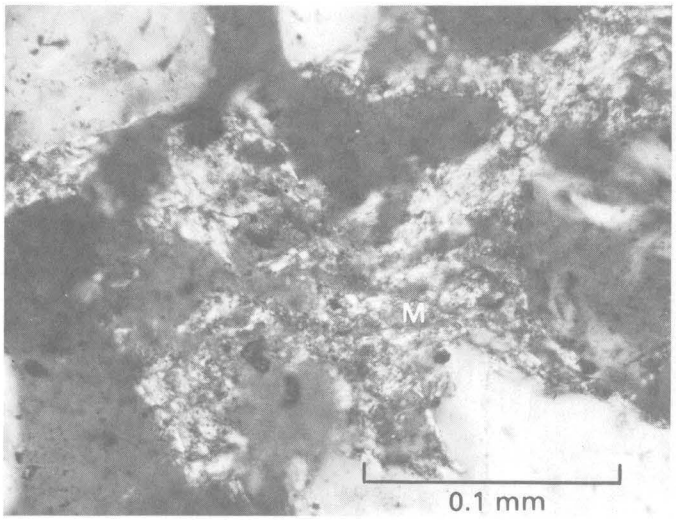

FIGURE 4.—Photomicrograph showing an example of the patchy distribution of matrix (M).

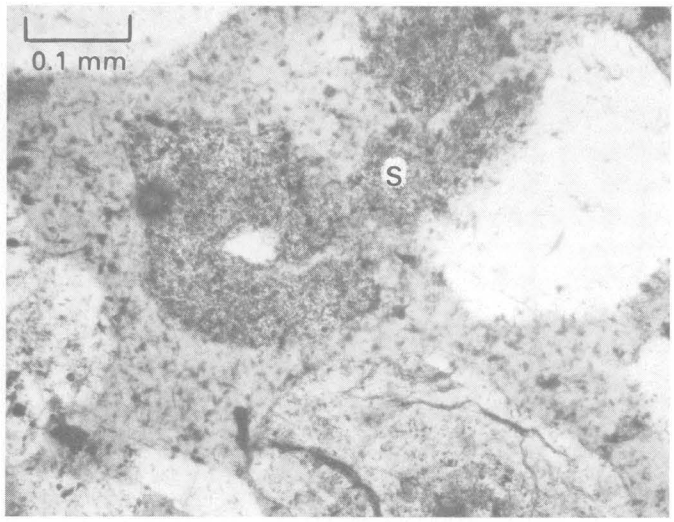

FIGURE 6.—Photomicrograph showing a fragmented detrital shale (S) grain.

chemical diagenesis of the sands is more extensive than that for physical diagenesis but is still not very common.

The most obvious chemical precipitates in the sands are early carbonate cements and feldspar overgrowths and late-stage (postcoring) halite and gypsum. Carbonate cement in the form of sparry and micritic calcite probably represents an early diagenetic product. Sparry calcite cement is locally abundant and completely encloses some detrital grains (fig. 9). Evidence of sparry calcite partially replacing detrital quartz and feldspar grains was seen only rarely. The widespread cementation of a few sands by sparry calcite was probably a result of primary precipitation during prolonged exposure to carbonate-supersaturated seawater. The existence of modern carbonate precipitation near the study area in Baffin Bay and Laguna Madre, Tex., has been documented by Rusnak (1960), Freeman (1962), and Land and others (1979). The sparry calcite cement is not as common as micrite cement.

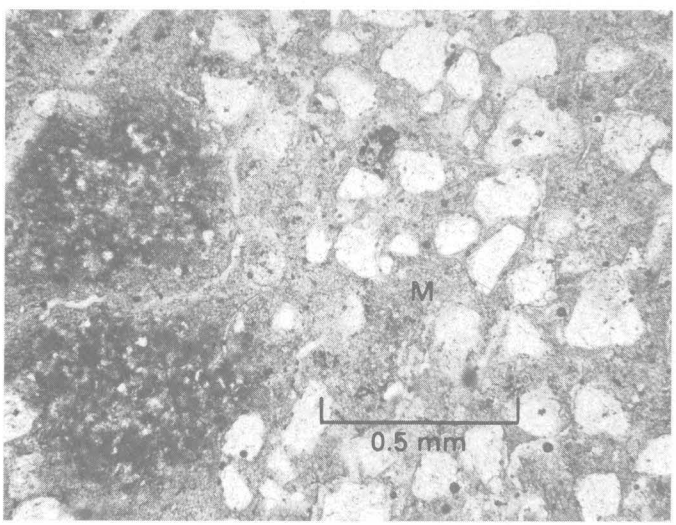

FIGURE 5.—Photomicrograph showing an example of widespread distribution of matrix (M) rich in organic matter.

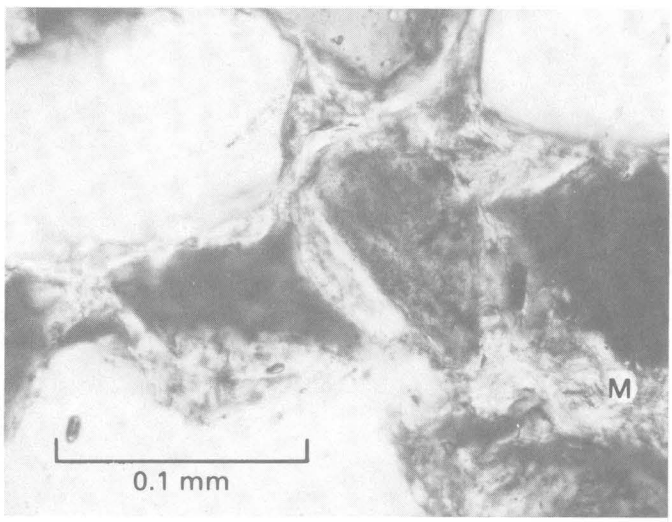

FIGURE 7.—Photomicrograph showing a detrital micaceous (M) fragment, varying degrees of crushing by adjoining framework grains, and the infiltration of crushed material into nearby voids as secondary matrix.

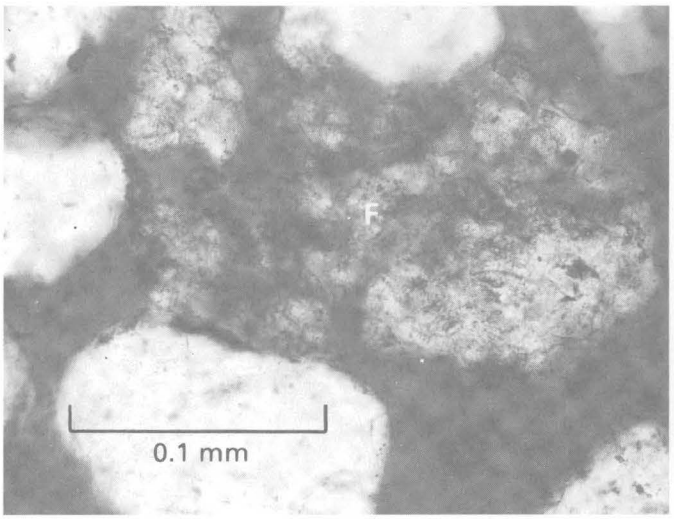

FIGURE 8.—Photomicrograph showing a feldspar (F) grain that has undergone leaching and subsequent fragmentation to become a source of matrix material.

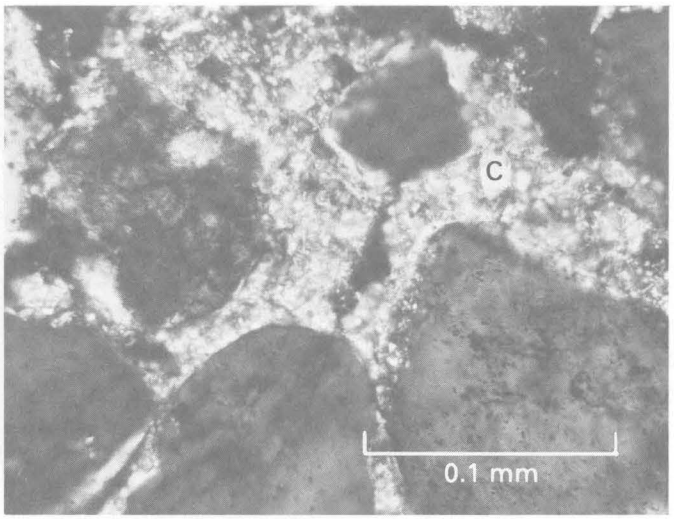

FIGURE 10.—Photomicrograph showing microcrystalline (micritic) calcite (C) cementing rounded framework grains.

Micrite cement occurs locally and commonly partly encloses detrital grains (fig. 10). Most of the micrite-cemented sands contain foraminiferal tests and pelecypod fragments. This association suggests partial dissolution of the skeletal calcite by pore water and reprecipitation of calcite as micrite cement. In some sands in which no skeletal materials were observed and in which micritic calcite cement was present, dissolution of allogenic carbonates may have served as a source of authigenic cement. The dissolution of carbonate shells and allogenic carbonates probably was enhanced by decomposition of organic matter. Kühn (1948) suggested that microcrystalline or micritic to cryptocrystalline carbonate cement was usually a fast-growing and early diagenetic feature. Heling (1963) proposed that macrocrystalline or sparry calcite cement was a much later diagenetic feature.

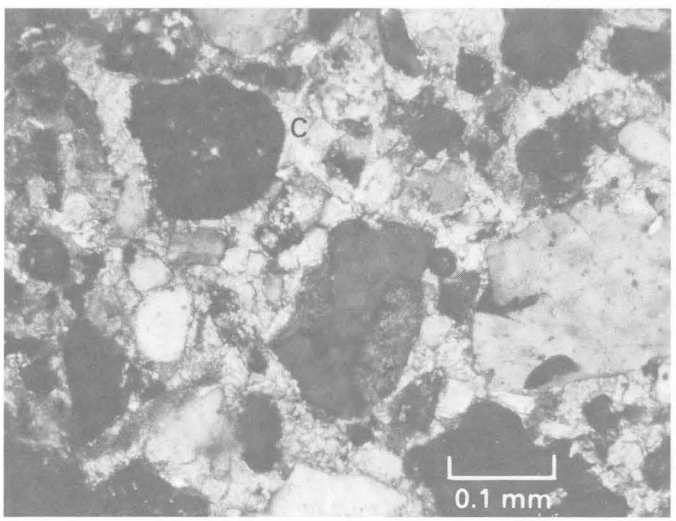

FIGURE 9.—Photomicrograph showing abundant sparry calcite (C) cementing subrounded framework grains.

Feldspar neoformation has taken place in the form of dissolution and overgrowth on detrital feldspar grains. Some detrital grains (fig. 11*A*) show evidence of dissolution that can be attributed to postdepositional processes. The shallow burial of the sediments favors dissolution of isolated feldspar minerals (Heald and Larese, 1973; Walker and others, 1978) similar to the intrastratal solution of heavy minerals proposed by Pettijohn (1957), rather than to pressure-induced dissolution. Dissolution resulted from leaching by interstitial waters. The dissolution of feldspar minerals may have served as a source for material that, in turn, precipitated in intergranular voids. This process formed rarely observed intergranular authigenic feldspar cement as shown in figure 11*B*. The feldspar overgrowth illustrated in figure 11*B* appears to be an early generation that was partially dissolved after transportation to its present site. The euhedral authigenic feldspar shown in figure 11*F* clearly grew in an open intergranular area and acts as a cement.

Authigenic clay coats of detrital grains are common in some Holocene sediments (Burns and Ethridge, 1979), in Tertiary sandstones (Galloway, 1974), and in continental red beds (Walker, 1976; Walker and others, 1978). The few clay coats observed by SEM (fig. 11*C*) were not authigenic. Petrographic observation (fig. 12) showed that clay coats partially surrounding detrital grains are micaceous flakes that generally are oriented parallel to the detrital-grain surface. Rarely, clay coats were observed petrographically as microcrystalline flakes oriented at an angle or perpendicular to the

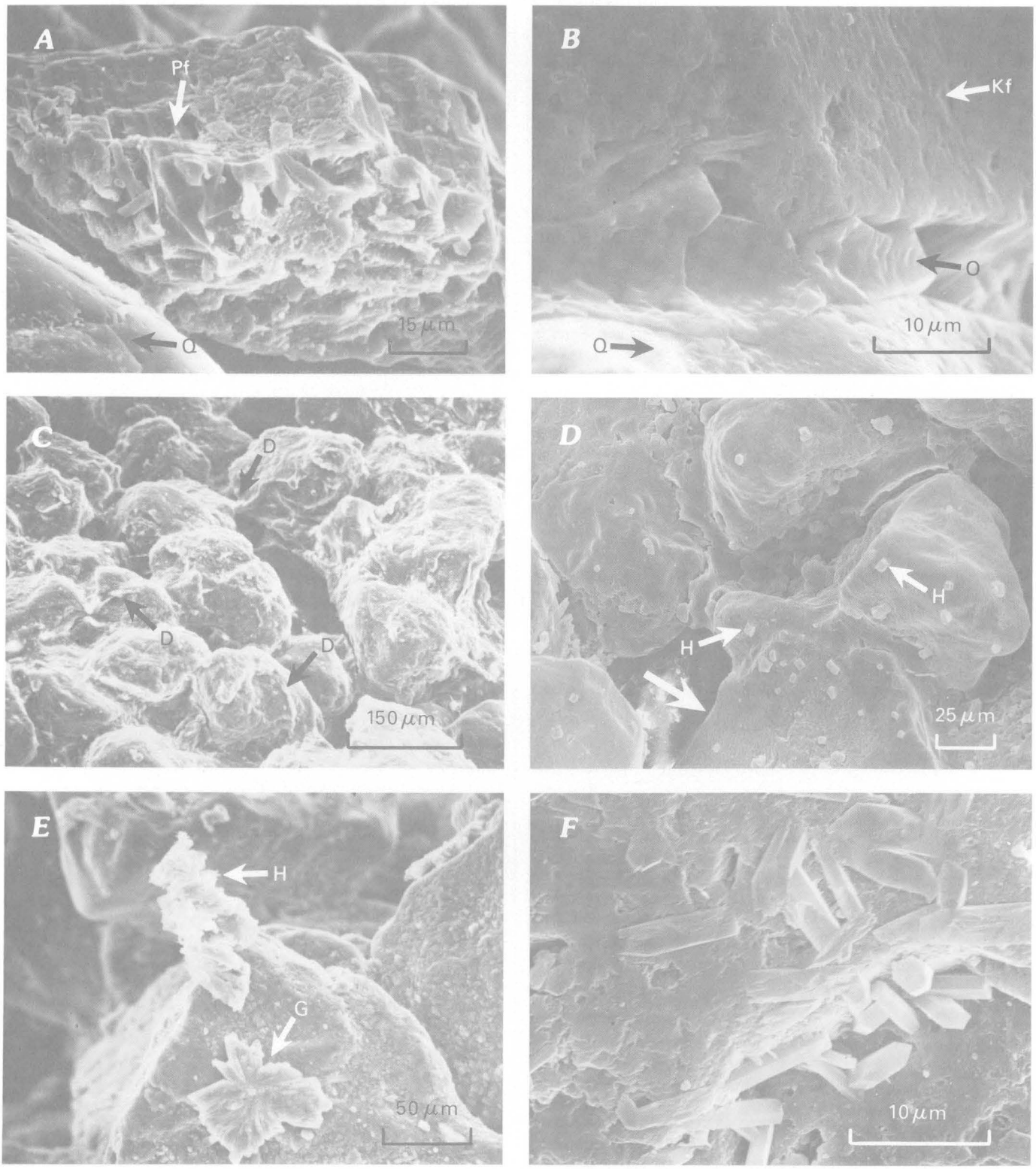

FIGURE 11.—SEM photomicrographs of detrital, matrix, and neogenetic minerals. *A*, Partially leached detrital Ca-plagioclase (Pf) and rounded detrital quartz (Q). *B*, Overgrowth of K-feldspar (O) acting as a cement between detrital K-feldspar (Kf) and detrital quartz (Q). Morphology indicates postdepositional leaching and suggests that the cemented grain shown is allogenic. *C*, Detrital clay (D) coating allogenic grains. *D*, Neogenetic halite (H) precipitated from evaporated pore water; note composite nature of grain (large arrow). *E*, Neogenetic gypsum (G) and halite (H) precipitated from pore water. Delicate nature of these minerals indicates that they were not mechanically transported. *F*, Unusually abundant authigenic feldspar(s?) formed on and between detrital grains.

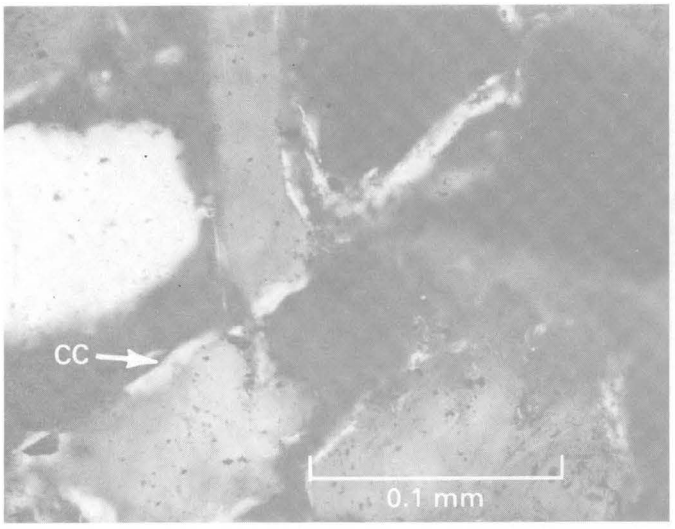

FIGURE 12.—Photomicrograph showing clay coats (CC) that partially surround quartz grains.

detrital-grain surface. These clay coats appear to have formed mainly by physical infiltration although some authigenic formation is possible.

NEOGENETIC MINERALS

Formation of neogenetic minerals is attributed to precipitation resulting from evaporation of trapped saline pore water after the cores were collected. The presence of these minerals in all sand types suggests that saline pore water is common in these fluvial-marine transition deposits. The most common neogenetic minerals are gypsum and halite. These minerals are not ubiquitous but are commonly sufficiently abundant to be detected by SEM and XRD; however, they were not detectable by examining thin sections under a petrographic microscope. The modes of occurrence (for example, partial to total coating of grain surfaces as shown in figs. 11*D*, *E*) and delicate crystal morphology (fig. 11*E*) of the minerals clearly indicate neogenetic growth.

PETROGRAPHIC CLASSIFICATION AND GENETIC DIFFERENTIATION

The petrographic classification of the late Quaternary sands was based on the framework-mineral composition and matrix content as described by Pettijohn and others (1972). The classification of the sands on the basis of their matrix content shows that 75 percent are arenites (less than 15 percent matrix) and 25 percent are wackes (greater than 15 percent matrix). The arenites were classified on the upper ternary diagram in figure 13 as quartz arenite (one sample), sublitharenites (46 percent), subarkoses (18 percent), and lithic arenites (10 percent). The wackes were classified on the lower ternary diagram in figure 13 as lithic graywackes (17 percent) and feldspathic graywackes (8 percent). Thus, on the basis of the matrix content, most of the sands are arenites that show a high textural maturity. The grain/matrix ratio of the arenites is 9.8 to 1. This ratio, however, is only a partial measure of the textural maturity of the sands, which, according to Folk (1951), also includes sorting and roundness of quartz grains.

The concept of mineralogical maturity of recent sands or ancient sandstones stems from the idea that progressive elimination and segregation by weathering and transport of unstable minerals result in an end product that is composed largely of stable minerals. Pettijohn (1957) defined the compositional maturity of sandstones as being inversely proportional to the frequency of those mineral constituents that are sensitive to transport, abrasion, and weathering. Thus, compositional maturity is best described by the ratio of quartz to feldspars plus rock fragments. On the whole, the compositional-maturity index of the late Quaternary sands is 3.5, which is greater than the index for lithic sandstones and approaches the index for quartzite, as described by Pettijohn (1957). Thus, the trend towards quartzose characteristics of the sands indicates moderately high mineralogical maturity.

The mineralogical maturity of the sands is a product of the intensity of modifying processes of erosion, transportation, and deposition as well as the length of time that the sands were exposed to these processes. As suggested by Folk (1951) and Keller (1954), if the processes have a high intensity and last a long time, then the end product will be mature. Thus, the moderately high mineralogical maturity of the sands suggests that they underwent intensive and prolonged process modification. In addition, the mineralogical maturity of the sands may reflect the number of times the framework grains have been recycled, each cycle contributing to the progressive loss of unstable framework components. This recycling appears to have been a significant contributing factor to the moderately high mineralogical maturity of the sands, as indicated by the abundance of sedimentary rock fragments composing the framework of the sands.

Perhaps the textural and mineralogical maturity of the sands is best expressed in the differences between genetic types. The environmental-stratigraphic framework of the study area (see Shideler, Chap. B, this volume), constructed on the basis of seismic and lithostratigraphic characteristics, as well as paleontological data (see Cronin, Chap. C, this volume), suggests that the sediments were deposited in two major environmental complexes—fluvial-deltaic and barrier-strandplain (marine-eolian) complexes. On the basis of

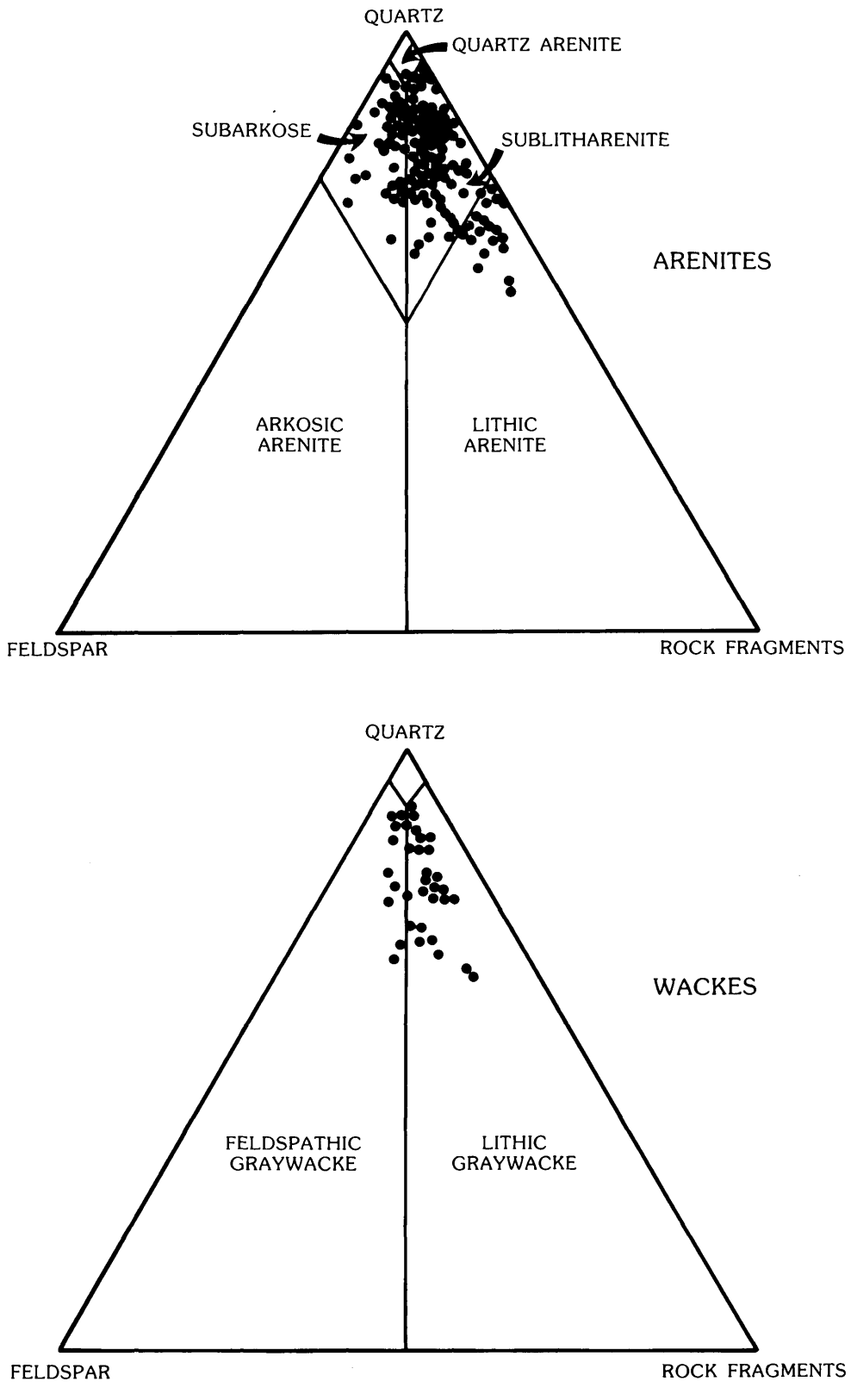

FIGURE 13.—Ternary diagrams of wackes and arenites showing petrographic classification of individual sand samples.

the salinity tolerance of the ostracode fauna, Cronin presented the following paleosalinity regimes for deposits of the study area: freshwater-fluvial, upper bay, mid-bay, lower bay-inlet, and sublittoral regimes. Deposits from specific paleoenvironments associated with these regimes, such as channel sands, were identified by Shideler on the basis of their seismic and lithostratigraphic properties. Thus, on the basis of stratigraphy, biological associations, and analogies with areal distributions of modern deposits, the core sands can be divided into three genetic types—barrier-strandplain, fluvial, and hybrid sands. The barrier-strandplain sands are elongate bodies that formed parallel to the shoreline, are very fine to fine grained, and generally contain a marine fauna. The fluvial sands are lenticular bodies formed landward of associated barrier-strandplain deposits, are generally medium grained, and either contain a freshwater fauna or are barren of organisms. The hybrid sands are deposits that formed under the influence of both fluvial and marine processes (for example, undifferentiated lagoon, bayfill, bayhead delta, and back-barrier deposits) and that do not belong in the first two categories. In addition, the hybrid sands may represent relatively dirty barrier shoreface deposits or clean fluvial deposits that could not be clearly differentiated by mineral composition. The petrographic and genetic sand types of the thin sections examined in this study are summarized in table 1.

The triangular plots (fig. 14) of all sand framework-compositional data show some variations among the barrier-strandplain, fluvial, and hybrid sand types; however, plots of all genetic types show areas of considerable overlap. The fluvial and hybrid sand types both occur as arenites and wackes; with one exception, the barrier-strandplain sand type occurs only as arenites. Fifty-five percent of the plot of the hybrid arenites overlaps the plot of the barrier-strandplain sand type. Forty-eight percent of the plot of the fluvial arenites overlaps the plot of the barrier-strandplain sand type.

Visual examination of the data on the mean framework composition (table 2) of all the genetic sand types shows that the barrier-strandplain sand is more quartzose than the fluvial and hybrid sands; the fluvial sand type contains the least amount of quartz. The fluvial and hybrid sand types contain more rock fragments than does the barrier-strandplain sand. The hybrid sand contains slightly more feldspar than do the fluvial and barrier-strandplain sands. The matrix contents of the sand types also differ. The barrier-strandplain sand contains the least amount of matrix; the fluvial and hybrid sands contain equal amounts of matrix. Thus, the framework mineralogy and matrix content of the hybrid sand appear to be more closely

TABLE 1.—*Petrographic and genetic sand types of the 138 thin sections examined from cores of the study area*

[Samples were collected from the upper, middle, and lower parts of each sand unit in cores A–D, EE, and F. From these samples, 138 thin sections were prepared for petrographic analyses. The unit numbers are shown in the lithologic logs of the cores in Chapter B, this volume, pls. 3–6, 8–9, in pocket]

Thin section	Origin of material in thin section		Depth below surface (meters)	Petrographic sand type	Genetic sand type
	Unit No.	Part of the unit			
Core A					
A–10	31	Upper	11.4	Wacke	Hybrid.
A–11	31	Middle	13.8	Wacke	Hybrid.
A–12	31	Lower	14.7	Arenite	Hybrid.
A–23a	21	Upper	28.8	Wacke	Hybrid.
A–23b	20	Upper	29.9	Wacke	Hybrid.
A–23c	20	Middle	30.8	Wacke	Hybrid.
A–25	18	Upper	32.0	Arenite	Hybrid.
A–41	5	Upper	50.8	Arenite	Fluvial.
A–42a	5	Middle	51.4	Arenite	Fluvial.
A–42b	5	Lower	51.9	Arenite	Fluvial.
A–43	4	Middle	53.0	Arenite	Fluvial.
A–44	3	Upper	53.7	Arenite	Fluvial.
Core B					
B–2a	57	Middle	2.0	Arenite	Barrier-strandplain.
B–2b	57	Middle	2.6	Wacke	Barrier-strandplain.
B–3	57	Lower	3.3	Arenite	Barrier-strandplain.
B–6a	53	Middle	7.5	Arenite	Hybrid.
B–6b	52	Middle	8.1	Arenite	Hybrid.
B–6c	51	Middle	8.6	Arenite	Hybrid.
B–6d	50	Upper	8.9	Arenite	Hybrid.
B–7a	50	Middle	9.4	Arenite	Hybrid.
B–7b	50	Lower	9.8	Arenite	Hybrid.
B–9	49	Lower	12.6	Wacke	Hybrid.
B–10a	48	Upper	12.8	Wacke	Fluvial.
B–10b	48	Lower	13.3	Wacke	Fluvial.
B–10c	47	Middle	13.8	Wacke	Fluvial.
B–11a	45	Middle	14.8	Arenite	Hybrid.
B–11b	44	Upper	15.2	Wacke	Hybrid.
B–11c	44	Lower	15.6	Arenite	Hybrid.
B–12a	42	Upper	16.8	Arenite	Hybrid.
B–12b	42	Lower	16.9	Wacke	Hybrid.
B–12c	41	Upper	17.0	Arenite	Hybrid.
B–13a	39	Upper	17.9	Arenite	Hybrid.
B–13b	37	Upper	18.7	Arenite	Hybrid.
B–13c	35	Upper	19.6	Arenite	Hybrid.
B–14	31	Upper	22.5	Arenite	Hybrid.
B–16	31	Middle	23.2	Arenite	Hybrid.
B–20	31	Lower	24.3	Wacke	Hybrid.
B–26a	23	Upper	35.1	Arenite	Hybrid.
B–26b	23	Lower	35.2	Wacke	Hybrid.
B–26c	21	Middle	35.7	Arenite	Hybrid.
B–38	11	Upper	48.4	Arenite	Hybrid.
B–40	11	Middle	49.8	Arenite	Hybrid.
B–43	11	Lower	51.9	Arenite	Hybrid.
B–48a	2	Upper	60.1	Arenite	Hybrid.
B–48b	2	Middle	60.3	Wacke	Hybrid.
B–49	2	Lower	60.5	Wacke	Hybrid.

TABLE 1.—*Petrographic and genetic sand types of the 138 thin sections examined from cores of the study area*—Continued

Thin section	Origin of material in thin section: Unit No.	Origin of material in thin section: Part of the unit	Depth below surface (meters)	Petrographic sand type	Genetic sand type
Core C					
C–4a	4	Upper	2.9	Arenite	Hybrid.
C–4b	4	Middle	4.1	Arenite	Hybrid.
C–5	4	Middle	5.3	Wacke	Hybrid.
Core D					
D–1	63	Middle	0.7	Arenite	Hybrid.
D–2	63	Lower	1.3	Arenite	Hybrid.
D–3	62	Lower	2.1	Arenite	Hybrid.
D–4a	60	Lower	4.2	Arenite	Hybrid.
D–4b	58	Upper	5.0	Wacke	Hybrid.
D–6	58	Lower	5.5	Wacke	Hybrid.
D–7	56	Upper	6.3	Wacke	Hybrid.
B–8a	55	Middle	7.8	Arenite	Hybrid.
D–8b	54	Upper	8.9	Arenite	Hybrid.
D–8c	54	Lower	10.6	Wacke	Hybrid.
D–11	49	Upper	14.5	Wacke	Hybrid.
D–12	48	Middle	15.9	Arenite	Hybrid.
D–15	47	Upper	16.8	Arenite	Hybrid.
D–16	43	Upper	19.6	Arenite	Fluvial.
D–17	43	Lower	20.3	Arenite	Fluvial.
D–18	40	Middle	21.1	Arenite	Fluvial.
D–19a	39	Middle	21.3	Arenite	Fluvial.
D–19b	38	Lower	22.0	Arenite	Fluvial.
D–20a	37	Middle	23.0	Arenite	Hybrid.
D–20b	37	Lower	23.9	Arenite	Hybrid.
D–29	26	Upper	34.9	Arenite	Hybrid.
D–30	26	Middle	36.0	Arenite	Fluvial.
D–32	26	Lower	37.3	Arenite	Fluvial.
D–34	24	Upper	38.2	Arenite	Hybrid.
D–35	23	Upper	38.8	Arenite	Hybrid.
D–36	23	Middle	39.4	Wacke	Hybrid.
D–40	12	Upper	48.2	Wacke	Fluvial.
D–43	12	Middle	50.7	Arenite	Fluvial.
D–46	12	Lower	53.6	Arenite	Fluvial.
D–48a	10	Upper	54.1	Arenite	Hybrid.
D–48b	10	Lower	54.7	Arenite	Hybrid.
D–49	5	Upper	57.0	Wacke	Hybrid.
D–50	5	Lower	58.3	Arenite	Hybrid.
Core EE					
EE–1a	43	Upper	0.2	Arenite	Hybrid.
EE–1b	43	Upper	.6	Arenite	Hybrid.
EE–1c	43	Upper	1.1	Arenite	Hybrid.
EE–7	43	Middle	2.5	Arenite	Hybrid.
EE–8	43	Lower	3.2	Arenite	Hybrid.
EE–9	41	Upper	4.2	Arenite	Hybrid.
EE–10	40	Upper	5.3	Arenite	Hybrid.
EE–11a	40	Upper	6.0	Arenite	Hybrid.
EE–11b	40	Middle	6.7	Arenite	Hybrid.
EE–12a	40	Lower	7.6	Wacke	Hybrid.

TABLE 1.—*Petrographic and genetic sand types of the 138 thin sections examined from cores of the study area*—Continued

Thin section	Origin of material in thin section: Unit No.	Origin of material in thin section: Part of the unit	Depth below surface (meters)	Petrographic sand type	Genetic sand type
Core EE—Continued					
EE–12b	39	Upper	8.0	Arenite	Hybrid.
EE–12c	39	Upper	8.5	Arenite	Hybrid.
EE–13a	37	Upper	12.3	Arenite	Hybrid.
EE–13b	37	Upper	13.0	Arenite	Hybrid.
EE–13c	37	Upper	13.9	Arenite	Hybrid.
EE–15	37	Middle	15.4	Arenite	Hybrid.
EE–17	37	Middle	16.1	Arenite	Hybrid.
EE–18	37	Lower	18.2	Arenite	Hybrid.
EE–21a	35	Middle	20.1	Arenite	Hybrid.
EE–21b	35	Lower	20.5	Arenite	Hybrid.
EE–21c	35	Lower	20.8	Arenite	Hybrid.
EE–26a	31	Upper	24.0	Arenite	Hybrid.
EE–26b	31	Middle	24.5	Arenite	Hybrid.
EE–26c	30	Upper	25.0	Wacke	Hybrid.
EE–26d	30	Lower	26.0	Wacke	Hybrid.
EE–36	28	Lower	32.6	Wacke	Hybrid.
EE–43	7	Upper	55.1	Arenite	Fluvial.
EE–47	4	Middle	57.8	Arenite	Fluvial.
EE–49	1	Middle	60.9	Wacke	Fluvial.
Core F					
F–1	42	Upper	0.1	Arenite	Barrier-strandplain.
F–5	39	Middle	7.1	Arenite	Barrier-strandplain.
F–9a	38	Upper	11.7	Arenite	Barrier-strandplain.
F–9b	38	Middle	12.9	Arenite	Barrier-strandplain.
F–10	38	Middle	13.5	Arenite	Barrier-strandplain.
F–11	38	Middle	16.0	Arenite	Barrier-strandplain.
F–12	38	Lower	18.8	Arenite	Barrier-strandplain.
F–15	38	Lower	20.9	Arenite	Barrier-strandplain.
F–16	36	Middle	23.5	Arenite	Barrier-strandplain.
F–18	35	Upper	23.9	Arenite	Barrier-strandplain.
F–19	34	Upper	25.4	Arenite	Barrier-strandplain.
F–21	34	Lower	28.4	Arenite	Barrier-strandplain.
F–29	21	Middle	39.7	Arenite	Fluvial.
F–31	21	Lower	40.0	Arenite	Fluvial.
F–32	21	Lower	40.2	Arenite	Fluvial.
F–34	17	Middle	41.3	Arenite	Fluvial.
F–36	16	Middle	42.4	Arenite	Fluvial.
F–37	15	Middle	43.0	Arenite	Fluvial.
F–39	12	Upper	44.8	Arenite	Fluvial.
F–40	12	Middle	46.5	Arenite	Fluvial.
F–44a	9	Lower	52.6	Wacke	Fluvial.
F–44b	8	Lower	53.4	Wacke	Fluvial.
F–45	6	Upper	53.9	Wacke	Fluvial.
F–47	4	Upper	55.1	Arenite	Fluvial.
F–50	4	Middle	56.0	Wacke	Fluvial.
F–52a	2	Middle	60.8	Arenite	Hybrid.
F–52b	1	Middle	61.1	Wacke	Hybrid.

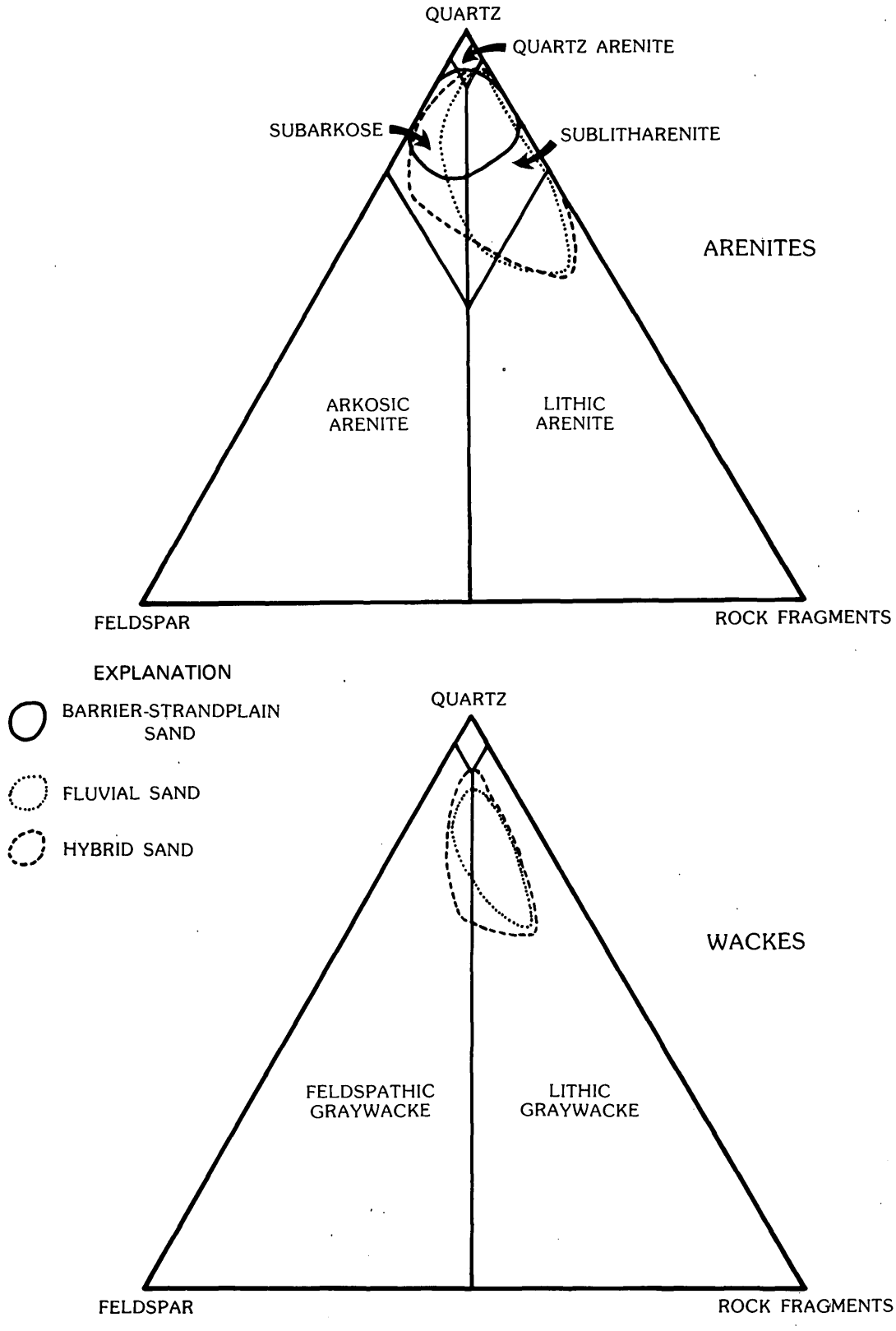

FIGURE 14.—Ternary diagrams of wackes and arenites showing petrographic classification of samples grouped as barrier-strandplain, fluvial, and hybrid sand types.

TABLE 2.—*Mean compositions of coastal-plain sands in the study area*

[All values are mean percentages determined by point counts]

Sands	Framework composition			Whole-sand composition		
	Quartz	Feldspar	Rock fragments	Matrix	Cement	Framework grains
All sands	77	9	14	8	13	79
Arenites and wackes:						
Barrier-strandplain	83	8	9	1	13	86
Fluvial	74	8	18	9	12	79
Hybrid	77	10	13	9	13	78
Arenites:						
Barrier-strandplain	83	8	9	1	13	86
Fluvial	75	7	18	4	14	82
Hybrid	78	9	13	6	13	81

related to those of the fluvial sand than to those of the barrier-strandplain sand. The test of significance of these mineralogical and textural differences among all three sand types was performed statistically. One statistical analysis tested the differences of these parameters among all sand types of combined arenites and wackes. A second statistical analysis tested the differences of the same parameters among all sand types of only the arenites.

An analysis of variance (table 3) among the barrier-strandplain, fluvial, and hybrid sand types of combined arenites and wackes showed a significant difference in their quartz, feldspar, rock-fragment, and matrix contents. However, an analysis of variance (table 4) among the barrier-strandplain, fluvial, and hybrid sand types of only the arenites showed no significant difference in the same framework and matrix constituents. Visual examination of the mean percentages (table 2) of these constituents of the sand types in the combined arenites and wackes shows that both fluvial and hybrid sand types contain more rock fragments and matrix than does the barrier-strandplain sand type. In contrast, the barrier-strandplain sand type contains more quartz than do the fluvial and hybrid sand types. All three sand types contain nearly equal amounts of feldspar. Thus, the significant differences in the framework and matrix constituents of the sand types can be attributed to their quartz, rock-fragment, and matrix contents. The insignificant difference in the quartz, feldspar, rock-fragment, and matrix contents of the sand types in the arenites probably can be attributed to minor differences in their mean percentages (table 2), particularly the feldspar content. An examination of the mean percentages of these constituents of the arenites and combined arenites and wackes shows that maximum differences exist between the barrier-strandplain and fluvial sand types. Futhermore, the maximum differences occur among their quartz, rock-fragment, and matrix contents. Thus, a more meaningful statistical test can be performed on these constituents between the barrier-strandplain and fluvial sand types of the combined arenites and wackes and of the arenites only.

Table 5 shows the results of a t-test analysis performed on the quartz, rock-fragment, and matrix contents of the barrier-strandplain and fluvial sand types of the combined arenites and wackes and of the arenites only. Significant differences exist in the quartz, rock-fragment, and matrix contents between the barrier-strandplain and fluvial sand types in the combined arenites and wackes as well as in the arenites only. The significant differences arise from the moderately high quartz content of the barrier-strandplain sand type in contrast to the lower quartz

TABLE 3.—*Results of analysis of variance of the framework composition and matrix content among the barrier-strandplain, fluvial, and hybrid sand types of combined arenites and wackes*

[df, degrees of freedom; SS, sum of squares; MS, mean square]

Source of variation	df	SS	MS	*F* test
Regression	2	10.67	5.33	4.46*
Deviation from regression	9	10,768.22	1,196.47	
Total	11	10,778.89	1,201.80	

*Significant at 0.1 level.

TABLE 4.—*Results of analysis of variance of the framework composition and matrix content among the barrier-strandplain, fluvial, and hybrid sand types of arenites*

[df, degrees of freedom; SS, sum of squares; MS, mean square]

Source of variation	df	SS	MS	*F* test
Regression	2	3.17	1.58	1.27*
Deviation from regression	9	11,219.79	1,246.64	
Total	11	11,222.96	1,248.22	

*Not significant at 0.1 level.

TABLE 5.—*Results of t-test analysis of differences between barrier-strandplain and fluvial sand types*

Source of variation	Quartz	Rock fragments	Matrix
Between barrier-strandplain and fluvial sand types of combined arenites and wackes	$t^1=2.65$	$t^1=4.90$	$t^1=3.97$
Between barrier-strandplain and fluvial sand types of arenites only	$t^2=2.63$	$t^2=4.66$	$t^2=3.79$

[1]Significant at 0.05 level with 40 degrees of freedom.
[2]Significant at 0.05 level with 48 degrees of freedom.

content of the fluvial sand type. In addition, the barrier-strandplain sand type has smaller rock-fragment and matrix contents than does the fluvial sand type.

The significant differences in the quartz, rock-fragment, and matrix contents between the barrier-strandplain and fluvial sand types probably reflect their environmental sensitivity. The abundance of unstable rock fragments and matrix in the fluvial sand type may be the result of first-cycle deposition, and the low concentrations of these constituents in the barrier-strandplain sand type may be a result of second-cycle deposition. The abundance of sedimentary rock fragments in the sand types indicates sedimentary source rocks. The rock fragments (for example, sandstone, siltstone, mudstone, chert, chalcedony, and limestone) are considered first cycle because they were deposited in fluvial environments that were near the source areas. However, where fluvial environments such as fluvial channels debouched into the sea, the abundance of rock fragments in this depositional environment depends, at least in part, upon abrasion and (or) size sorting by coastal processes as demonstrated by Davies and Ethridge (1975). In this coastal environment, intensive wave and current action upon unstable rock fragments can cause progressive size diminution; the fragments eventually are reworked and redistributed farther offshore. Thus, coastal deposits such as the barrier-strandplain sand type formed, in part, as a result of the concentration of lags composed of chemically and physically stable minerals. The low concentration of matrix in the barrier-strandplain sand type also may be the result of size sorting and removal of the very fine particles. Thus, the low concentrations of rock fragments and matrix in the barrier-strandplain sand type make this deposit a mineralogically and texturally more mature genetic type than the fluvial sand type. The maturity of the barrier-strandplain sand type is perhaps best measured by its moderately high concentration of stable quartz. The quartzose nature of the barrier-strandplain sand type probably evolved from progressive recycling of older Pleistocene coastal-plain sediments. This reworking of earlier formed deposits may have been enhanced by marine transgressions during Pleistocene and Holocene time.

The immature characteristics of the fluvial sand type, which are, in part, caused by the common occurrence of rock fragments and matrix, are perhaps directly related both to the nature of the source rocks and to postdepositional compaction. That is, the incisement of the ancestral Nueces River system into mainly sedimentary terrane during the late Pleistocene lowering of sea level may explain the common occurrence of the sedimentary rock fragments. These sedimentary rock fragments probably were an important source of the matrix of the fluvial and hybrid sand types. Postdepositional compaction and crushing resulted in the fragmentation of the soft sandstone, siltstone, and mudstone fragments. The pieces of these fragments were infiltrated into intergranular voids, forming patches of matrix of secondary origin probably similar to the pseudomatrix described by Dickinson (1970). The deformation of the sandstone fragments may also have enhanced the concentration of quartz in the fluvial sand type.

Table 6 displays the results of a t-test analysis performed on the quartz, rock-fragment, and matrix contents of the barrier-strandplain and hybrid sand types and of the fluvial and hybrid sand types of the arenites only and combined arenites and wackes. Overall, significant differences exist in the quartz, rock-fragment, and matrix contents between the barrier-strandplain and hybrid sands in the arenites alone and in the combined arenites and wackes; significant differences also exist in these components between fluvial and hybrid sands in the arenites alone and in the combined arenites and wackes. Specifically, however, no significant difference exists in the quartz content between the barrier-strandplain and hybrid sand types in both the arenites only and the combined arenites and wackes. In addition, no significant difference exists in the matrix content between the fluvial and hybrid sand types in the combined arenites and wackes. Thus, although visual observation of data in table 2 on framework mineralogy and matrix content suggests that the hybrid sands are more closely related to the fluvial sands than to the barrier-strandplain sands, this observation is not borne out by the statistical analysis. Nevertheless, the statistical analysis supports previous conclusions that

TABLE 6.—*Results of t-test analysis of differences between barrier-strandplain and hybrid sand types and between fluvial and hybrid sand types*

Source of variation	Quartz	Rock fragments	Matrix
Between barrier-strandplain and hybrid sand types of combined arenites and wackes	$t^1=1.43$	$t^2=2.84$	$t^2=3.78$
Between barrier-strandplain and hybrid sand types of arenites	$t^1=1.45$	$t^2=2.62$	$t^2=4.27$
Between fluvial and hybrid sand types of combined arenites and wackes	$t^3=3.77$	$t^2=2.66$	$t^1=1.24$
Between fluvial and hybrid sand types of arenites	$t^3=3.42$	$t^3=2.83$	$t^3=2.30$

[1]Not significant at 0.05 level with 84, 103, and 121 degrees of freedom.
[2]Significant at 0.05 level with 84 and 94 degrees of freedom.
[3]Significant at 0.05 level with 103 and 121 degrees of freedom.

the hybrid sands may represent dirty barrier and clean fluvial sands that cannot be clearly classified according to their mineral composition. The occurrence of mixed mineralogical suites in these coastal sands probably reflects effects of combined regressive, transgressive, and static shoreline processes.

SUMMARY

The Pleistocene and Holocene sands of southern Mustang Island, northern Laguna Madre, southern Corpus Christi Bay, and the adjacent mainland are arenites and wackes, and arenites are more abundant. The arenites sampled consist of, in descending order of abundance, sublitharenites, subarkoses, lithic arenites, and one quartz arenite. The wackes are commonly represented by lithic graywackes and subordinate feldspathic graywackes.

The arenites and wackes show quantitative differences in their framework-grain composition and matrix content according to genetic types, as indicated by stratigraphy, faunal assemblage, and analogy with modern environmental conditions. Two kinds of statistical analysis were performed in order to test the apparent quantitative mineralogical and textural differences among the sand types. Analyses of variance show significant differences in the quartz, feldspar, rock-fragment, and matrix contents of barrier-strandplain, fluvial, and hybrid sand types in the combined arenites and wackes but not in the arenites alone. Additional statistical analysis using a t-test shows that the quartz, rock fragments, and matrix are the most environmentally sensitive constituents in differentiating the genetically distinct barrier-strandplain and fluvial sand types. That is, the barrier-strandplain sand type is more quartzose than the fluvial sand type, which contains significantly greater amounts of rock fragments and matrix. The concentration of rock fragments, which are dominated by sedimentary types, in the fluvial sand type probably reflects first-cycle detritus deposited by the ancestral Nueces River system that was incised into a pre-Pleistocene sedimentary terrane. In addition, a significant amount of matrix in the fluvial sand type may have been of secondary origin, resulting from postdepositional compaction of the soft sedimentary rock fragments. Pieces of these fragments were then mechanically infiltrated into intergranular voids. The mineralogical and textural maturity of the barrier-strandplain sand type resulted from recycling older coastal-plain sediments and reworking by coastal processes that accompanied marine transgressions during Pleistocene and Holocene time. Although quartz and matrix contents of the hybrid sands are somewhat similar to those of the barrier-strandplain and fluvial sands, an overall mineralogical difference suggests that the hybrid sands were modified by combined fluvial- and marine-influenced shoreline processes and belong in a separate genetic class.

The diagenetic features observed in the sand types include authigenic calcite and feldspar cements and mechanically infiltrated clay coats. The calcite occurs as either microcrystalline or sparry cement. Calcite partially or totally binds framework grains; the latter condition is less common. Minor feldspar overgrowths act as a cement between detrital feldspar and quartz. The clay coats, which occur as microcrystalline flakes surrounding framework grains, are common diagenetic features; however, they seldom behave as cements.

Clear evidence exists for the occurrence of diagenetic reactions (for example, modest dissolution of feldspars and chert grains, precipitation of sparry calcite and micrite cements, and partial replacement of feldspars and quartz by calcite); however, diagenesis is not extensive. Although confining pressure and temperature were low, diagenetic reactions do not require drastic temperature or pressure conditions (Burns and Ethridge, 1979; Walker and others, 1978). Abundant pore fluid was available, as indicated by the appearance of the cores when removed from the core barrel, and by the formation of neogenetic gypsum and halite when the saline pore waters partially evaporated. The pore fluid could easily have enhanced chemical diagenesis. Because evidence for chemical diagenesis is rather limited, however, we suggest that migration of pore fluid through the sediments was limited, possibly because of their youth.

REFERENCES CITED

Barton, D. C., 1930, Surface geology of coastal southeast Texas: American Association of Petroleum Geologists Bulletin, v. 14, no. 10, p. 1301–1320.

Bernard, H. A., and LeBlanc, R. J., 1965, Résumé of the Quaternary geology of the northwestern Gulf of Mexico province, *in* Wright, H. E., Jr., and Frey, D. G., eds., The Quaternary of the United States: Princeton, N.J., Princeton University Press, p. 137–185.

Burns, L. K., and Ethridge, F. G., 1979, Petrology and diagenetic effects of lithic sandstones—Paleocene and Eocene Umpqua Formation, southwest Oregon, *in* Scholle, P. A., and Schluger, P. R., eds., Aspects of diagenesis: Society of Economic Paleontologists and Mineralogists Special Publication 26, p. 307–317.

Davies, D. K., and Ethridge, F. G., 1975, Sandstone composition and depositional environment: American Association of Petroleum Geologists Bulletin, v. 59, no. 2, p. 239–264.

Deussen, Alexander, 1924, Geology of the Coastal Plain of Texas west of Brazos River: U.S. Geological Survey Professional Paper 126, 139 p.

Dickinson, W. R., 1970, Interpreting detrital modes of graywacke and arkose: Journal of Sedimentary Petrology, v. 40, no. 2, p. 695–707.

Folk, R. L., 1951, Stages of textural maturity in sedimentary rocks: Journal of Sedimentary Petrology, v. 21, no. 3, p. 127–130.

Freeman, Tom, 1962, Quiet water oölites from Laguna Madre, Texas: Journal of Sedimentary Petrology, v. 32, no. 3, p. 475–483.

Galloway, W. E., 1974, Deposition and diagenetic alteration of sandstone in northeast Pacific arc-related basins—Implications for graywacke genesis: Geological Society of America Bulletin, v. 85, no. 3, p. 379–390.

Gibbons, G. S., 1967, Shell content in quartzose beach and dune sands, Dee Why, New South Wales: Journal of Sedimentary Petrology, v. 37, no. 3, p. 869–878.

Heald, M. T., and Larese, R. E., 1973, The significance of the solution of feldspar in porosity development: Journal of Sedimentary Petrology, v. 43, no. 2, p. 458–460.

Heling, Dietrich, 1963, Zur Petrographie des Stubensandsteins: Beiträge zur Mineralogie und Petrographie, v. 9, no. 3, p. 251–284.

Keller, W. D., 1954, The energy factor in sedimentation: Journal of Sedimentary Petrology, v. 24, no. 1, p. 62–68.

Kühn, Robert, 1948, Über einen rezenten Sandstein: Neues Jahrbuch für Mineralogie, Geologie und Paläontologie, Monatshefte, Abt. B, v. 9–12, p. 334–336.

Land, L. S., Behrens, E. W., and Frishman, S. A., 1979, The ooids of Baffin Bay, Texas: Journal of Sedimentary Petrology, v. 49, no. 4, p. 1269–1278.

LeBlanc, R. J., and Hodgson, W. D., 1959, Origin and development of the Texas shoreline: Gulf Coast Association of Geological Societies Transactions, v. 9, p. 197–220.

Pettijohn, F. J., 1957, Sedimentary rocks, 2d ed.: New York, Harper and Bros., 718 p.

Pettijohn, F. J., Potter, P. E., and Siever, R., 1972, Sand and sandstone: New York, Springer Verlag, 618 p.

Price, W. A., 1958, Sedimentology and Quaternary geomorphology of South Texas: Gulf Coast Association of Geological Societies Transactions, v. 8, p. 41–75.

Rusnak, G. A., 1960, Some observations of recent oolites: Journal of Sedimentary Petrology, v. 30, no. 3, p. 471–480.

Snedecor, G. W., 1956, Statistical methods applied to experiments in agriculture and biology, 5th ed.: Ames, Iowa, Iowa State College Press, 534 p.

Texas University Bureau of Economic Geology, 1974, Environmental geologic atlas of the Texas coastal zone—Corpus Christi sheet: Austin, scale 1:125,000.

———1975, Geologic atlas of Texas, Corpus Christi sheet: Austin, scale 1:250,000.

Walker, T. R., 1976, Diagenetic origin of continental red beds, *in* Falke, Horst, ed., The continental Permian in central, west, and south Europe—Proceedings of the NATO Advanced Study Institute held at the Johannes Gutenberg University, Mainz, F.R.G., 23 September–4 October, 1975: Dordrecht, Holland, D. Reidel, p. 240–282.

Walker, T. R., Waugh, Brian, and Crone, A. J., 1978, Diagenesis in first-cycle desert alluvium of Cenozoic age, southwestern United States and northwestern Mexico: Geological Society of America Bulletin, v. 89, no. 1, p. 19–32.

Geochemistry and Mineralogy of Late Quaternary Fine-Grained Sediments, South Texas Coastal Complex

By ROMEO M. FLORES *and* GERALD L. SHIDELER

STRATIGRAPHIC STUDIES OF A
LATE QUATERNARY BARRIER-TYPE COASTAL COMPLEX,
MUSTANG ISLAND–CORPUS CHRISTI BAY AREA,
SOUTH TEXAS GULF COAST

U.S. GEOLOGICAL SURVEY PROFESSIONAL PAPER 1328–E

CONTENTS

ILLUSTRATIONS

TABLES

STRATIGRAPHIC STUDIES OF A LATE QUATERNARY BARRIER-TYPE COASTAL COMPLEX, MUSTANG ISLAND–CORPUS CHRISTI BAY AREA, SOUTH TEXAS GULF COAST

GEOCHEMISTRY AND MINERALOGY OF LATE QUATERNARY FINE-GRAINED SEDIMENTS, SOUTH TEXAS COASTAL COMPLEX

By ROMEO M. FLORES and GERALD L. SHIDELER

ABSTRACT

The geochemical and mineralogical variations of fine-grained sediments in late Quaternary deposits of the southern Mustang Island–Corpus Christi Bay area, South Texas, can be attributed to their environments of deposition and differences in grain size. Concentrations of 28 important elements and oxides representing the composition mainly of clay minerals (kaolinite, illite, mixed-layer illite-smectite, smectite, and undifferentiated kaolinite-chlorite), heavy minerals, and other minor minerals were used in an effort to differentiate sediments of fluvial-channel, freshwater-upper bay, mid-bay, lower bay-inlet, estuary-lagoon, and barrier-strandplain environments.

Univariate statistical analysis of the concentrations of the 28 elements and oxides distinguished the freshwater-upper bay sediments from the marine barrier-strandplain sediments. Seventy-nine percent of the 28 elements and oxides were present in larger amounts in the freshwater-upper bay sediments than in sediments from any other environment. In contrast, 89 percent of the elements and oxides were present in smaller amounts in the barrier-strandplain sediments than in sediments from any other environment.

Q-mode factor analysis showed that the geochemical variations also can be attributed to the relative proportions of clay and sand-silt particles composing the sediments. The clay particles are significantly concentrated within the freshwater-upper bay sediments, reflecting settling in low-energy, protected basins. The relatively high sand-silt content of the barrier-strandplain sediment can be explained by lag sedimentation resulting from reworking.

In addition, sediments from the freshwater-upper bay and barrier-strandplain environments can be differentiated by their detrital kaolinite and illite contents. The fluvial-channel sediments can be mineralogically differentiated from other sediment types by the presence of detrital smectite.

Thus, geochemical and mineralogical variations were used to distinguish sediments deposited within freshwater and marine end members of the coastal environmental spectrum. The sediments deposited within intermediate environments of this spectrum were not sufficiently distinct for successful differentiation.

INTRODUCTION

During the late Quaternary, numerous geochemical, physical, and biological processes affected sedimentary environments within the coastal complex of the southern Mustang Island–Corpus Christi Bay area of South Texas. The physical and biological attributes of this environmental complex are discussed in the other chapters of this volume, which describe paleoenvironments and the differentiation of the sediments into specific facies. The objective of this chapter is to examine the bulk geochemistry and mineralogy of the fine-grained sediments deposited within the various coastal environments.

Studies of the geochemistry and clay mineralogy of sediments deposited within a spectrum of coastal-plain environments were made by Millot (1949), Brooks and Ferrell (1970), and Keller (1970); these studies suggested that concentrations of certain trace elements and mineral matter are influenced by local chemical processes within the environment of deposition. These concentrations were interpreted to be diagnostic of the response of elements to processes that are inherent in specific environmental settings. Thus, the work described in this chapter is an outgrowth of these observations, which were compared to observations made within the coastal complex of the southern Mustang Island–Corpus Christi Bay area.

METHODS

Samples analyzed for this study were collected from longitudinal halves of six cores designated A, B, C, D, EE, and F; the corehole locations are shown in figure 1 of Chapter B of this volume. Table 1 shows the depths in each core where samples were collected from different types of fine-grained sediments. The classification of the fine-grained sediment follows the system of Shepard (1954), which is based on the relative proportions of sand, silt, and clay components. Lithologic logs of the sampled cores are shown in plates 3–6, 8, and 9 of Chapter B of this volume. In order to collect uncontaminated samples, a 26.5-g vial was inserted into the middle part of the core half. In all, 68 samples were collected for geochemical analysis (table 1). The samples were assigned to the following six depositional environments: fluvial channel, freshwater-upper bay, mid-bay, lower bay-inlet, estuary-lagoon, and marine barrier-strandplain environments. Identification of the depositional environments was based on the information presented in Chapters B, C, and D of this volume.

In an attempt to ensure analytical consistency, a system of elemental analysis was followed, as described by Sutton (1976). The geochemical analysis consisted of

TABLE 1.—*Numbers, lithologies, core depths, and depositional environments of the 68 samples collected for geochemical analysis*

Sample number	Lithology	Depth below surface (meters)	Depositional environment
Core A			
A–2	Silty sand	0.61	Estuary-lagoon.
A–7	Sand-silt-clay	7.62	Freshwater-upper bay.
A–14	Silty sand	17.98	Mid-bay.
A–21	Sand-silt-clay	26.21	Freshwater-upper bay.
A–36	Clay	42.67	Freshwater-upper bay.
A–41	Silty sand	50.90	Fluvial channel.
A–42	Medium sand*	52.00	Fluvial channel.
Core B			
B–4	Sand-silt-clay	5.79	Freshwater-upper bay.
B–8	Sand-silt-clay	11.89	Freshwater-upper bay.
B–12	Silty sand	17.37	Lower bay-inlet.
B–21	Clayey silt	28.04	Lower bay-inlet.
B–24	Silty sand	33.83	Freshwater-upper bay.
B–32	Silty clay	41.45	Freshwater-upper bay.
B–36	Clayey silt	46.33	Freshwater-upper bay.
B–44	Clayey silt	53.95	Freshwater-upper bay.
B–47–1	Sand-silt-clay	57.00	Freshwater-upper bay.
B–47–2	Sandy silt	58.52	Freshwater-upper bay.
Core C			
C–1	Sand-silt-clay	0.61	Mid-bay.
C–3	Fine sand	3.05	Lower bay-inlet.
C–7–1	Silty sand	7.62	Lower bay-inlet.
C–7–2	Sandy silt	9.14	Lower bay-inlet.
C–8	Sand-silt-clay	10.36	Mid-bay.
Core D			
D–3	Silty sand	4.57	Estuary-lagoon.
D–10	Silty clay	14.02	Mid-bay.
D–16	Very fine sand*	19.81	Lower bay-inlet.
D–23	Clayey silt	27.43	Freshwater-upper bay.
D–25	Sand-silt-clay	30.78	Mid-bay.
D–26	Sand-silt-clay	32.31	Mid-bay.
D–27	Silty sand	33.53	Mid-bay.
D–36	Clayey silt	41.76	Mid-bay.
D–38	Silty clay	44.81	Mid-bay.
D–39	Clayey silt	46.33	Freshwater-upper bay.
D–40	Silty sand	47.85	Freshwater-upper bay.
D–48	Silty sand	56.08	Fluvial channel.
D–51	Sand-silt-clay	60.35	Freshwater-upper bay.
D–52	Clayey silt	61.57	Freshwater-upper bay.
Core EE			
EE–10	Fine sand*	12.50	Barrier-strandplain.
EE–12	Fine sand*	14.33	Barrier-strandplain.
EE–19	Silty sand	22.56	Barrier-strandplain.
EE–20	Sandy silt	24.38	Freshwater-upper bay.
EE–22	Silty clay	27.74	Freshwater-upper bay.
EE–25	Clayey sand	32.31	Freshwater-upper bay.
EE–26	Silty sand	33.53	Mid-bay.
EE–28	Silty clay	35.97	Mid-bay.
EE–30	Clayey silt	38.40	Mid-bay.
EE–33	Clayey silt	42.06	Mid-bay.
EE–35	Silty clay	44.20	Freshwater-upper bay.
EE–37	Silty clay	46.94	Freshwater-upper bay.
EE–39	Silty clay	49.68	Freshwater-upper bay.
EE–41–1	Silty clay	51.82	Freshwater-upper bay.
EE–41–2	Sand-silt-clay	52.73	Fluvial channel.
EE–42	Silty sand	54.25	Fluvial channel.
Core F			
F–17	Silty sand	22.86	Barrier-strandplain.
F–21	Silty sand	28.96	Estuary-lagoon.
F–22	Clayey silt	30.18	Estuary-lagoon.
F–23	Sand-silt-clay	31.39	Estuary-lagoon.
F–25	Silt	34.75	Estuary-lagoon.
F–26	Clayey silt	35.97	Freshwater-upper bay.
F–27	Clayey silt	37.19	Freshwater-upper bay.
F–28	Silty sand	38.40	Fluvial channel.
F–32	Sandy silt	40.54	Fluvial channel.
F–34	Medium sand*	41.15	Fluvial channel.
F–38	Sandy silt	44.81	Fluvial channel.
F–41	Silty clay	48.46	Freshwater-upper bay.
F–43	Silty clay	51.21	Fluvial channel.
F–45	Silty sand	53.34	Fluvial channel.
F–51	Sandy silt	60.05	Mid-bay.
F–52	Silty sand	60.96	Mid-bay.

*In samples composed mainly of sand, only the argillaceous matrix was analyzed.

emission spectroscopy, in which 65 elements were detected simultaneously down to the part-per-million level. Of these, 25–30 elements were detected in most samples, and 28 elements were found to be present in all the samples. A computerized plate-reading procedure described by Dorrzapf (1973) and Helz (1973) was followed in order to gain a faster and more versatile analysis. In addition, the procedure provided a more sensitive analysis for certain elements. The above-described analyses were performed by L. Mei, W. B. Crandell, and D. W. Golightly of the U.S. Geological Survey (USGS) in Reston, Va.

Separate samples of the fine-grained sediments were collected from the cores at the same stratigraphic levels from which the geochemical samples were acquired; these samples were used for X-ray diffraction (XRD) analysis by R. Brown of the USGS in Denver, Colo. In all, 20 samples, each weighing 10 g, were collected from the sediments of the six environments. The samples were dried, powdered, pressed into cellulose-backed pellets, and analyzed for clay mineralogy. X-ray patterns were obtained for each untreated sample. In addition, a few selected samples were treated with ethylene glycol and heated to 300°C to investigate expandable clay minerals.

Statistical analyses were performed on the geochemical data in order to determine whether sediments from the six depositional environments could be differentiated on the basis of contents of the chemical elements and compounds. Factor analysis (Miesch, 1976a) was used to evaluate the geochemical variations of fine-grained sediments among the various environments. For detailed descriptions of the mathematical and practical applications of factor analysis to geochemical and petrological data, the reader is referred to Imbrie (1963), Miesch (1976b), and Flores and Shideler (1978).

DISCUSSION OF GEOCHEMICAL DATA

The mean concentrations of the 28 elements and oxides in samples collected from the six environments are presented in table 2. In addition, table 3 summarizes the minimum and maximum values (ranges) of the element and oxide concentrations in these same samples.

In the total of 68 samples (table 2), the two elements having the highest mean concentrations are Mn (338 ppm) and Ba (287 ppm), and the two elements having the lowest mean concentrations are Yb (1.85 ppm) and Be (1.58 ppm). The oxides having the highest means in all 68 samples are SiO_2 (68.1 percent) and Al_2O_3 (8.71 percent), and the oxides that show the lowest means are TiO_2 (0.262 percent) and Na_2O (1.24 percent). The most variable element (table 3) is Mn (62–780 ppm), and the least variable element is Be (0.7–2.6 ppm). The most variable oxide is SiO_2 (42.8–103.9 percent), and the least variable oxide is TiO_2 (0.02–0.40 percent).

Table 2 shows which of the six environments have the highest and lowest mean concentrations of the elements and oxides. Visual inspection of these concentrations shows that most (79 percent) of the highest mean concentrations of the elements and oxides occur within the freshwater-upper bay sediments. The remainder of the highest mean concentrations are distributed among lower bay-inlet, barrier-strandplain, and estuary-lagoon sediments. In contrast, 89 percent of the lowest mean concentrations of the elements and oxides occur in the marine barrier-strandplain sediments. The remainder of the lowest concentrations of the elements and oxides are distributed among the freshwater-upper bay, mid-bay, and lower bay-inlet sediments. Thus, the greatest proportions of the highest and lowest mean concentrations of elements and oxides are probably influenced by processes within their environments of deposition. More importantly, within a spectrum ranging from freshwater to marine environments, the highest mean concentrations of the elements and oxides occur mainly in one end member (freshwater-upper bay) of the environmental spectrum, and the lowest mean concentrations occur mainly in the other end member (marine) of the spectrum. In order to determine the factors that controlled the environmental variation patterns of the elements and oxides, a Q-mode factor analysis was performed.

The Q-mode factor analysis, as adopted from Miesch (1976a), appears to be a method well suited for summarizing complex multivariate geochemical data. It was used in this study in an attempt to reduce the data matrix to a smaller matrix that would facilitate interpretation by being a concise representation of the geochemical variation within a sample suite.

The initial step in the analysis required the data matrix to be transformed so that the concentration of each variable (elements and oxides) was expressed as a proportion of the total range of concentrations for that variable. The next step in generating the Q-mode factor model was to compute a matrix of sums of squares and cross products among the columns of the transformed data matrices. The eigenvalues of these matrices of cosine theta derived from the original and transformed data matrices, and their cumulative percentages, indicated the corresponding number of factors that accounted for all the variability within the data matrices. As shown by the factor-variance diagram (fig. 1), a plot of the eigenvalues against the number of factors indicates that a three-factor model (where the slope flattens) appears to be the most efficient. Models having fewer than three factors would fail to explain much of the variation in most of the geochemical constituents, and models having more than three factors would not

TABLE 2.—*Arithmetic means of concentrations of 8 oxides and 20 elements in samples from 6 depositional environments*
[Oxide contents are in weight percent; element contents are in parts per million]

Oxide or element	Total (68 samples)	Fluvial channel (11 samples)	Freshwater-upper bay (26 samples)	Mid-bay (15 samples)	Lower bay-inlet (6 samples)	Estuary-lagoon (6 samples)	Barrier-strandplain (4 samples)
SiO_2	68.1	78.1	59.6**	67.5	76.7	68.3	93.4*
Al_2O_3	8.71	6.63	10.7*	7.92	8.41	7.81	3.98**
Na_2O	1.24	.99	1.26	1.21	1.09	2.02*	.98**
K_2O	1.96	1.32	2.31*	1.92	1.99	2.08	.92**
Fe_2O_3	3.73	2.53	4.73*	3.28	4.05	3.10	1.55**
MgO	1.52	.894	1.92*	1.49	1.39	1.47	.634**
CaO	2.75	2.82	3.38*	2.51	2.24	1.56	1.49**
TiO_2	.262	.203	.309*	.238	.264	.281	.128**
Mn	338	258	374	360	271	407*	186**
B	74.6	52.8	89.4*	66.7	70.7	81.3	46.3**
Ba	287	290	270**	281	312	368*	270**
Be	1.58	1.28	1.89*	1.46	1.53	1.28	1.03**
Co	7.70	4.30	9.29*	8.57	8.48	6.22	2.35**
Cr	25.1	14.8	29.5*	26.8	23.9	27.5	11.2**
Cu	14.0	11.0	17.3*	13.3	12.9	11.3	6.55**
La	26.4	21.7	31.9*	23.6	24.7	22.7	16.75**
Nb	8.14	6.36	9.8	6.94	9.92*	6.33	5.09**
Ni	12.6	7.52	15.4*	12.9	13.8	10.4	4.88**
Pb	14.4	8.91	18.3*	12.8	15.5	12.3	7.37**
Sc	7.65	4.99	9.8*	6.95	7.42	6.70	3.05**
Sn	2.80	2.97	3.35*	2.80	1.25**	2.13	1.63
Sr	205	198	235*	197	174	162	141**
V	56.3	41.6	67.6*	54.2	55.2	53.0	26.2**
Y	14.3	13.2	16.7*	13.3	12.7	13.1	8.25**
Zn	45.1	27.3	63.4*	39.1	41.6	21.5	19.5**
Zr	170	198	149	144**	187	215	259*
Ga	7.86	4.86	10.5*	6.90	7.82	6.23	2.64**
Yb	1.85	1.65	2.10*	1.75	1.77	1.87	.950**

*Highest mean value.
**Lowest mean value.

substantially improve the situation. Thus, a three-factor model appears to be optimum and accounts for 80 percent of the total variability in the normalized data matrix.

In order to determine the nature of the three factors used in the analysis, table 4 presents the correlations between the varimax loadings and the geochemical variables. The varimax loadings in factor I show that high scores (absolute value >0.8) for Al_2O_3, K_2O, Fe_2O_3, MgO, and TiO_2 can be attributed to a relative abundance of clay-sized particles composed of clay minerals. The high loadings for the trace elements Co, Cr, Ni, Sc, V, Y, and Ga can be attributed to their significant absorption by the highly chemically reactive clay minerals. The varimax loadings in factor II show high scores (absolute value >0.7) for SiO_2, MgO, and Fe_2O_3. The high score for SiO_2 is attributed to a relative abundance of quartz occurring as both sand- and silt-sized particles; the high scores for the other oxides may have resulted from the weathering of ferromagnesian heavy-mineral admixtures. Factor III varimax loadings show high scores (absolute value >0.7) for TiO_2, Y, and Yb that may be attributed to a relative abundance of the heavy minerals ilmenite, leucoxene, rutile, and monazite. Visual inspection of the factor loadings in table 4 shows that the high loading scores (absolute value >0.7) occur mainly in factors I (clay-sized particles) and II (sand- and silt-sized particles), suggesting that they are the two most significant factors. Thus, a large part of the geochemical variations in the fine-grained

sediments of the various environments appears to be caused by differences in grain size (clay or sand and silt).

The stratigraphic variations of factor I (clay-sized particles) and factor II (sand- and silt-sized particles) in relation to the sediments of the fluvial-deltaic and barrier-strandplain environmental complexes are shown in figures 2 and 3. In order to summarize the data, the varimax loadings or mixing proportions of the end-member compositions for each sample were plotted on a cross section drawn through coreholes A, B, D, EE, and F and were then used to construct isolines. The cross section was adopted from Shideler (this volume, Chap. B, fig. 4); however, it is modified here to indicate only the fluvial-deltaic and barrier-strandplain complexes in order to simplify and facilitate visual observation of the varimax-loading variations. The fluvial-deltaic complex includes fluvial-channel, freshwater-upper bay, mid-bay, lower bay-inlet, and estuary-lagoon sediments.

Figure 2, which illustrates the stratigraphic variation of factor I (clay-sized particles), shows five areas (hachured) of high absolute values (>0.9) of varimax loadings within the fluvial-deltaic sediments. The values of varimax loadings in the fluvial-deltaic sediments from cores A, B, and D appear to be uniformly high. In contrast, the absolute values of varimax loadings in the same type of sediments from cores EE and F are highly variable, ranging from 0.4 to 0.9 within a short distance both laterally and vertically. The loadings in the fluvial-deltaic sediments from cores A, B, D, and EE suggest that the five local areas of high absolute values (>0.9) tend to be rich in clay-sized particles. These areas rich in clay-sized particles are all distributed within sediments of the freshwater-upper bay and mid-bay environments, suggesting that these

TABLE 3.—*Ranges of concentrations of 8 oxides and 20 elements in samples from 6 depositional environments*
[Oxide contents are in weight percent; element contents are in parts per million]

Oxide or element	Total (68 samples)	Fluvial channel (11 samples)	Freshwater-upper bay (26 samples)	Mid-bay (15 samples)	Lower bay-inlet (6 samples)	Estuary-lagoon (6 samples)	Barrier-strandplain (4 samples)
SiO_2	42.8–103.9*	49.2–103.9*	42.8–103.9*	49.2–103.9*	51.3–103.9*	53.5–103.9*	62.0–103.9*
Al_2O_3	1.17–15.7	4.16–10.77	5.86–15.7	4.35–11.90	3.97–13.98	5.10–9.83	1.17–6.61
Na_2O	0.26–3.50	0.35–1.89	0.26–3.50	0.75–2.29	0.54–2.16	0.89–2.83	0.28–1.77
K_2O	0.28–2.58	0.64–2.58	0.95–2.58	0.94–2.58	0.57–2.58	1.00–2.58	0.28–1.51
Fe_2O_3	0.34–8.44	1.17–4.86	2.00–7.28	1.86–4.86	1.43–8.44	2.00–4.15	0.34–3.00
MgO	0.23–2.65	0.31–1.99	0.53–2.65	0.55–2.49	0.41–2.65	0.98–1.99	0.23–1.38
CaO	0.31–13.01	0.31–7.14	0.35–13.01	0.62–8.54	0.57–4.20	0.97–2.38	0.35–3.22
TiO_2	0.02–0.40	0.11–0.32	0.20–0.40	0.12–0.35	0.13–0.38	0.18–0.33	0.02–0.18
Mn	62–780	87–470	150–780	96–760	98–540	150–640	62–370
B	13–150	22–89	37–150	40–100	45–99	65–100	13–69
Ba	150–680	200–380	180–390	190–350	250–340	280–680	150–340
Be	0.7–2.6	0.7–1.7	1.2–2.6	0.7–2.1	0.7–2.3	0.7–1.6	0.7–1.6
Co	0.7–36	1.4–8.1	3–23	3.8–36	1.6–19	3.5–8.0	0.7–4.7
Cr	1.7–65	4–25	8.7–65	10–49	4.4–54	13–46	1.7–21
Cu	3.5–30	5.7–30	7.5–28	6.6–23	6.6–23	10–14	3.5–12
La	7–47	15–29	16–47	14–34	10–43	14–28	7–22
Nb	2.2–16	4.3–8.2	5.7–14	2.2–11	3.5–16	4.9–7.8	2.2–8
Ni	1.9–28	2.5–16	5.1–28	5.7–24	3–28	6.4–13	1.9–9.9
Pb	4.8–40	4.8–12	7.2–40	4.8–21	3–28	4.8–16	4.8–9.8
Sc	0.7–13	1.9–8.2	5.4–13	3.9–11	2.6–13	4.4–8.2	0.7–6.7
Sn	1.05–11	1.05–11	1.05–9.6	1.05–5.0	1.05–1.7	1.05–3.1	1.05–2.9
Sr	42–350	120–280	110–330	140–350	85–260	120–230	42–230
V	7.6–94	18–60	32–94	34–82	21–90	33–67	7.6–53
Y	1.7–23	8.5–17	10–23	8.6–18	6.4–19	9.5–15	1.7–13
Zn	10.5–120	10.5–50	24–120	10.5–72	10.5–87	10.5–39	10.5–29
Zr	82–610	91–300	82–280	82–330	120–260	140–460	84–610
Ga	1.05–18	2.2–9.4	4.1–18	2.6–12	2.6–15	3.4–8.8	1.05–5.0
Yb	0.16–3.3	0.88–2.9	1.4–3.3	1.0–2.3	0.99–2.8	1.1–2.3	0.16–1.7

*SiO_2 contents exceeding 100 percent are a computational artifact of the analytical technique.

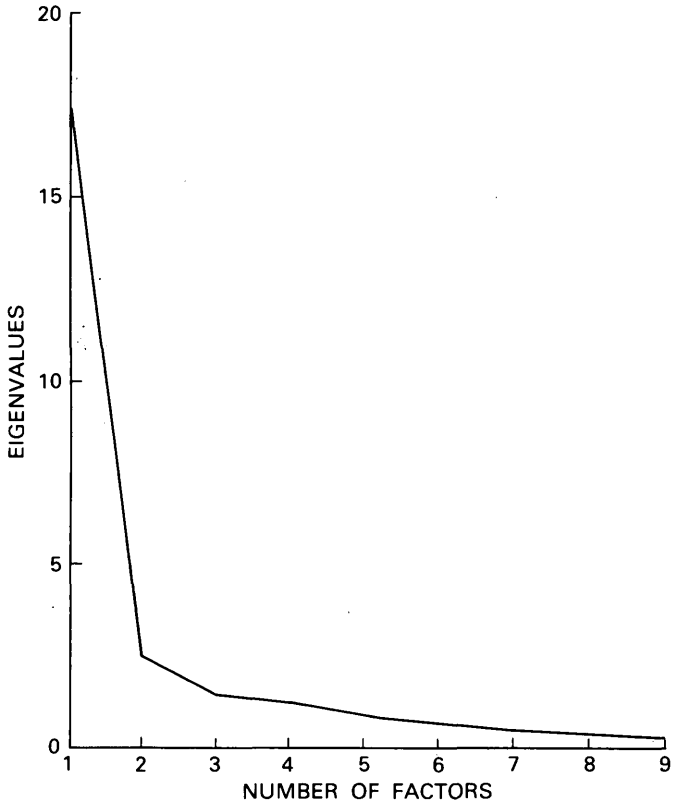

FIGURE 1.—Factor-variance diagram derived from the geochemical data matrix for the fine-grained sediments.

environments contained protected low-energy basins where clay particles preferentially settled.

In contrast, relatively low loading values (absolute value ≤0.6) tend to be somewhat associated with channel deposits. The winnowing action of high-energy flow regimes in the channels may have caused an enrichment of coarser particles relative to clay particles. In addition, the presence of relatively abundant channel deposits in the fluvial-deltaic complex at corehole F probably contributed to the high degree of variability of the clay particles within this seaward area. Figure 2 shows a range from very low to high values of varimax loadings on the back side of the Mustang Island barrier (core EE), suggesting that sorting of the particles in this backbarrier environment was not as efficient as sorting on the seaward side of the barrier island.

The stratigraphic variation of factor II (sand- and silt-sized particles), which is shown in figure 3, is characterized by highly variable and some high (absolute value ≥0.8) varimax-loading values in both the fluvial-deltaic and barrier-strandplain sediments of cores EE and F. The fluvial-deltaic sediments in the landward cores (A, B, and D) are less variable and show lower

TABLE 4.—*Correlations between the varimax loadings and the 28 geochemical variables*

Variables	Factor I (clay-sized particles)	Factor II (silt- and sand-sized particles)	Factor III (heavy minerals)
SiO_2	−0.7119	0.7674*	0.6960
Al_2O_3	.8923*	−.6694	−.6552
Na_2O	.3863	−.1742	−.5375
K_2O	.8475*	−.6935	−.6096
Fe_2O_3	.9017*	−.7065*	−.6639
MgO	−.8329*	−.7848*	−.5866
CaO	.3046	−.0478	−.5386
TiO_2	.8539*	−.4401	−.7374*
Mn	.6334	−.4609	−.5971
B	.7764	−.5771	−.6073
Ba	.0327	.3816	−.1395
Be	.7997	−.8228*	−.4932
Co	.8118*	.6970	−.5439
Cr	.8028*	−.6512	−.5727
Cu	.7886	−.7446*	−.5807
La	.7435	−.5489	−.6340
Nb	.5959	−.4045	−.4781
Ni	.8211*	−.7769*	−.4789
Pb	.6276	−.6392	−.3173
Sc	.9118*	−.7033*	−.6809
Sn	.3150	−.2725	−.1794
Sr	.6659	−.3319	−.6967
V	.9286*	−.7313*	−.6885
Y	.8557*	−.4128	−.8327*
Zn	.6980	−.8124*	−.3822
Zr	−.3289	.7303*	−.1012
Ga	.8507*	−.7974*	−.5857
Yb	.7987	−.3306	−.7537*

*High scores.

varimax-loading values than the same type of sediments in cores EE and F. In essence, the high absolute values are associated mainly with the sandy channel and barrier-island sediments, which are abundant in cores EE and F. The high variability, as well as the concentration of high varimax-loading values in these sediments at coreholes EE and F, suggests deposition in environments having higher energy conditions (for example, channels and barrier islands) than the environments in which sediments of cores A, B, and D were deposited. Within these higher energy environments, selective sorting preferentially deposited coarser sand- and silt-sized lag particles rather than clay-sized particles. Thus, size segregation by lag sedimentation appears to have been an important factor controlling the distribution of clay, silt, and sand particles in deposits of the various depositional environments.

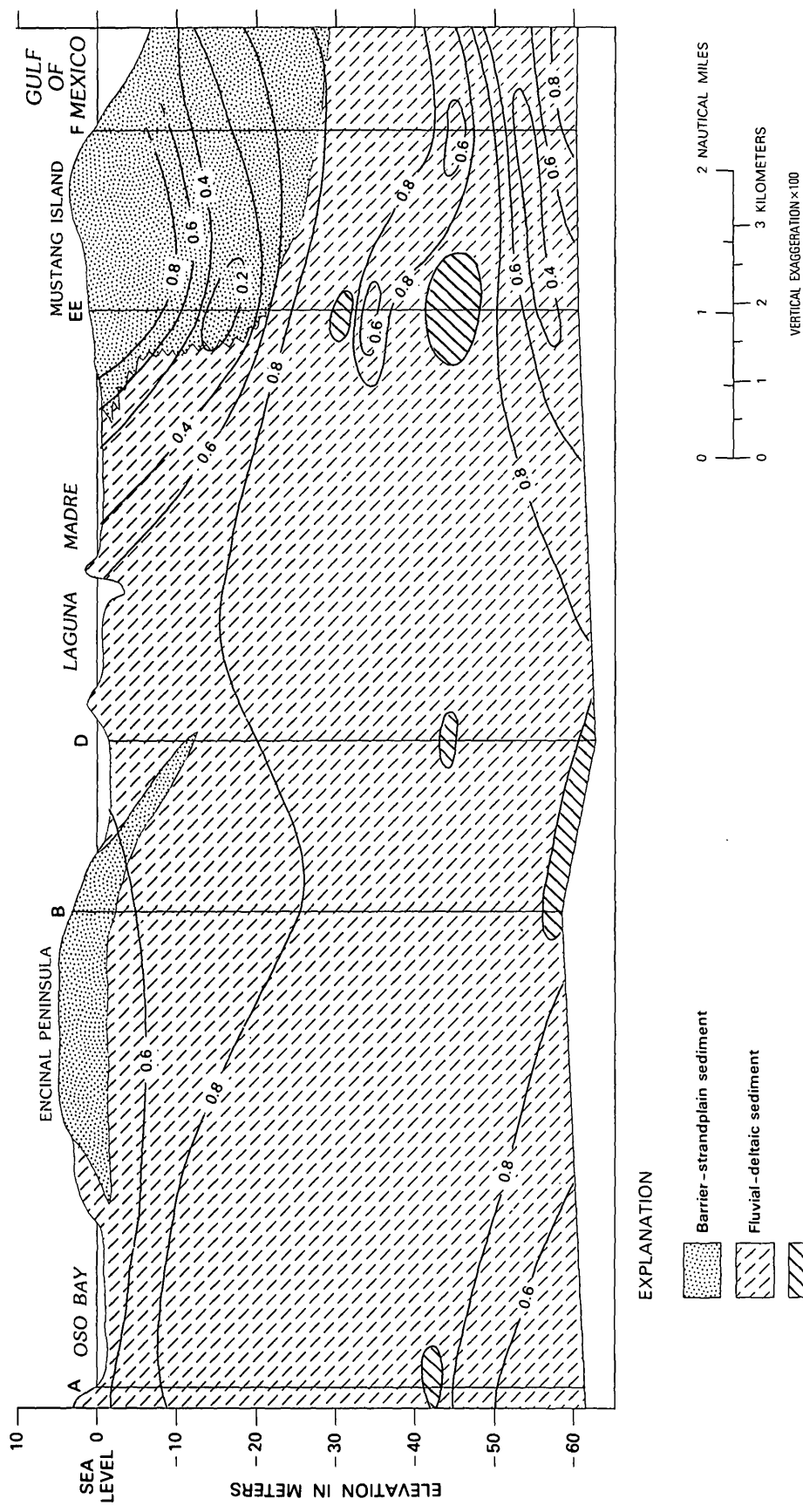

FIGURE 2.—Cross section of the study area through coreholes A, B, D, EE, and F showing lateral and vertical variations of varimax-loading scores for factor I (clay-sized particles).

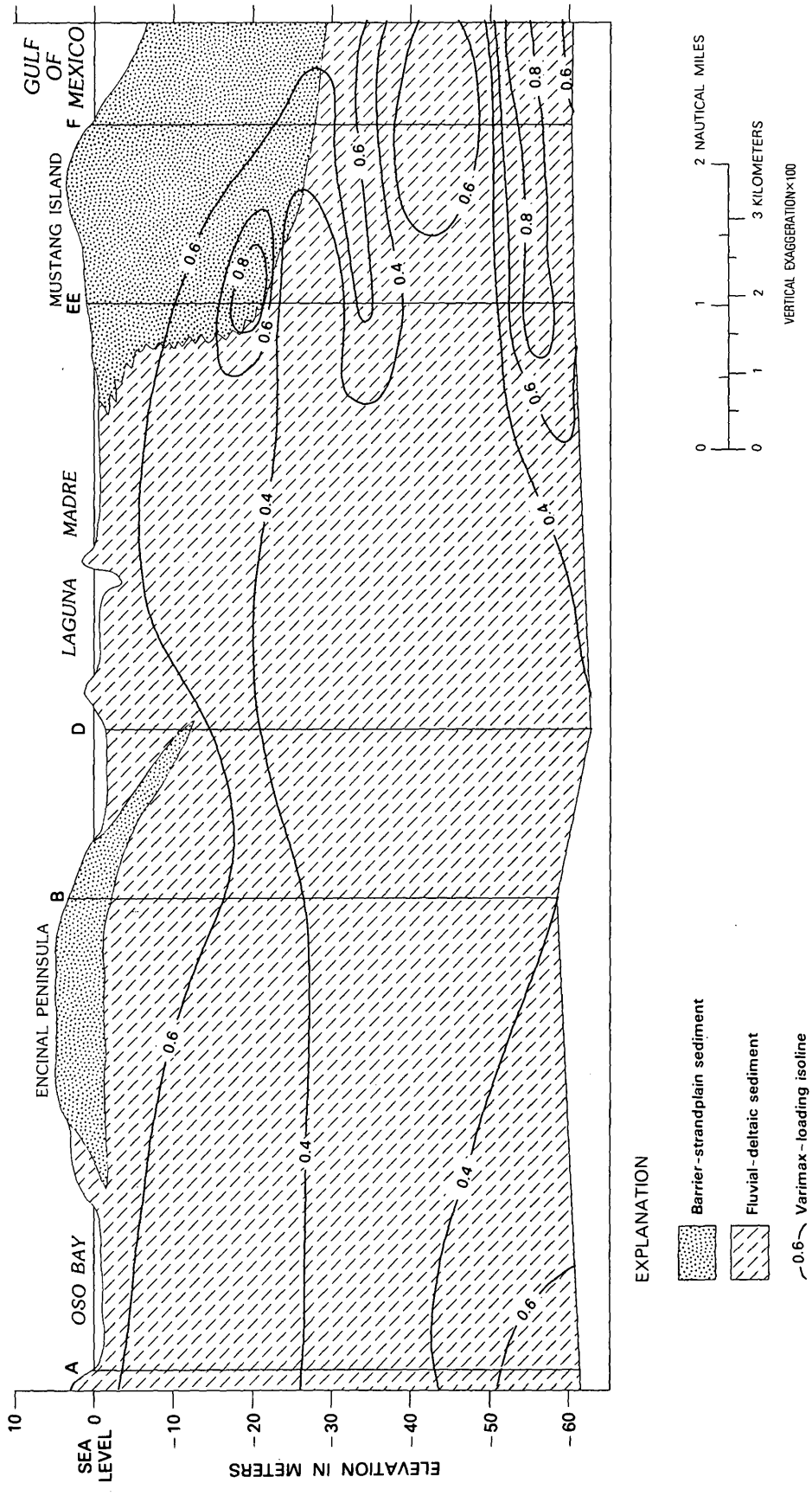

FIGURE 3.—Cross section of the study area through coreholes A, B, D, EE, and F showing lateral and vertical variations of varimax-loading scores for factor II (sand- and silt-sized particles).

Perhaps another clue to the importance of lag sedimentation is the variation of heavy minerals (factor III) in sediments of the fluvial-deltaic and barrier-strandplain complexes. The stratigraphic variation of the varimax-loading values of the heavy-mineral factor (fig. 4) indicates relatively high values in the barrier-strandplain sediments and generally lower values in the fluvial-deltaic sediments. The difference in loading values between sediments of these environments probably reflects the nature of reworking and recycling of sediments. In the barrier-strandplain environment, sediments were reworked and perhaps were recycled several times; thus, the resulting deposits are relatively mature. Associated with these mature sediments are lag concentrations of stable heavy minerals such as zircon, as indicated by the high mean content of Zr shown in the barrier-strandplain deposits (table 2). In contrast, the low loading values of heavy minerals in the fluvial-deltaic sediments probably are the effects of masking by other minerals present because these sediments have been reworked less than the barrier-strandplain sediments and have a correspondingly lower degree of maturity.

DISCUSSION OF MINERALOGICAL DATA

The mineralogical analysis of the fine-grained sediments involved a qualitative determination of clay-mineral composition by XRD. The detected clay minerals include kaolinite, illite, smectite, mixed-layer illite-smectite, and undifferentiated kaolinite-chlorite. The most common clay minerals are kaolinite and illite. The least common clay minerals are smectite and undifferentiated kaolinite-chlorite. The mixed-layer illite-smectite is fairly common.

Representative X-ray diffractograms of the clay-mineral suites in untreated samples from the various depositional environments are illustrated in figure 5, and the clay minerals found in each environment are summarized in table 5. In addition, representative X-ray diffractograms of glycol-treated samples, showing peaks for mixed-layer and undifferentiated clay minerals, are illustrated in figure 6. Kaolinite and illite are present in sediments from all the environments. The channel and freshwater-upper bay sediments contain the most clay-mineral varieties, in contrast to the mid-bay, lower bay-inlet, and barrier-strandplain sediments, which contain the least. More importantly, smectite occurs only in the channel sediments, and the undifferentiated kaolinite-chlorite occurs only in the channel and freshwater-upper bay sediments.

Overall, the common occurrence of kaolinite and illite in all environmental settings suggests a detrital origin, although a possible authigenic origin cannot be totally discounted. A detrital origin is consistent with the detrital occurrence of kaolinite and illite in Pleistocene and Holocene sediments from the Guadalupe Delta and San Antonio Bay, as described by Morton (1972). In addition, Simons and Taggart (1954) obtained samples of rocks ranging in age from Late Cretaceous to Quaternary along a traverse from Corpus Christi to San Antonio, and from San Antonio to Uvalde, Tex., for clay-mineral analysis. They determined that the predominant clay minerals in these rocks were kaolinite, illite, and smectite. The lines of traverse in the Simons and Taggart study lie within the watershed of the ancestral Nueces River that drained the present study area during the Pleistocene and Holocene. The similarity of the clay-mineral assemblages of the fine-grained sediments in the present study area and of the rocks in the watershed of the ancestral Nueces River suggests source-area derivation of the clay minerals. Kaolinite may have been derived from the weathering of feldspars in pre-existing source rocks. Illite was probably derived mainly from pre-existing illite in marine shale source rocks, which, in turn, may have formed authigenically in a marine environment (Feuillet and Fleischer, 1976). The restricted presence of smectite in the fluvial-channel deposits of the fluvial-deltaic complex suggests that it may have been derived from the source area following primary-stage weathering as an in situ alteration product of volcanic ash (Keller, 1970). The occurrence of detrital kaolinite and illite across the entire environmental spectrum from freshwater to marine end members and the absence of detrital smectite within the brackish-marine environments can be explained by the more rapid settling of kaolinite and illite in a saline environment relative to smectite, which may be altered to illite (Whitehouse and McCarter, 1958). These different settling rates are caused by different rates of flocculation among the clay minerals.

RELATIONSHIPS BETWEEN GEOCHEMISTRY AND MINERALOGY

Relationships between the geochemistry and clay mineralogy of the fine-grained sediments deposited in the various environmental settings are discussed below. A comparison of the geochemistry of illite ($KAl_2(OH)_2[AlSi_3(O,OH)_{10}]$) and kaolinite ($Al_2O_3 \cdot 2SiO_2 \cdot 2H_2O$), which occur in the sediments of all the six environments, may provide clues to the variations in the mean concentrations of the oxides and elements between freshwater-upper bay and barrier-strandplain environments, as shown in table 2. The

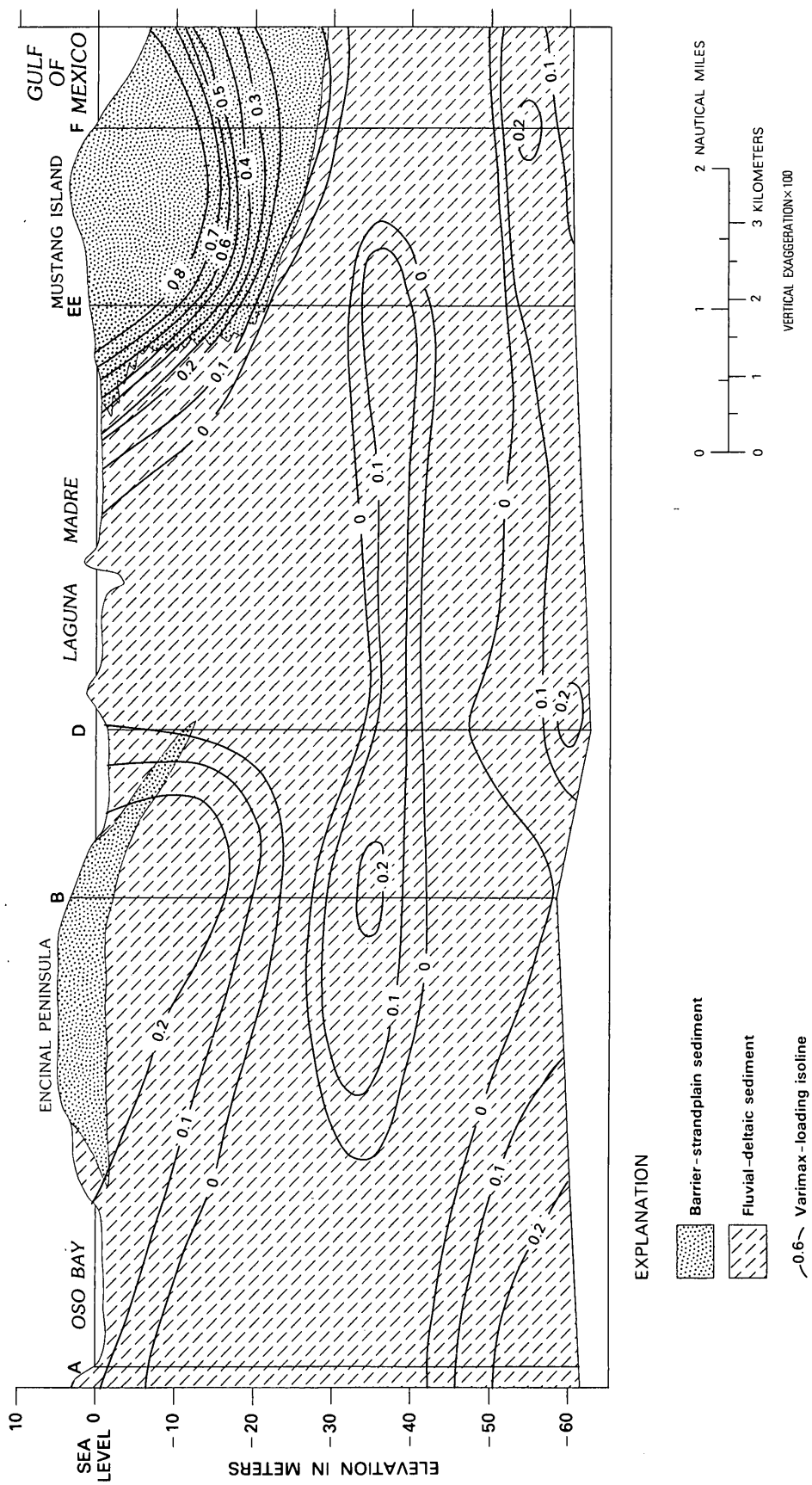

FIGURE 4.—Cross section of the study area through coreholes A, B, D, EE, and F showing lateral and vertical variations of varimax-loading scores for factor III (heavy minerals).

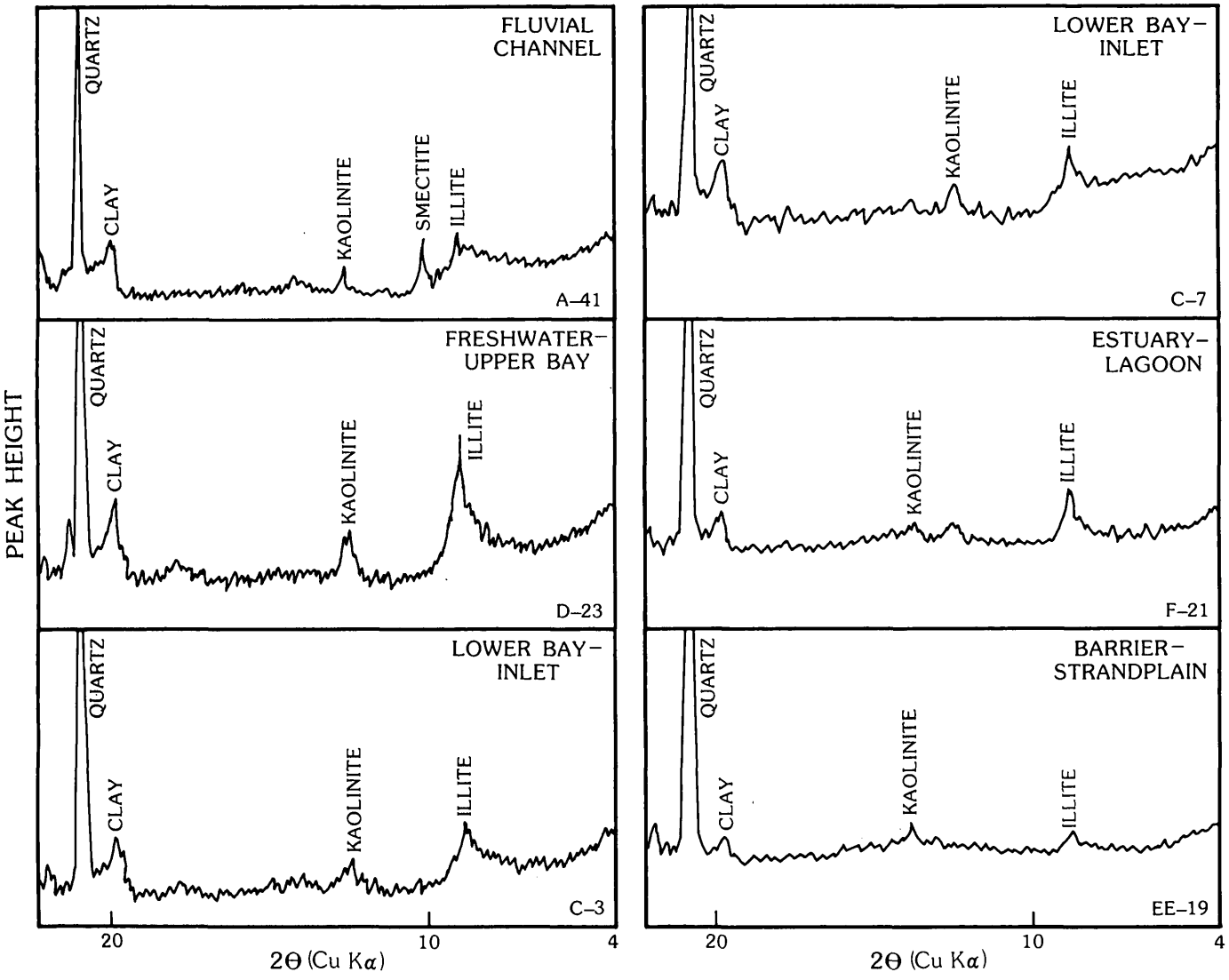

FIGURE 5.—Representative X-ray diffractograms of untreated samples of sediments from six depositional environments showing peaks for quartz and clay minerals.

following geochemical comparison is based on the premise that a large part of these clay minerals was river derived.

Table 2 shows that the mean content of SiO_2 is highest in the barrier-strandplain sediments and is lowest in the freshwater-upper bay sediments. In contrast, the mean content of Al_2O_3 is highest in the freshwater-upper bay sediments and is lowest in the barrier-strandplain sediments. If these oxides are assumed to represent quartz and kaolinite compositions, then the high Al_2O_3 content of the fine-grained sediments of the freshwater-upper bay environment can be attributed to the presence of high-alumina kaolinite. The unusually high (93.4 percent) SiO_2 content of the barrier-strandplain environment is probably the result of a large quartz component that may have depressed the kaolinite concentration by dilution. The depressed occurrence of kaolinite in the barrier-strandplain sediments may reflect reworking that resulted in the clay minerals being redistributed further offshore. The association of K_2O with Al_2O_3 and SiO_2 represents the composition of illite. As shown in table 2, the mean value of K_2O is highest in the freshwater-upper bay sediment and is lowest in the barrier-strandplain sediment. The relatively high K_2O mean content of the freshwater-upper bay sediments probably can be attributed to a high degree of flocculation of the clay minerals from riverine muds. On the other hand, the relatively low K_2O mean content of the barrier-strandplain sediments may also partially result from

TABLE 5.—*Clay-mineral distribution in the fine-grained sediments of the six depositional environments*

Depositional environment	Clay minerals
Fluvial channel	Kaolinite, illite, smectite, mixed-layer illite-smectite, and undifferentiated kaolinite-chlorite.
Freshwater-upper bay	Kaolinite, illite, mixed-layer illite-smectite, and undifferentiated kaolinite-chlorite.
Mid-bay	Kaolinite and illite.
Lower bay-inlet	Kaolinite and illite.
Estuary-lagoon	Kaolinite, illite, and mixed-layer illite-smectite.
Barrier-strandplain	Kaolinite and illite.

reworking and the redistribution of detrital illite elsewhere. Thus, conditions within the environment of deposition may have controlled the variation of oxides composing kaolinite and illite between the freshwater-upper bay and barrier-strandplain end members. Where the clay minerals settled as first-cycle detritus in the freshwater-upper bay environment, the oxides of kaolinite and illite are highest in concentration. However, where the clay minerals were reworked and redistributed as second- or third-cycle detritus, as in the barrier-strandplain sediments, the oxides of kaolinite and illite are lowest in concentration.

An additional important relationship between the geochemistry and mineralogy of the fine-grained sediments in the various environments is indicated by the heavy minerals. The most readily identifiable oxide and element of heavy minerals are TiO_2 (ilmenite, leucoxene, and rutile or anatase) and Zr (zircon). Table 2 shows the highest mean content of TiO_2 in the freshwater-upper bay sediments and lowest mean content in the barrier-strandplain sediments. In contrast, the highest mean content of Zr is in the barrier-strandplain sediments, and a very low mean content is in the freshwater-upper bay sediments. The high mean content of TiO_2 in the freshwater-upper bay sediments may reflect the derivation of some detritus from igneous and metamorphic rocks in the source area. The high mean content of Zr in the barrier-strandplain sediments probably resulted from the concentration of zircon as a stable, multicycle heavy mineral in a highly mature sediment derived primarily from sedimentary source rocks.

SUMMARY AND CONCLUSIONS

The fine-grained sediments of the late Quaternary deposits in the southern Mustang Island–Corpus Christi Bay area of South Texas contain 28 important elements and oxides, and as much as 89 percent of them can be used to differentiate freshwater-upper bay and barrier-strandplain sediments. The mean concentrations of the elements and oxides are generally highest in the freshwater-upper bay sediments and lowest in the barrier-strandplain sediments. In addition, Q-mode factor analysis of the samples shows that variations in the element and oxide contents can be attributed to differences in grain size. The freshwater-upper bay sediments contain relatively abundant clay-sized particles probably deposited in low-energy, protected settling basins. In contrast, where sediments were deposited in high-energy environments, such as barrier islands and stream channels, the concentration of coarser sand- and silt-sized particles by lag sedimentation was an

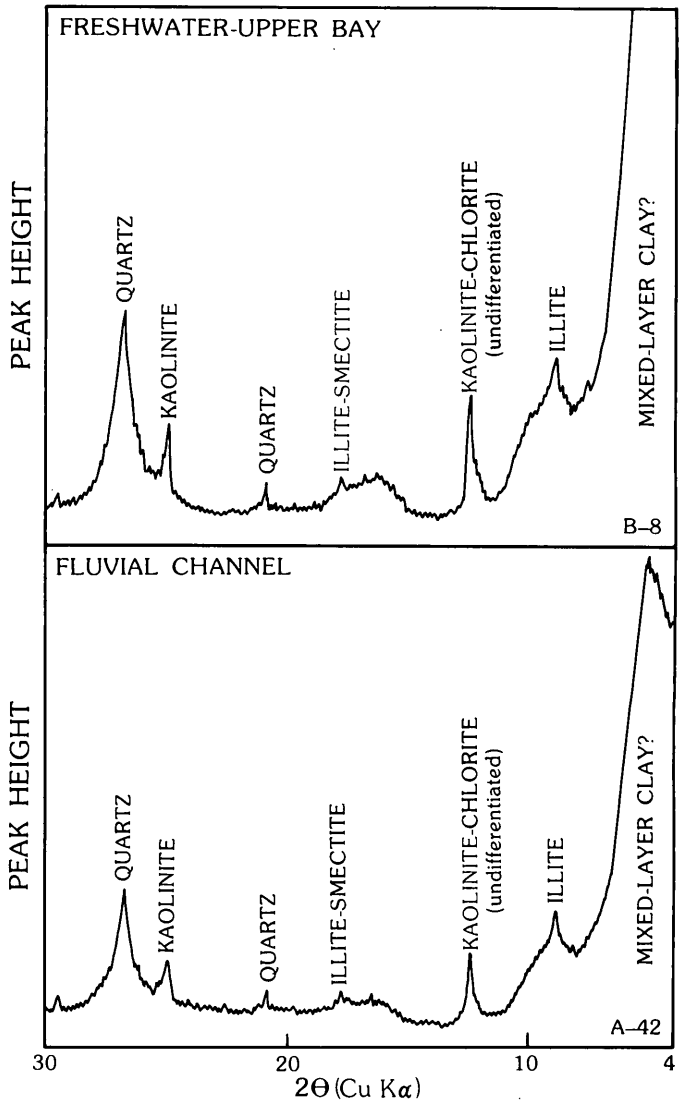

FIGURE 6.—Representative X-ray diffractograms of glycol-treated sediment samples showing peaks for quartz and clay minerals, including expanded mixed-layer clay minerals.

important contributor to the geochemical variations. A third factor that may be a significant contributor to the geochemical variation is heavy minerals. The elements and oxides of ilmenite, leucoxene, and rutile are preferentially concentrated within the freshwater-upper bay sediments. The barrier-strandplain sediments contain a high concentration of Zr, probably reflecting their zircon content. The differences in the concentrations of heavy-mineral populations in these environments probably also reflect the results of lag sedimentation.

The clay minerals of the fine-grained sediments are, in descending order of abundance, kaolinite, illite, mixed-layer illite-smectite, smectite, and undifferentiated kaolinite-chlorite. On the basis of the mean concentrations of the elements and oxides composing these clay minerals, kaolinite and illite represent the most common minerals in the freshwater-upper bay sediments. These clay minerals, as well as smectite, which occurs exclusively in fluvial-channel sediments, probably were derived from source rocks within the watershed of the ancestral Nueces River that drained the study area during Pleistocene and Holocene time.

In conclusion, the geochemical and mineralogical variations of the fine-grained sediments in the study area result mainly from two contributing factors—differences in depositional environment and differences in grain size. The end members of the coastal environmental spectrum are freshwater-upper bay and marine barrier-strandplain environments. The difference in sediment grain size between these end-member environments is marked, and it is a significant contributor to the observed geochemical and mineralogical variability.

REFERENCES CITED

Brooks, R. A., and Ferrell, R. E., Jr., 1970, The lateral distribution of clay minerals in Lakes Pontchartrain and Maurepas, Louisiana: Journal of Sedimentary Petrology, v. 40, no. 3, p. 855–863.

Dorrzapf, A. F., Jr., 1973, Spectrochemical computer analysis—Argon-oxygen d-c arc method for silicate rocks: U.S. Geological Survey Journal of Research, v. 1, no. 5, p. 559–562.

Feuillet, J.-P., and Fleischer, Peter, 1976, James River estuary, Virginia—Control of clay mineral distribution by estuarine circulation [abs.]: Geological Society of America Abstracts with Programs, v. 8, no. 2, p. 169.

Flores, R. M., and Shideler, G. L., 1978, Factors controlling heavy-mineral variations on the South Texas Outer Continental Shelf, Gulf of Mexico: Journal of Sedimentary Petrology, v. 48, no. 1, p. 269–280.

Helz, A. W., 1973, Spectrochemical computer analysis—Instrumentation: U.S. Geological Survey Journal of Research, v. 1, no. 4, p. 475–482.

Imbrie, John, 1963, Factor and vector analysis programs for analyzing geologic data: U.S. Office of Naval Research, Geography Branch, Technical Report 6 of ONR Task No. 389–135, 83 p.

Keller, W. D., 1970, Environmental aspects of clay minerals: Journal of Sedimentary Petrology, v. 40, no. 3, p. 788–813.

Miesch, A. T., 1976a, Q-mode factor analysis of compositional data: Computers & Geosciences, v. 1, no. 3, p. 147–159.

———1976b, Q-mode factor analysis of geochemical and petrologic data matrices with constant row-sums: U.S. Geological Survey Professional Paper 574–G, 47 p.

Millot, Georges, 1949, Relations entre la constitution et la genèse des roches sédimentaires argileuses: Géologie Appliquée et Prospection Minière (Nancy), v. 2, nos. 2–4, 352 p.

Morton, R. A., 1972, Clay mineralogy of Holocene and Pleistocene sediments, Guadalupe Delta of Texas: Journal of Sedimentary Petrology, v. 42, no. 1, p. 85–88.

Shepard, F. P., 1954, Nomenclature based on sand-silt-clay ratios: Journal of Sedimentary Petrology, v. 24, no. 3, p. 151–158.

Simons, L. H., and Taggart, M. S., Jr., 1954, Clay mineral content of Gulf Coast outcrop samples, *in* Swineford, Ada, and Plummer, N. V., eds., Clays and clay minerals—Proceedings of the 2d National Conference on Clays and Clay Minerals, Columbia, Missouri, October 15–17, 1953: National Research Council Publication 327, p. 104–110.

Sutton, A. L., Jr., 1976, Spectrochemical computer analysis, *in* Geochemical survey of the western energy regions: U.S. Geological Survey Open-File Report 76–729, p. 131–138.

Whitehouse, U. G., and McCarter, R. S., 1958, Diagenetic modification of clay mineral types in artificial sea water, *in* Swineford, Ada, ed., Clays and clay minerals—[Proceedings of the] 5th National Conference on Clays and Clay Minerals, University of Illinois, October 8–10,1956: National Research Council Publication 566, p. 81–119.

*U.S. GOVERNMENT PRINTING OFFICE: 1986- 491-409:40006